ASPHALT PAVEMENT AGING AND TEMPERATURE DEPENDENT PROPERTIES USING FUNCTIONALLY GRADED VISCOELASTIC MODEL

BY

ESHAN V. DAVE

B.E., Sardar Patel University, 2001
M.S., University of Illinois at Urbana-Champaign, 2003

DISSERTATION

Submitted in partial fulfillment of the requirements
for the degree of Doctor of Philosophy in Civil Engineering
in the Graduate College of the
University of Illinois at Urbana-Champaign, 2009

Urbana, Illinois

Doctoral Committee

Professor William G. Buttlar, Chair, Director of Research
Professor Glaucio H. Paulino, Chair, Director of Research
Professor Harry H. Hilton
Professor Hervé DiBenedetto, University of Lyon
Mr. Philip B. Blankenship, Asphalt Institute

ABSTRACT

ASPHALT PAVEMENT AGING AND TEMPERATURE DEPENDENT PROPERTIES THROUGH A FUNCTIONALLY GRADED VISCOELASTIC MODEL

Eshan V. Dave

Department of Civil and Environmental Engineering
University of Illinois at Urbana Champaign

William G. Buttlar, Advisor

Glaucio. H. Paulino, Advisor

Asphalt concrete pavements are inherently graded viscoelastic structures. Oxidative aging of asphalt binder and temperature cycling due to climatic conditions being the major cause of non-homogeneity. Current pavement analysis and simulation procedures dwell on the use of layered approach to account for these non-homogeneities. The conventional finite-element modeling (FEM) technique discretizes the problem domain into smaller elements, each with a unique constitutive property. However the assignment of unique material property description to an element in the FEM approach makes it an unattractive choice for simulation of problems with material non-homogeneities. Specialized elements such as "graded elements" allow for non-homogenous material property definitions within an element. This dissertation describes the development of graded viscoelastic finite element analysis method and its application for analysis of asphalt concrete pavements.

Results show that the present research improves efficiency and accuracy of simulations for asphalt pavement systems. Some of the practical implications of this work include the new technique's capability for accurate analysis and design of asphalt pavements and overlay systems and for the determination of pavement performance with varying climatic conditions and amount of in-service age. Other application areas include simulation of functionally graded fiber-reinforced concrete, geotechnical materials, metal and metal composites at high temperatures, polymers, and several other naturally existing and engineered materials.

To my parents.

ACKNOWLEDGEMENTS

This study would not have been possible without support of many people. First of all I would like to acknowledge my advisers, Prof. William G. Buttlar and Prof. Glaucio H. Paulino. They have provided endless support, excellent guidance and encouragement throughout the study. I am also grateful to my committee members Professor Harry H. Hilton, Mr. Philip B. Blankenship, and Prof. Hervé DiBenedetto, for their help and valuable input to thesis. I would also like to thank my colleagues, Dr. Michael P. Wagoner, Dr. Seong H. Song, Dr. Andrew B. Braham, Dr. MinKyum Kim, Dr. Bin Shen, Dr. Hyunwook Kim, Mr. Sarfraz Ahmed, Mr. Behzad Behnia, Mr. Kyoungsoo Park, Ms. Sofia Leon, Mr. Salman Hakimzadeh, and many others who always encouraged and helped me during course of this study. Thanks to SemMaterials L.P., USDOT's NexTrans Research Center, USDOT Pooled Fund Study and Department of Civil and Environmental Engineering for providing financial support to complete this research. And finally, thanks to my family for being with me and always offering support and love.

TABLE OF CONTENTS

LIST OF TABLES ix

LIST OF FIGURES x

CHAPTER 1 – INTRODUCTION 1

1.1 Background 1

1.2 Asphalt Pavement Systems 2

1.2.1 Conventional Asphalt Pavements 2

1.2.2 Full-Depth Asphalt Pavements: 3

1.2.3 Surface Treatments 3

1.2.4 Overlay Systems 4

1.3 Reflective and Thermal Cracking in Asphalt Pavements 5

1.4 Problem Statement 7

1.5 Research Objectives and Outline 7

1.6 Organization of Dissertation 9

CHAPTER 2 – REVIEW OF FGMs AND VISCOELASTIC MODELS 11

2.1 Functionally Graded Materials 11

2.2 Asphalt Concrete Pavements as Graded Structures 12

2.3 Asphalt Concrete Material Behavior 14

2.4 Review of Viscoelastic Models 16

2.4.1 Generalized Models 17

2.4.2 Parabolic Models 19

2.4.3 Power-Law Model 21

2.4.4 Sigmoidal Models 21

2.5 Simulation of Functionally Graded Materials 21

2.5.1 Generalized Isoparametric Formulation for Graded Elements 22

2.5.2 Example: Comparison of Homogeneous and Graded Element 23

2.5.3 Application of GIF Elements 25

2.6 Analysis of Viscoelastic Functionally Graded Materials 26

2.6.1 Correspondence Principle (CP) for Analysis of Viscoelastic FGMs 27

2.7 Modeling of Asphalt Concrete Pavements 27

2.8 Summary 28

CHAPTER 3 – VISCOELASTIC CHARACTERIZATION OF ASPHALT CONCRETE 30

3.1 Introduction....30
3.2 Motivation and Background....30
3.3 Indirect Tensile Creep Test Data Analysis....35
3.3.1 Elastic Solution....35
3.3.2 Viscoelastic Solution....37
3.4 Testing and Analysis....39
3.4.1 Material Details....40
3.4.2 Data Analysis....41
3.4.3 Results....41
3.5 Summary....45

CHAPTER 4 – FUNCTIONALLY GRADED VISCOELASTIC FINITE ELEMENT ANALYSIS USING CORRESPONDENCE PRINCIPLE....47
4.1 Introduction....47
4.2 Viscoelastic Constitutive Relationships....47
4.3 Elastic-Viscoelastic Correspondence Principle (CP)....48
4.3.1 Introduction....48
4.3.2 Limitation of CP for Non-Homogeneous Viscoelastic Problems....49
4.3.3 CP for Non-Separable Models....50
4.4 Selection of Material Model....52
4.4.1 Applicability to Material....53
4.4.2 Flexibility of Model....53
4.4.3 Compatibility with Current Research....53
4.4.4 Other Factors....53
4.5 Viscoelastic FGM Finite Element Formulation....54
4.6 Finite Element Implementation....57
4.6.1 Numerical Integral Transform....58
4.7 Verification Examples....61
4.7.1 Verification of Graded Elements....61
4.7.2 Verification of Viscoelastic Analysis....62
4.8 Comparisons with Commercial Software....64
4.8.1 Boundary Conditions....64
4.8.2 Material Distribution....65
4.8.3 FE Models....66
4.8.4 Results and Discussions....66
4.9 Summary....67

CHAPTER 5 – FUNCTIONALLY GRADED VISCOELASTIC FINITE ELEMENT ANALYSIS USING TIME-INTEGRATION SCHEME....69
5.1 Introduction....69
5.2 Time Integration Approaches....70

5.2.1 Brief Review of Time-Integration Approaches for Viscoelastic Analysis ...70
5.3 Analysis using Incremental Scheme ...72
5.3.1 Problem Description ...73
5.3.2 Results and Comparison with Analytical Solution ...73
5.4 Finite Element Analysis using Recursive Scheme ...75
5.4.1 Recursive Formulation ...75
5.4.2 Implementation and Verification ...76
5.4.3 Comparisons with Commercial Software ...82
5.5 Boundary Layer Analysis of Viscoelastic FGM ...87
5.5.1 Introduction ...87
5.5.2 Problem Description and FE Mesh ...88
5.5.3 Material Gradation ...89
5.5.4 Results ...90
5.5.5 Summary of Boundary Layer Analysis ...96
5.6 Summary ...96

CHAPTER 6 – CASE STUDIES: ASPHALT CONCRETE PAVEMENT SYSTEMS ...98

6.1 Introduction ...98
6.2 Practical Implications of the Present Research ...98
6.3 Pavement System 1, Conventional Asphalt Pavement ...101
6.3.1 Pavement Section ...101
6.3.2 Asphalt Concrete Properties ...101
6.3.3 Boundary Conditions ...102
6.3.4 Results and Discussions ...103
6.4 Pavement System 2, Full-Depth Asphalt pavement ...104
6.4.1 Pavement Section ...104
6.4.2 Asphalt Concrete Properties ...104
6.4.3 FE Model and Boundary Conditions ...106
6.4.4 Results ...108
6.4.5 Discussion of Results ...111
6.5 Pavement System 3, Overlay-Interlayer System with Graded Interface ...113
6.5.1 Introduction and Motivation ...113
6.5.2 Pavement Section ...114
6.5.3 FE Model and Boundary Conditions ...114
6.5.4 AC Material Properties ...116
6.5.5 Results ...118
6.5.6 Summary and Findings ...120
6.6 Summary ...121

CHAPTER 7 – CONCLUSIONS AND EXTENSIONS ...122

7.1 Summary and Findings ...122
7.2 Conclusions ...124

7.3 Future Extensions....124
7.4 Some Applications of the Present Research....127

CHAPTER 8 – NOMENCLATURE....130
8.1 Constitutive Relationship....130
8.2 Finite-Element Formulation....131
8.3 Time Integration Schemes....131

REFERENCES....132

APPENDIX A – MATLAB® CODE, CP-BASED VISCOELASTIC FGM FE IMPLEMENTATION....146

APPENDIX B – MATLAB® CODE, RECURSIVE FORMULATION BASED VISCOELASTIC FGM FE IMPLEMENTATION....163

AUTHOR'S BIOGRAPHY....177

LIST OF TABLES

Table 3.1: Aggregate Structure 40
Table 3.2: Binder Characteristics 40
Table 4.1: Mesh Attributes for Different Analysis Options 66
Table 5.1: Mesh Attributes for Different Analysis Options 86

LIST OF FIGURES

Figure 1-1: Layered versus smoothly-graded modeling approach 1
Figure 1-2: Typical Cross Section of Conventional Asphalt Pavement.....3
Figure 1-3: Typical Cross Section of Full-Depth Asphalt Pavement.....3
Figure 1-4: Typical Cross Section of Surface Treatments 4
Figure 1-5: Typical Cross Section of Overlay Systems 4
Figure 1-6: Thermal Cracking in Asphalt Pavement 5
Figure 1-7: Reflective Cracking in Asphalt Overlay 6
Figure 1-8: Outline of Doctorate Research.....8
Figure 2-1: Asphalt Concrete Complex Modulus after Eight-Years in Service (predicted using Mirza and Witczak's global aging model) 13
Figure 2-2: Temperature Variation through the Thickness of Asphalt Concrete Pavement.....14
Figure 2-3: Creep Compliance of 9.5-mm NMAS PG64-22 Asphalt Concrete 15
Figure 2-4: Relaxation Modulus Master-curve of 9.5-mm NMAS PG64-22 Asphalt Concrete.....15
Figure 2-5: Generalized Maxwell Model.....18
Figure 2-6: Generalized Kelvin Model 19
Figure 2-7: Huet-Sayegh Model 20
Figure 2-8: 2S2P1D Model (Di Benedetto et al. [49]) 20
Figure 2-9: Generalized Isoparametric Formulation for Graded Elements 23
Figure 2-10: Comparison of Standard (Uniform) Element with Graded Element.....24
Figure 2-11: Unaveraged Horizontal Stresses in an Aged Flexible Pavement (reproduced from Buttlar et al. [39]).....25
Figure 3-1: Field Core Sample Procurement (inset: Cored Sample) 31
Figure 3-2: Indirect Tensile Creep and Strength Test Setup (AASHTO T-322) 31
Figure 3-3: Crushing Under the Loading Head 32
Figure 3-4: Flattened IDT Specimen Geometry (left: Test Schematics; right: Flattened IDT test setup).....33
Figure 3-5: Stress Contours in Vertical (y) Direction (left: regular IDT, right: flattened IDT).....34
Figure 3-6: Ratio of Peak Compressive and Tensile Stresses.....34

Figure 3-7: Geometry and Boundary Conditions for the Hondros Solution.....37
Figure 3-8: 50° Flattened (left) and Standard (right) IDT Test Specimens 39
Figure 3-9: Mix-22 Creep Compliance Mastercurve (reference temperature = -20°C).....42
Figure 3-10: Mix-28 Creep Compliance Mastercurve (reference temperature = -20°C).....42
Figure 3-11: Mix-40 Creep Compliance Mastercurve (reference temperature = -20°C).....43
Figure 3-12: Comparison of Mix-22 Regular and Flattened Creep Compliances.....43
Figure 3-13: Comparison of Mix-28 Regular and Flattened Creep Compliances.....44
Figure 3-14: Comparison of Mix-40 Regular and Flattened Creep Compliances.....44
Figure 4-1: Outline of Finite Element Analysis Procedure.....58
Figure 4-2: Numerical Laplace Inversion using Collocation Method 61
Figure 4-3: Comparison of Exact (line) and Numerical Solution (circular markers) for Bending of FGM Bar (insert illustrates the boundary value problem along with material gradation).....62
Figure 4-4: Comparison of Exact and Numerical Solution for the Creep of Exponentially Graded Viscoelastic Bar 63
Figure 4-5: Comparison of Exact and Numerical Solution for the Relaxation of Exponentially Graded Viscoelastic Bar 64
Figure 4-6: Graded Viscoelastic Beam Problem Configuration 65
Figure 4-7: Relaxation Moduli on Top and Bottom of the Graded Beam 65
Figure 4-8: Mesh Discretization for Various Simulation Cases ($1/5^{th}$ beam span shown for each case).....66
Figure 4-9: Normalized Mid-Span Deflection for the Beam.....67
Figure 5-1: Problem Geometry.....73
Figure 5-2: Comparison of Analytical and Numerical Evaluation of Tangential Stresses.....74
Figure 5-3: Comparison of Analytical and Numerical Evaluation of Radial Stresses.....75
Figure 5-4: Computation Times for Different Solution Schemes.....78
Figure 5-5: Error Analysis for Different Solution Schemes 78
Figure 5-6: Viscoelastic Beam Problem Configuration.....79
Figure 5-7: Relaxation Modulus for the Beam Bending Verification Example.....80
Figure 5-8: Normalized Mid-Span Deflections for the Viscoelastic Beam 80

Figure 5-9: Comparison of Exact and Numerical Solution for the Exponentially Graded 81
Figure 5-10: Comparison of Exact and Numerical Solution for the Exponentially Graded 82
Figure 5-11: Boundary Conditions and Temperature Distribution (legend on right provides temperature in °C) 83
Figure 5-12: Temperature Input for Different Simulation Cases (solid line: FGM approach (present formulation), dashed line: layered approach (ABAQUS®) 84
Figure 5-13: Relaxation Modulus (inset: Time temperature superposition shift factors) 85
Figure 5-14: Mesh Discretization for Various Simulation Cases (1/5th beam span shown for each case) 86
Figure 5-15: Normalized Mid-Span Deflections for Thermally Induced Graded Beam 86
Figure 5-16: Deviation of Layered Results with FGM Results 87
Figure 5-17: Problem Description and FE Model 89
Figure 5-18: Relaxation Modulus Variation with Radial Distance and Time 90
Figure 5-19: Elastic Stresses for Homogeneous "Stiff" Properties at Different Radial Distances 91
Figure 5-20: Elastic Stresses for All Material Distributions (Homogeneous and FGM) 92
Figure 5-21: Elastic Stresses (y-Direction) for FGM (at Four Radial Distances) and Homogeneous Materials 92
Figure 5-22: Viscoelastic Normal Stresses (y-Direction) for All Material Distributions (Homogeneous and FGM) 94
Figure 5-23: Peak Normal Stresses (y-Direction) for All Material Distributions (Homogeneous and FGM) 94
Figure 5-24: Viscoelastic Shear Stresses for All Material Distributions (Homogeneous and FGM) 95
Figure 5-25: Peak Shear Stresses for All Material Distributions (Homogeneous and FGM) 96
Figure 6-1: Pavement Section at ATREL (left: immediately after construction right: 19 months after construction) 99
Figure 6-2: Relevance of Present Research in Context of Pavement Analysis and Design 100
Figure 6-3: Pavement Section and FE Mesh 101

Figure 6-4: Relaxation Modulus of Asphalt Concrete (variation with height of AC layer and time) 102
Figure 6-5: Stresses in Horizontal Direction (x-direction) directly under the Tire Load 103
Figure 6-6: Full-Depth Asphalt Pavement Section (I-155, Lincoln, IL)....104
Figure 6-7: Relaxation Modulus of Full-Depth AC Pavement (variation with Height of AC Layer and Time) 105
Figure 6-8: FE Meshes for Full Depth AC Pavements (Inset: Region of AC Layers) 107
Figure 6-9: FE Model Schematic....108
Figure 6-10: Strain in y-y Direction across AC Thickness for Unaged Conditions 109
Figure 6-11: Peak Strain in Vertical (y) Direction 110
Figure 6-12: Peak Strain in Horizontal (x) Direction 110
Figure 6-13: Peak Shear Strains (x-y Direction)....111
Figure 6-14: Strain in Vertical Direction at Interface of Surface and Binder Courses....112
Figure 6-15: Cross Section of Asphalt Pavements showing Interfaces between Different Construction Courses 113
Figure 6-16: Pavement Section (LA34 near Monroe, LA)....115
Figure 6-17: Pavement Cross Section and FE Model Schematics....115
Figure 6-18: Relaxation Modulus for Surface and Interlayer Mixtures 116
Figure 6-19: Relaxation Modulus Variation for Step Interface....117
Figure 6-20: Relaxation Modulus Variation for Graded Interface....117
Figure 6-21: Stress in Horizontal Direction (x-direction) directly under the Tire Load (different loading times are shown)....118
Figure 6-22: Stress in Horizontal Direction (x-direction) at Interface 119
Figure 6-23: Peak Tensile Stresses in the Overlay....120
Figure 7-1: Fractured Faces of Asphalt Concrete Specimens....126
Figure 7-2: Tack Coat Emulsion Wicking up (reproduced from [150]) 128

CHAPTER 1 - INTRODUCTION

1.1 BACKGROUND

Asphalt concrete pavements are inherently graded viscoelastic structures. Oxidative aging of asphalt binder and temperature cycling due to climatic conditions represent the major cause of this non-homogeneity. Current pavement analysis and simulation procedures involve the use of a layered approach to account for these non-homogeneities; a common example of such an approach is the recently developed American Association of State Highway and Transportation Officials (AASHTO) Mechanistic-Empirical Design Guide (MEPDG) [1]. Figure 1-1 illustrates the difference between layered and smoothly-graded approaches for a simple geometry consisting of material variation in one direction. In this example the layered approach is shown with sub-division of body into three layers and each modeled using average properties (E_i), where as in case of smoothly-graded modeling approach the material variation is accounted for through spatial dependence of material property, given by $E(x)$.

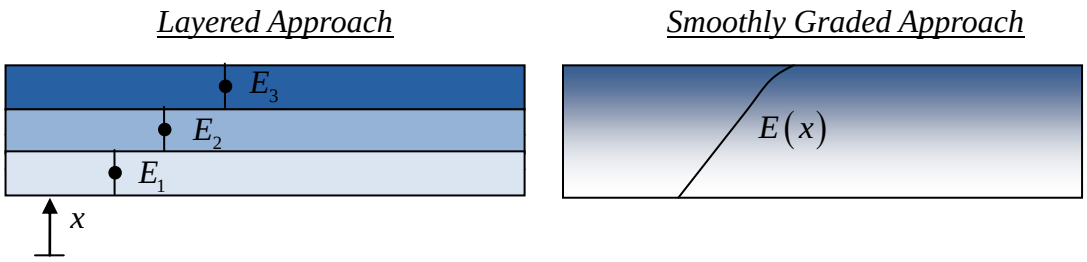

Figure 1-1: Layered versus smoothly-graded modeling approach

The conventional finite-element modeling (FEM) technique discretizes the problem domain into smaller elements, each with a unique constitutive property. The capability to effectively discretize the problem domain makes it an attractive simulation technique for

modeling of complicated boundary value problems such as asphalt concrete pavements. However the assignment of unique material property description to an element in the conventional FEM approach makes it an unattractive choice for simulation of problems with material non-homogeneities. Specialized elements such as "graded elements" allow for non-homogenous material property definitions within an element. This dissertation describes the development of a graded viscoelastic finite element analysis method and its application for analysis of asphalt concrete pavements. Apart from simulation of asphalt pavements, the present approach could also be utilized for the analysis of other engineering systems that exhibit graded viscoelastic behavior. Examples of such systems include metals and metal composites at high temperatures [2, 3]; polymeric and plastic based systems that undergo oxidative and/or ultraviolet hardening [4-6] and graded fiber reinforced cement and concrete structures [7]. Other application areas for the graded viscoelastic analysis includes accurate simulation of the interfaces between viscoelastic materials such as the layer interface between different asphalt concrete lifts or simulations of viscoelastic gluing compounds used in the manufacture of layered composites [8].

1.2 ASPHALT PAVEMENT SYSTEMS

There are over 2.2 million miles of paved roads across the United States, out of which 94% are surfaced with asphalt concrete [9]. Asphalt concrete pavements (also known as flexible pavements) can be broadly classified into four types.

1.2.1 Conventional Asphalt Pavements

These types of pavement systems are most commonly utilized and the pavement structure consists of subbase, base, and asphalt concrete layer on top of soil subgrade. The layer thicknesses depend on the traffic loading as well as the soil subgrade conditions. Figure 1-2 shows typical cross-section of conventional asphalt pavement systems.

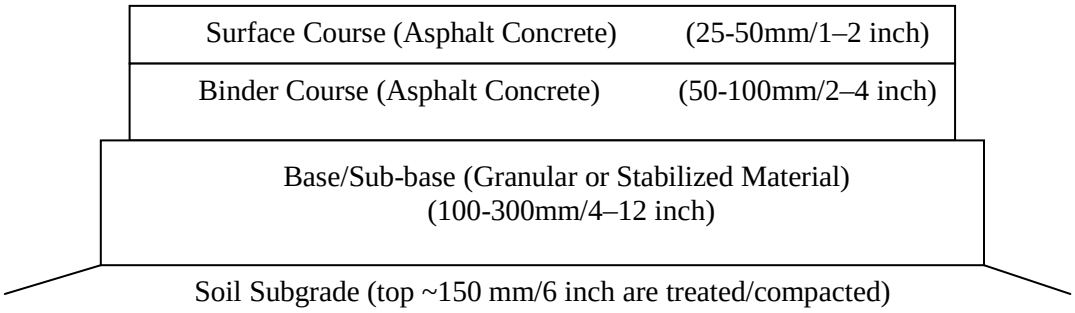

Figure 1-2: Typical Cross Section of Conventional Asphalt Pavement

1.2.2 Full-Depth Asphalt Pavements:

As the name suggests this type of pavement systems eliminates the need for base or subbase layers and instead a thicker asphalt concrete layers is constructed directly on top of the soil subgrade. In case of poor subgrade conditions, the top few inches of soil subgrade may be stabilized to improve the support conditions. A typical full-depth asphalt pavement cross-section is illustrated in Figure 1-3.

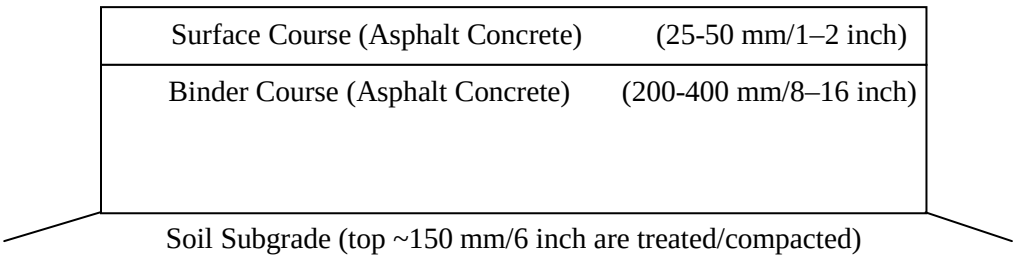

Figure 1-3: Typical Cross Section of Full-Depth Asphalt Pavement

1.2.3 Surface Treatments

The primary applications for surface treatments can be divided into two categories: (1) low volume roads, and (2) surface improvement (non structural overlays). For low volume roads, the surface treatments provide a low cost riding surface with limited structural capacity. On a deteriorated pavement surface, treatments such as open graded

friction courses (OGFC) are constructed to improve drivability and reduce surface distresses such as low friction resistance or raveling or to improve drainage.

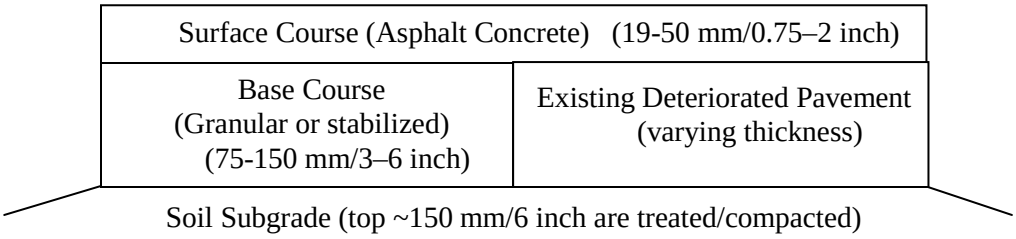

Figure 1-4: Typical Cross Section of Surface Treatments

1.2.4 Overlay Systems

Asphalt concrete overlay systems provide an economical and rapid means for improving the structural and functional capabilities of deteriorated asphalt or concrete pavements. Apart from usage of traditional dense graded asphalt concrete layers a variety of specialty systems have been developed. For instance the reflective crack relief interlayer (RCRI) system described by Blankenship et al. [10], RCRI is engineered to improve the reflective cracking resistance of asphalt overlays.

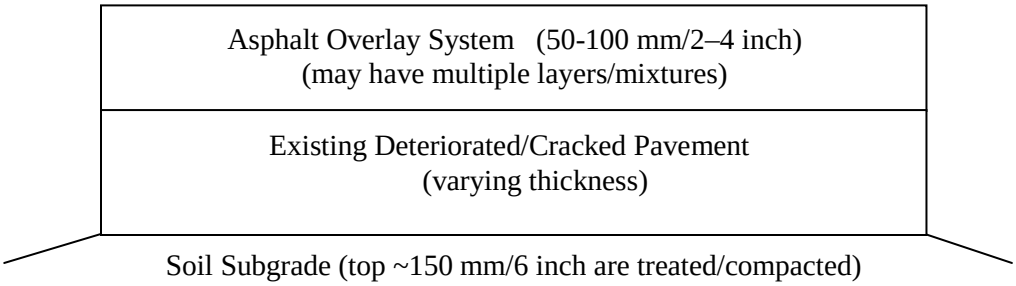

Figure 1-5: Typical Cross Section of Overlay Systems

1.3 REFLECTIVE AND THERMAL CRACKING IN ASPHALT PAVEMENTS

Reflective and thermal cracking in asphalt pavements and overlays are a major source of pavement deterioration and structural failure. Thermal cracks in asphalt pavements form as a result of high cooling rates and/or low pavement temperature as a result of climatic events. When the thermally induced straining causes stresses in the longitudinal direction to exceed material capacity, damage is initiated. This damage can eventually result in the development of fully grown transverse crack. A typical thermal crack in an asphalt pavement is shown in Figure 1-6. An ongoing United State Department of Transportation (USDOT) pooled fund study is focused on the development of laboratory testing and computer simulation procedures for improving the prediction of thermal cracking in asphalt pavements. The first phase of this study made tremendous strides in development of analytical and numerical prediction models on cracking in asphalt concrete [11]. One of the future extensions to the fracture prediction procedures developed in this study is to capture the effects of aging in the asphalt pavements.

Figure 1-6: Thermal Cracking in Asphalt Pavement

When an overlay is placed on an existing pavement, physical separation of the overlay often takes place as a result of movement at the joints and cracks in the underlying pavement layer. Temperature and tire-induced movements, concentrated at underlying joints and cracks in the existing pavement lead to stresses in the overlay, which significantly contribute to reflective cracking. Reflective cracking in the overlay allows water to percolate into the pavement structure and weaken the subbase and also contributes to many forms of pavement deterioration, including increased roughness and spalling. Figure 1-7 shows a reflective crack in the field for a pavement section located at IA9 near Decorah, IA.

Figure 1-7: Reflective Cracking in Asphalt Overlay

Paulino et al. [12] undertook a joint study between the National Science Foundation (NSF), the University of Illinois and an industry partner on integrated approach for reflective cracking control treatment analysis and design procedures. This study produced significant developments on laboratory fracture characterization and numerical

simulations of cracking in asphalt pavements. Wagoner et al. [13-17] developed fracture tests for asphalt concrete and performed extensive testing on laboratory and field samples for overlay and interlayer mixtures. Cohesive zone fracture models tailored for asphalt concrete have been developed by Song et al. [18-21]. The integration of laboratory fracture testing and cohesive zone fracture model has been successfully performed for the NSF study and other follow up studies on thermal and reflective cracking of asphalt pavements and overlays [22, 23].

Besides the two research projects described previously several other researchers have explored modeling approaches for study of cracking in pavements. However, most of these studies ignored the property gradients in asphalt pavements due to oxidative aging and effect of non-homogeneous temperature distributions.

Non-homogeneous viscoelastic analysis procedures are developed through the doctorate research described in this dissertation. When incorporated with the previous research preformed at the University of Illinois [12-22, 24] the research described herein will increase simulation reliability of thermal and reflective cracking in asphalt pavements through accurate and efficient consideration of aging and thermally induced property gradients in asphalt pavements.

1.4 PROBLEM STATEMENT

The main objective of this research is to develop a procedure that can accurately and efficiently simulate linear viscoelastic response of asphalt concrete pavements. The scheme should be capable of accounting for the linear viscoelastic material behavior at moderate and low temperatures, and the material property gradients caused by the effects of oxidative aging and thermal gradients. The formulations and implementations should undergo in-depth verification to ensure the accuracy and comparisons with conventional approaches should be made to demonstrate the efficiency of procedures developed herein.

1.5 RESEARCH OBJECTIVES AND OUTLINE

In order to develop a simulation scheme according to the problem statement described above the objectives for this research were identified as follows:

- Development and implementation of a finite-element analysis method (code) that can effectively and accurately solve linear viscoelastic problems
- Implementation of specialized graded element(s) to capture time-dependent material gradation
- Application of the aforementioned analysis techniques for the simulation of asphalt concrete pavements under typical loading conditions.

The research outline employed to meet the objectives listed above has been summarized in Figure 1-8. The key development includes implementation of finite-element analysis code for solving functionally graded viscoelastic boundary value problems. This can be performed by two approaches: (1) the use of an elastic-viscoelastic correspondence principle, and; (2) the use of a time-integration scheme. More details on each item within this outline are discussed in subsequent chapters.

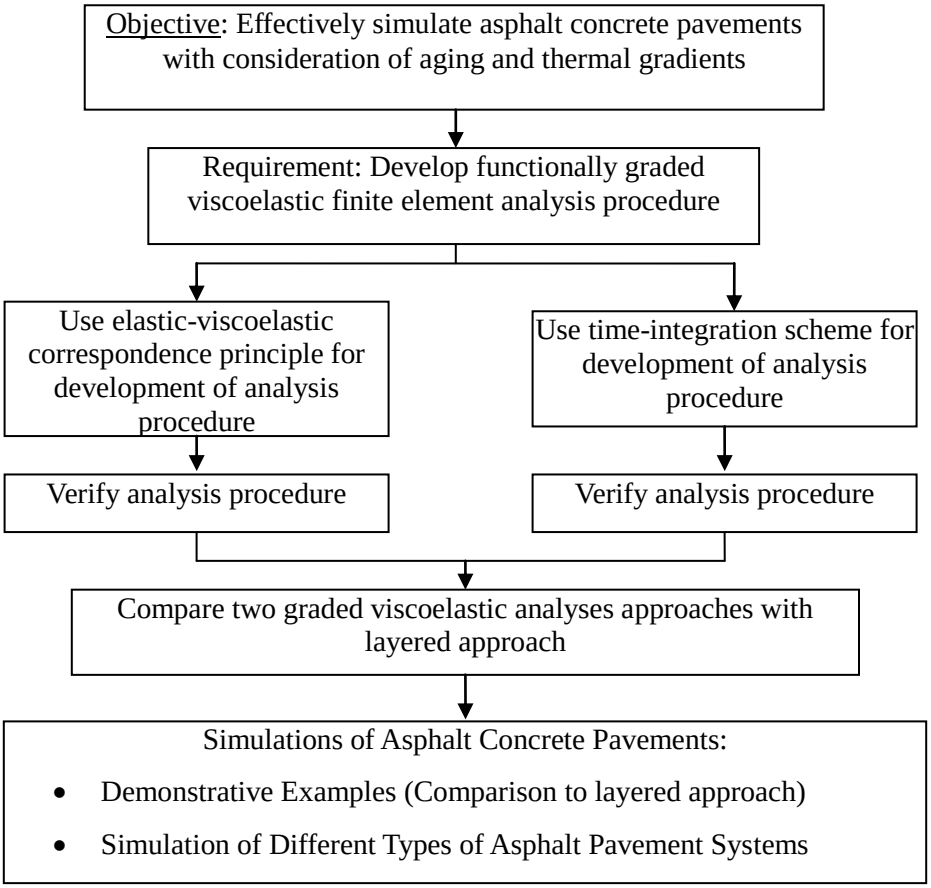

Figure 1-8: Outline of Doctorate Research

1.6 ORGANIZATION OF DISSERTATION

This dissertation consists of eight chapters. The subsequent chapters are organized as follows,

- Review of FGMs and Viscoelastic Models: This chapter describes the background information on FGMs and commonly used viscoelastic constitutive models. In addition to the background information, this chapter provides the summary of previous research that has been conducted in fields of simulation of FGMs, simulation of viscoelastic materials, and modeling of asphalt pavements.
- Viscoelastic Characterization of Asphalt Concrete: The testing and analysis procedures in regular and flattened indirect tensile configuration are discussed in this chapter. Viscoelastic characterization of three mixtures is presented and comparisons are made between results from regular and flattened geometries.
- Functionally Graded Viscoelastic Finite Element Analysis using Correspondence Principle: The basic viscoelastic constitutive relations are presented in this chapter followed by the formulation of the viscoelastic graded finite-element procedure. The implementation details along with verification examples are presented in the later portion of this chapter.
- Functionally Graded Viscoelastic Finite Element Analysis using Time Integration Scheme: Background information on various time-integration schemes for viscoelastic finite-element analysis is presented. Detailed description of the time-integration schemes of interest are presented in this chapter followed by the verification examples.
- Case Studies, Asphalt Concrete Pavement Systems: This chapter describes a variety of example problems where the analysis procedures developed in chapters 4 and 5 are utilized for simulation of three types of asphalt pavements systems. The simulation results are discussed and comparisons are made between the procedure proposed in this dissertation and the typical simulation approaches.

- Conclusions and Extensions: The contributions and key findings from this study are described in this chapter along with the recommendations and future extensions.
- Nomenclature: This chapter describes the list of symbols that have been used throughout this dissertation. Unless otherwise indicated the symbols used in the write-up, figures, equations and tables refer to this chapter.
- References, Appendices, and Author's Biography

CHAPTER 2 – REVIEW OF FGMS AND VISCOELASTIC MODELS

2.1 FUNCTIONALLY GRADED MATERIALS

Functionally Graded Materials (FGMs) are characterized by spatially varied microstructures created by non-uniform distributions of the reinforcement phase with different properties, sizes and shapes, as well as, by interchanging the role of reinforcement and matrix materials in a continuous manner [25]. They are usually engineered to produce property gradients aimed at optimizing structural response under different types of loading conditions (thermal, mechanical, electrical, optical, etc) [26]. These property gradients are produced in several ways, for example by gradual variation of the content of one phase (ceramic) relative to other (metallic) used in thermal barrier coatings, or by using a sufficiently large number of constituent phases with different properties [27]. Hilton [28, 29] has proposed designer viscoelastic FGMs (VFGMs) that are tailored to meet the design requirements such as viscoelastic columns subjected to axial and thermal loads. Muliana [30] has recently proposed micro-mechanical model for thermo-viscoelastic response of FGMs.

Apart from the engineered or tailored FGMs, several engineering materials naturally exhibit graded material properties. Silva et al. [31] have extensively studied and simulated bamboo, which is a naturally occurring graded material. Apart from natural occurrence a variety of materials and structures exhibit non-homogeneous material distribution and constitutive property gradations as an outcome of manufacturing or construction practices, aging, different amount of exposure to deteriorating agents etc. Asphalt concrete pavements are one such example, whereby aging and temperature variation yield continuously graded non-homogeneous constitutive properties.

2.2 ASPHALT CONCRETE PAVEMENTS AS GRADED STRUCTURES

The constituents of asphalt concrete include asphalt binder (bitumen) and mineral aggregates. Asphalt binder is derived from crude oil as a by-product of fractional distillation. Due to its organic nature asphalt binder undergoes oxidative aging as time progresses, the effect of which is most prominent in form of hardening or stiffening. The effect of aging creates graded material properties due to variation in the amount of aging across the depth of pavement. The Strategic Highway Research Program (SHRP) Project A-368 dealt with the chemical composition changes during the aging process of asphalt binders. The final report from this project identifies the process of age hardening as a non-reversible and continuous process that extends throughout the life of a pavement [32]. The aging and temperature induced property gradients have been well documented by several researchers in the field of asphalt pavements [30, 33-35]. The current state-of-the-art in viscoelastic simulation of asphalt pavements is limited to either ignoring non-homogeneous property gradients [22, 36-38] or considering them through a layered approach, for instance, the model used in the American Association of State Highway and Transportation Officials (AASHTO) Mechanistic Empirical Pavement Design Guide (MEPDG) [1]. Significant loss of accuracy from the use of the layered approach for elastic analysis of asphalt pavements has been demonstrated [39].

Age hardening can be divided into two stages. Mirza and Witczak [33] refers to them as short term hardening, which occurs during the mix production and construction and in-situ field aging which occurs during the service life of a pavement. In-situ field aging or long-term aging is the source of property gradient through the pavement. Illustration of aging gradient through the asphalt concrete pavement thickness is shown in Figure 2-1. The illustration is based on prediction made by “Global Aging Model” used in AASHTO MEPDG [1] for an eight year old asphalt concrete pavement located in central Illinois type climatic conditions.

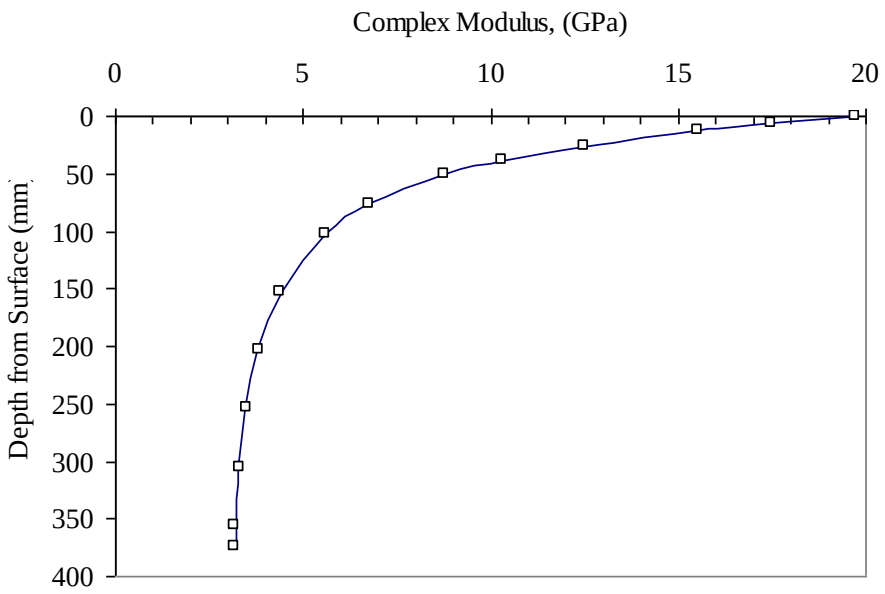

Figure 2-1: Asphalt Concrete Complex Modulus after Eight-Years in Service (predicted using Mirza and Witczak's global aging model)

Constitutive properties of asphalt concrete are significantly temperature dependent. Asphalt concrete creep compliance varies significantly with temperature (c.f. Figure 2-2). Nam and Bahia [40] have measured and reported a significant dependence of coefficient of thermal expansion of asphalt binder and mixtures on temperature. Due to climatic variations the pavement structure undergoes transient thermal conditions. Typical variation of temperature in asphalt concrete pavement during the course of a winter day is shown in Figure 2-2. Due to temperature gradients, material property gradients are essentially always present within asphalt pavements.

Other sources of graded material properties through the pavement includes effects of moisture, material gradation formed due to non-uniform compaction, bad construction practices (such as segregation), etc.

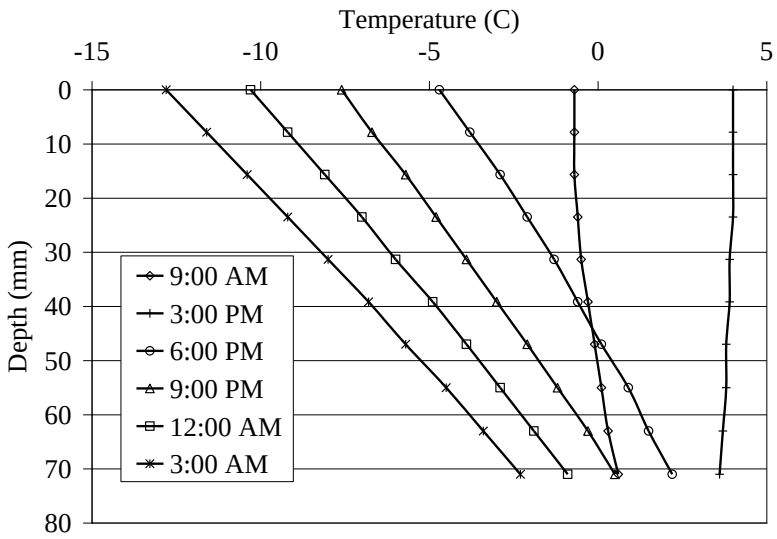

Figure 2-2: Temperature Variation through the Thickness of Asphalt Concrete Pavement

2.3 ASPHALT CONCRETE MATERIAL BEHAVIOR

Krishnan and Rajagopal [41] have reviewed the history of asphalt usage, its mechanical behavior and historical modeling approaches. Asphalt concrete exhibits viscoelastic material behavior at low and moderate pavement service temperatures [42]. The indirect tensile test (IDT) developed by Buttlar and Roque [43] and adopted as AASHTO T-322 [44] is the most commonly used procedure for viscoelastic characterization of asphalt concrete materials. The test procedure typically involves 1000-second creep testing of three replicate samples at three test temperatures. Creep-compliance at various test temperatures is calculated from the IDT creep testing. Chapter 3 describes the analysis procedure for extraction of viscoelastic properties from indirect tensile creep tests. Creep-compliances for a 9.5-mm nominal maximum aggregate size (NMAS) mixture, manufactured with a typical Illinois roadway binder (PG64-22 [45]) at temperatures of 0, -10, and -20°C, are shown in Figure 2-3 [16]. The creep compliance measured at three temperatures could be shifted using time-temperature superposition principle to obtain creep-compliance master-curve. Creep compliance master-curve could thereafter be interconverted to obtain the relaxation modulus master-curve, which is shown in Figure 2-4 [43, 46]. Notice that as common with other polymeric materials the bulk compliance/modulus seems to have a delayed creep/relaxation behavior.

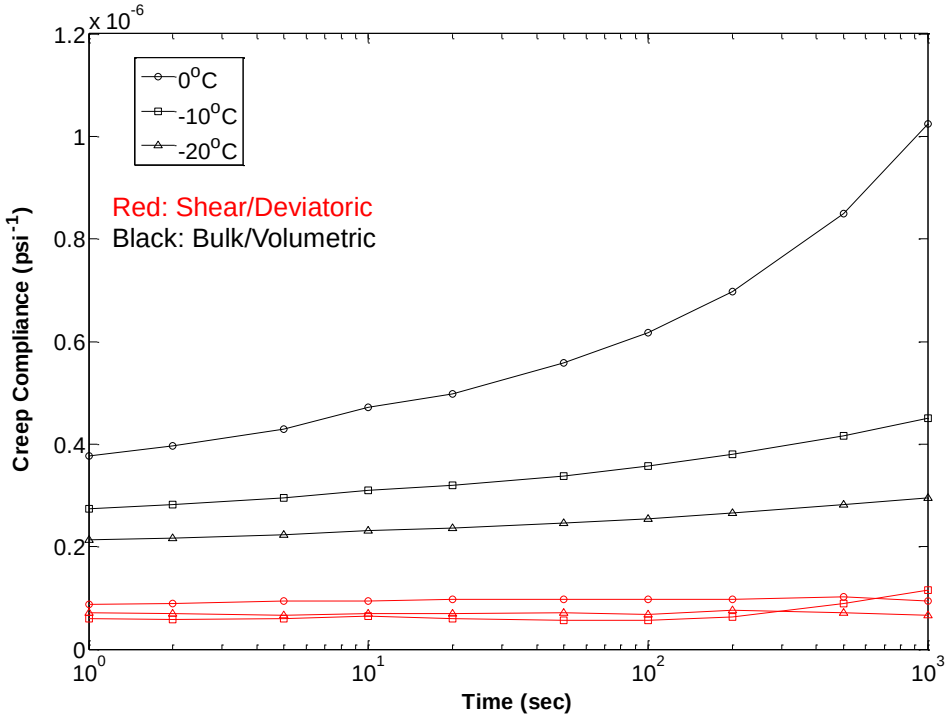

Figure 2-3: Creep Compliance of 9.5-mm NMAS PG64-22 Asphalt Concrete

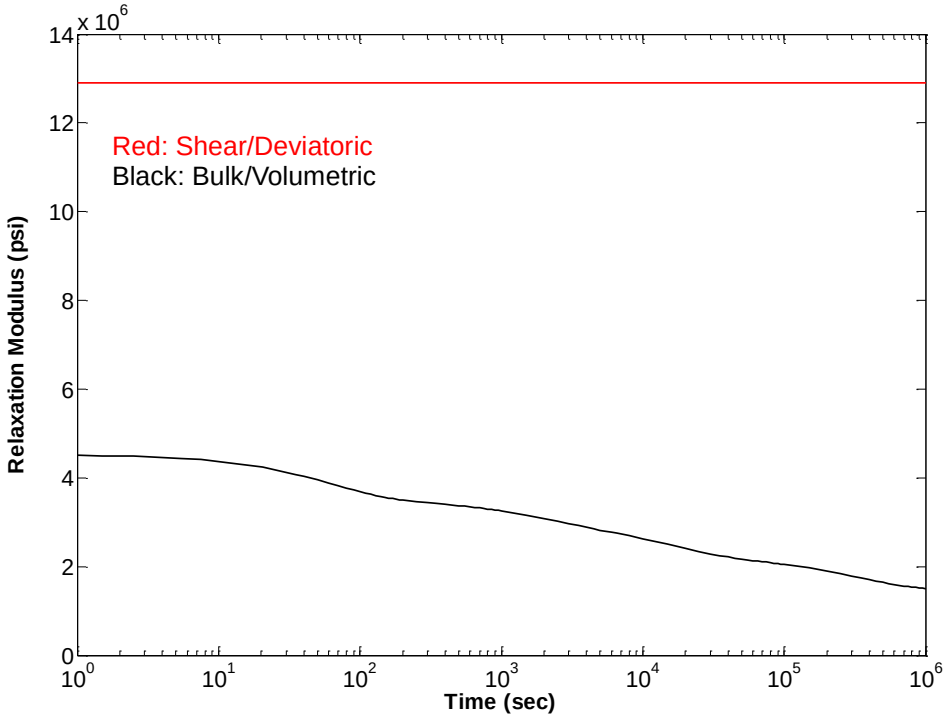

Figure 2-4: Relaxation Modulus Master-curve of 9.5-mm NMAS PG64-22 Asphalt Concrete

By comparing Figure 2-2 and Figure 2-3 the severity of the material property gradient created due to temperature variation can be seen. For example, if the pavement surface temperature is -10°C and the temperature at the bottom of the asphalt concrete layer is 0°C the properties could have as much as 50% difference even at loading times as short as 10-seconds. This effect becomes exaggerated at longer loading times. Apart from the temperature dependence of material properties the thermal gradients also cause inaccuracies in commercially available finite-element simulation codes (such as *Abaqus*) since they usually utilize an averaged element temperature in the calculations rather than allowing for temperature variation within the element.

2.4 REVIEW OF VISCOELASTIC MODELS

It is common practice to visualize viscoelastic material models by means of different arrangements of linear spring(s) and linear dashpot(s). Major benefits of using springs and dashpots for visualization of viscoelastic material models are:

- Springs and dashpots allow us to visualize behavior of material with more ease, which may not be the case of purely mathematical models
- It is easy to arrange springs and dashpots in various series and parallel arrangements, whereby if material behavior is well understood, it is easy to come up with a model that will duplicate this behavior
- Spring-Dashpot systems allow user to add or remove springs and dashpots on basis of the complexity of material behavior

The basic response of a linear spring is same as that of a linear elastic material and of a dashpot is same as of Newtonian fluid. The constitutive relationships for these basic elements are given as,

$$\begin{aligned} &\text{Linear Spring, } \sigma_{ij} = C_{ijkl}\varepsilon_{kl} \\ &\text{Linear Dashpot, } \sigma_{ij} = \eta_{ijkl}\frac{d\varepsilon_{kl}}{dt} \end{aligned} \tag{2.1}$$

Please refer to the Chapter 8: Nomenclature for description of the symbols throughout this dissertation.

In the case of asphaltic materials, the basic viscoelastic models such as Maxwell, Kelvin, 3-parameter solid and 3-parameter liquid models are too simple to properly capture the actual material behavior. Burger's model could probably capture the behavior of asphalt binder. However in general, it is not very suitable for asphalt mixtures. More commonly used viscoelastic models for asphalt concrete include:

- Generalized models (Prony series models)
- Parabolic models
- Power law model
- Sigmoidal models

2.4.1 Generalized Models

Generalized models are developed by series or parallel combinations of number of simpler models (such as Maxwell or Kelvin Model). Through the combination of simpler models it is possible to capture complex responses, such as those exhibited by asphalt mixtures. The most commonly used form of generalized viscoelastic models are generalized Maxwell model and generalized Kelvin model. Both of these models are inter-convertible to each other depending on prescribed condition. For strain prescribed conditions generalized Maxwell model can be expressed in form of Prony series, the generalized Kelvin model takes similar form for stress prescribed condition. Therefore these models are also known as Prony series form.

Generalized Maxwell Model: This model is obtained through parallel arrangement of a number of Maxwell models. Figure 2-5 illustrates a common form of generalized Maxwell model. The material properties such as shear and bulk moduli for the generalized Maxwell model are given as,

$$C_{ijkl} = \sum_{h=1}^{n} \left(C_{ijkl}\right)_h Exp\left[-t / \left(\tau_{ijkl}\right)_h\right] \tag{2.2}$$

where, $\left(C_{ijkl}\right)_h$ are the spring (elastic) constants, and $\left(\tau_{ijkl}\right)_h$ are the relaxation time of each Maxwell unit. Relaxation time is related to spring constant and dashpot viscosity as,

$$\tau = \frac{\eta}{C} \tag{2.3}$$

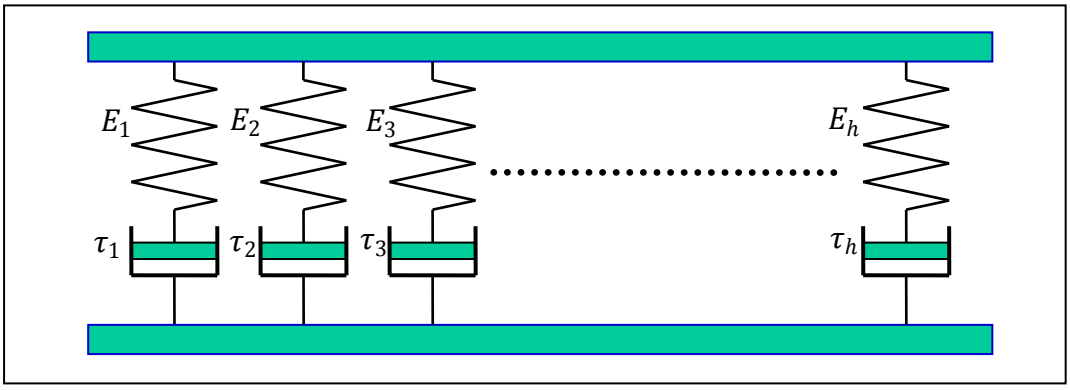

Figure 2-5: Generalized Maxwell Model

Generalized Kelvin Model: This model is obtained by series arrangement of a number of Kelvin models as shown in Figure 2-6. Notice that the generalized Kelvin model illustrated here is the Prony series form corresponding to the generalized Maxwell model discussed previously. This model being of preference for stress prescribed conditions, the material properties such as shear or bulk compliances are commonly represented by it. The compliance for the generalized Kelvin model is given by,

$$D_{ijkl}(t) = \left(D_{ijkl}\right)_0 + \sum_{h=1}^{n}\left(D_{ijkl}\right)_h \left(1 - Exp\left[-t / \left(\lambda_{ijkl}\right)_h\right]\right) + \frac{t}{\left(\eta_{ijkl}\right)_0} \tag{2.4}$$

where $\left(D_{ijkl}\right)_h$ are the spring compliances and $\left(\lambda_{ijkl}\right)_h$ are the retardation time of the Kelvin units which is related to spring compliances and dashpot viscosities $\left(\eta_{ijkl}\right)_h$ as,

$$\lambda = D\,\eta \tag{2.5}$$

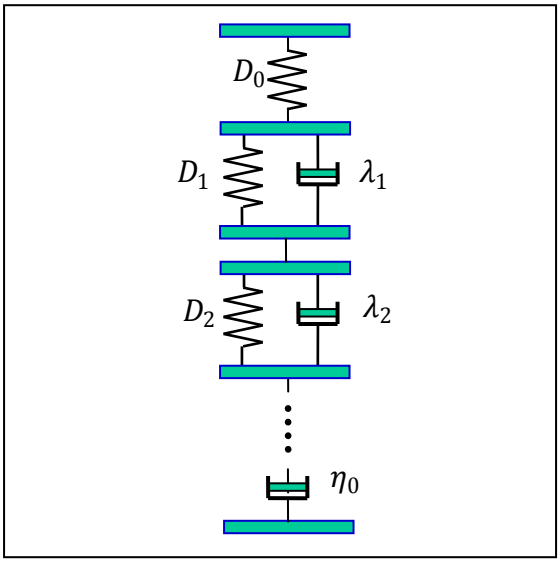

Figure 2-6: Generalized Kelvin Model

2.4.2 Parabolic Models

Huet [47] proposed the parabolic relationship for viscoelastic behavior of hydrocarbon based materials. The relationship proposed by Huet can be visualized in the form of a special type of dashpot whereby the constitutive relationship has a parabolic form as function of time. Strain for a prescribed stress σ for parabolic model proposed by Huet is given as,

$$\varepsilon(t) = \frac{\sigma}{A} t^k, 0 < k < 1 \tag{2.6}$$

The parameters A and k are generally determined through experiments.

Sayegh [48] proposed the Huet-Sayegh model for asphalt concrete materials; the Huet-Sayegh model uses the linear springs and the parabolic dashpots. This model consists of total of six material parameters, one for each spring and two for each parabolic unit. The Huet-Sayegh model is illustrated in Figure 2-7.

In recent years Di Benedetto and colleagues [49-52] have further extended the Huet-Sayegh model, they have proposed a 2S2P1D (2-springs, 2-parabolics, and 1-dashpot) model, whereby a dashpot has been added in series combination with the spring and parabolic unit. An illustration of the 2S2P1D model is shown in Figure 2-8. The 2S2P1D model has been shown to have fit the asphalt concrete data with significantly fewer

parameters when compared to generalized models [51]. Another merit of the 2S2P1D model for application to asphaltic materials is presence of unique model parameters going from binders to mastics to mixtures as show by Di Benedetto et al. [51, 52]. A functional form of 2S2P1D model for creep compliance can be given by,

$$J(t) = \frac{1}{E_0} + \frac{1}{E_\infty}\left(1 + \delta\frac{(t/\tau)^k}{\Gamma[k+1]} + \frac{(t/\tau)^h}{\Gamma[h+1]} + \frac{t}{\beta\tau}\right) \tag{2.7}$$

where, $E_0, E_\infty, \delta, k, h, \beta, \tau$ are all model parameters and Γ is the gamma function.

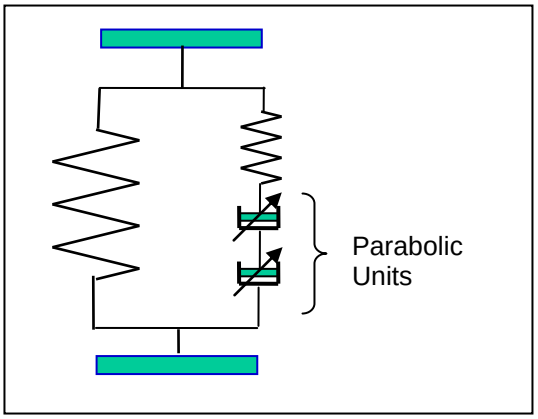

Figure 2-7: Huet-Sayegh Model

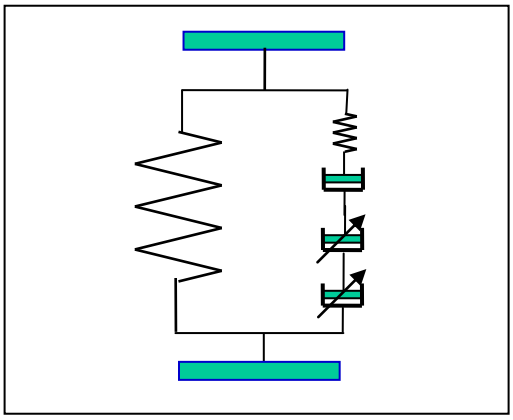

Figure 2-8: 2S2P1D Model (Di Benedetto et al. [49])

2.4.3 Power-Law Model

Power law type of relationship has been extensively used for asphalt binders. The bending beam rheometer [53] test for determining flexural creep stiffness of asphalt binder utilizes power law model to fit the test data. Unlike previously presented models this model is presented in only mathematical form (it is not illustrated through combination of springs and dashpots). As the name suggests this model is characterized by power-law type of functional form. An example of power-law model representing creep-compliance would be,

$$D(t) = D_0 + D_1 t^a + D_2 t^b \tag{2.8}$$

where, parameters D_i, a, b are all experimentally determined.

2.4.4 Sigmoidal Models

Asphalt concrete complex modulus prediction models such as Witczak predictive equation [54-57] and Hirsch model [58] use sigmoidal function for fitting the predicted data as well as measure lab data. The sigmoidal function is a generic function that is used to fit for both complex modulus as well as relaxation modulus due to its s-shaped nature. However as in case of power law model the sigmoidal model does not have a physical interpretation. An example of sigmoidal function used by Witczak et al. [54] is as follows,

$$E(t) = \delta + \frac{\alpha}{1 + Exp\left[\beta + \gamma(\log t)\right]} \tag{2.9}$$

where α, β, γ and δ are all material constants determined through experiment or predictive (regression) equations.

2.5 SIMULATION OF FUNCTIONALLY GRADED MATERIALS

Extensive research has been carried out to efficiently and accurately simulate functionally graded materials. Cavalcante et al. [26], Zhang and Paulino [59], Reddy [5],

Paulino and Kim [60, 61], Song and Paulino [62], have all recently worked on finite-element simulations of FGMs.

Graded elements have significant benefits over standard elements types in the context of simulating non-homogeneous isotropic and orthotropic materials using a finite-element framework [61]. Lee and Erdogan [63] and Santare and Lambros [64] have used graded elements with direct Gaussian integration. This type of formulation involves selection of material properties directly at the Gauss integration points. Kim and Paulino [65] proposed graded elements with generalized isoparametric formulation (GIF). The details on the generalized isoparametric formulation for graded elements are discussed in following subsection.

2.5.1 Generalized Isoparametric Formulation for Graded Elements

In the conventional finite-element method a single set of properties are assigned to an element. In case of graded elements with GIF the constitutive material properties are selected at each nodal point and interpolated back to the Gauss-quadrature points (Gaussian integration points) using isoparametric shape functions. Using GIF, the non-homogeneous viscoelastic material properties such as, shear relaxation modulus $G(t)$ and bulk modulus $K(t)$ are interpolated as,

$$G(t) = \sum_{i=1}^{m} N_i \left[G(t) \right]_i, \qquad K = \sum_{i=1}^{m} N_i \left[K(t) \right]_i \tag{2.10}$$

where N_i are the iso-parametric shape functions corresponding to node i, and m is the number of nodal points in the element.

This concept is illustrated in Figure 2-9. The figure shows the sampling of the material properties at element nodes. The non-homogeneous material properties are shown by the shaded plane and property sampling is indicated by the arrows in z-direction. The bold faced (red-colored) arrows show the interpolation of material properties from node points to one of the Gaussian integration points (shown by plus marks).

Paulino and Kim [61] recently presented a series of weak patch tests for the graded elements. This work demonstrated the existence of two length scales: (a) length scale associated with element size, and (b) length scale associated with material non-homogeneity. Consideration of both length scales is necessary in order to ensure convergence.

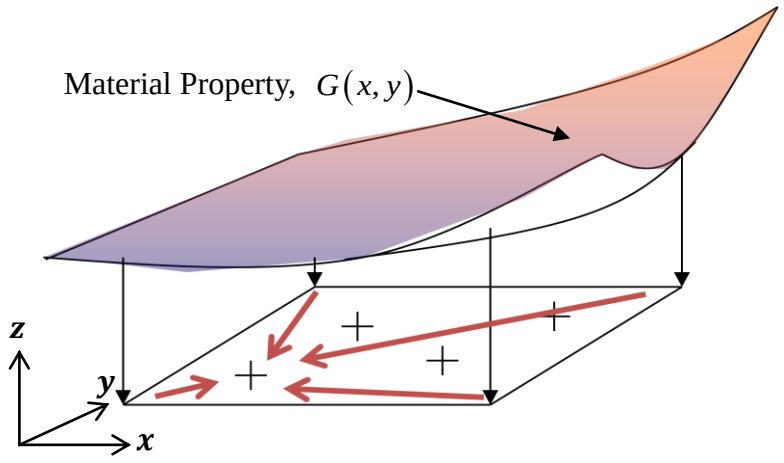

Figure 2-9: Generalized Isoparametric Formulation for Graded Elements

2.5.2 Example: Comparison of Homogeneous and Graded Element

A simple example is presented here to illustrate the use of generalized isoparametric graded finite element. Simulations were performed for a functionally graded body loaded in uniaxial tension. The problem geometry is as shown in Figure 2-10. Notice that the material variation is in both *x* and *y* directions. The simulations are performed by discretizing the body into four six-node triangular elements each with three Gauss-integration points. In case of standard (homogeneous) element average material properties were assigned to each element. The results for each approach are shown in terms of the stresses in the *x*-direction. Notice that the stress evaluation for the graded element was performed at the integration points using shape function interpolation.

The results clearly illustrate the superiority of graded elements in capturing the material non-homogeneity.

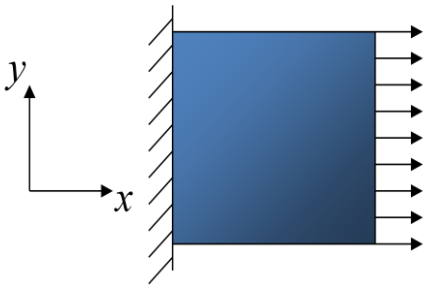

$$E(x,y) = E_0 Exp\left[3x - 2y\right]$$

(a) Problem Description

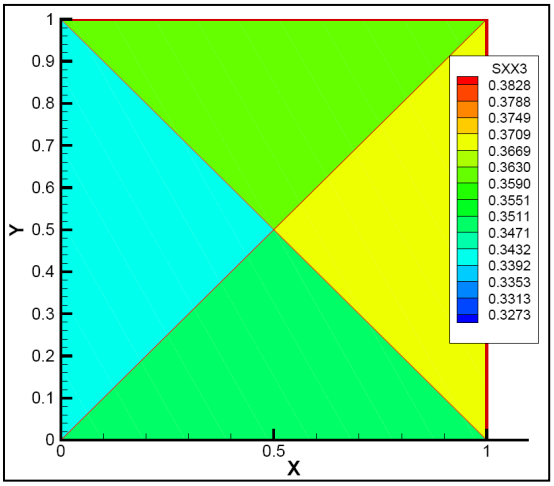

(b) Homogeneous Elements: Stresses in *x*-direction

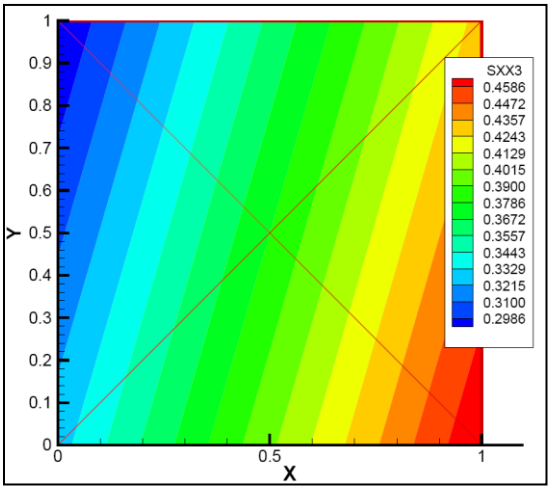

(c) Graded Elements: Stresses in *x*-direction

Figure 2-10: Comparison of Standard (Uniform) Element with Graded Element

2.5.3 Application of GIF Elements

Buttlar et al. [39] have used GIF elements for simulation of an aged flexible pavement system (I-155, near Lincoln, IL). Figure 2-11 shows one of their results. This figure compares the simulation results for graded and layered approaches. Notice that this work was limited to elastic material behavior and effects of time and temperature on properties of asphalt concrete were not considered.

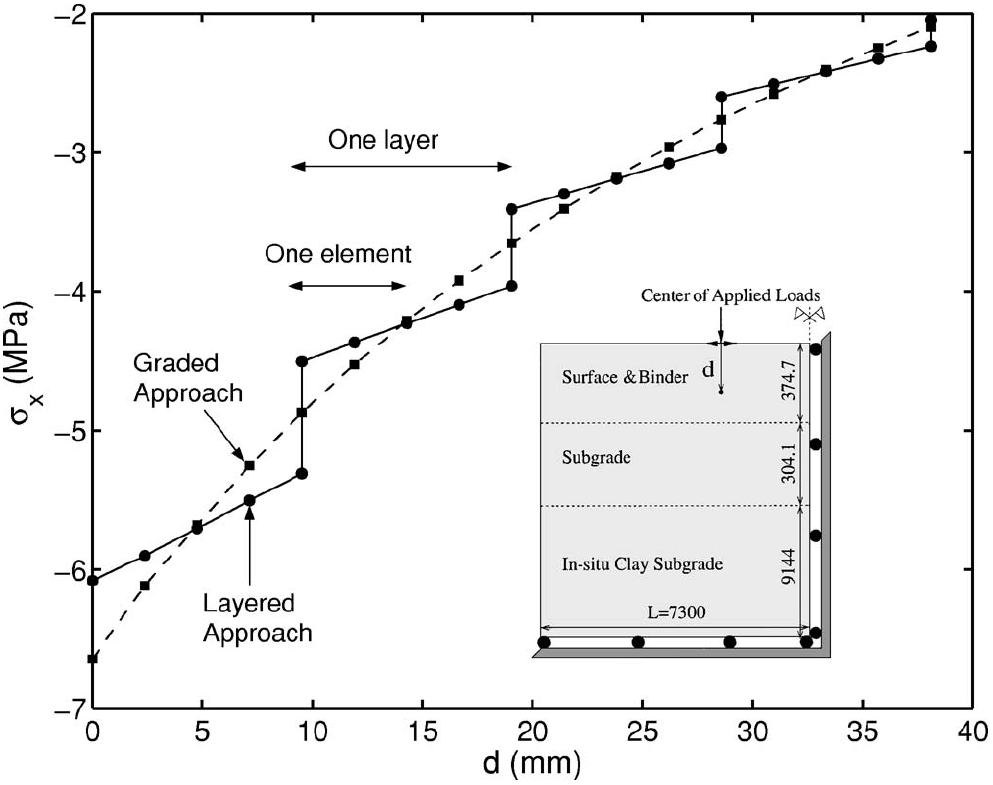

Figure 2-11: Unaveraged Horizontal Stresses in an Aged Flexible Pavement (reproduced from Buttlar et al. [39])

Zhang and Paulino [59] have recently used graded elements for dynamic analysis of graded beams. They have also illustrated the use of graded elements for simulation of interface between different material layers. Song and Paulino [62] have used graded element for evaluation of dynamic stress-intensity factors in functionally graded materials. Walter et al. [66] evaluated stress-intensity factors (SIFs) for FGMs under mode-I thermo-mechanical loading. Silva et al. [67] extended graded elements for

multiphysics applications and have shown the properties of the elements in such circumstances.

2.6 ANALYSIS OF VISCOELASTIC FUNCTIONALLY GRADED MATERIALS

Analysis of viscoelastic problems is typically approached in two ways:

- Correspondence Principle (CP): It allows for readily using the elastic solution or derived viscoelastic solution based on existing elastic solution, such as beam bending etc. However CP has limitations on its applicability for solving boundary value problems with non-homogeneous material properties.
- Time-Integration: Solve the convolution integral by means of either exact integration or numerical integration. For numerical methods such as finite-element analysis, the solution requires use of numerical integration scheme.

This can be more clearly explained by means of an example. For a simple one-dimensional (1D) problem, the stress-strain relationship for viscoelastic material is given by convolution integral shown in equation (2.11).

$$\sigma(t) = \int_0^t E\left(t - t'\right)\varepsilon\left(t'\right)dt' \tag{2.11}$$

If one is interested in solving for the stress and material properties and imposed strain conditions are know. Using the elastic-viscoelastic correspondence principle the convolution integral could be deduced to the following relationship using an integral transform such as the Laplace transform:

$$\tilde{\sigma}(s) = \tilde{E}(s)\tilde{\varepsilon}(s) \tag{2.12}$$

Notice that the above functional form is similar to that of the elastic problem, thus the analytical solution available for elastic problems could be directly applied to the viscoelastic problem. The transformed stress quantity, $\tilde{\sigma}(s)$ is solved with known $\tilde{E}(s)$ and $\tilde{\varepsilon}(s)$. Inverse transformation of $\tilde{\sigma}(s)$ provides the stress $\sigma(t)$.

For this 1D problem the time-integration based solution is obtained by directly solving the time integration. However as the problem gets more involved the analytical integration may not be possible and numerical integration becomes necessary.

2.6.1 Correspondence Principle (CP) for Analysis of Viscoelastic FGMs

Over the years. the correspondence principle has been extensively used for the analysis of non-homogeneous viscoelastic materials.. Hilton and Piechocki [68] used this principle for exploring the shift in shear center of non-homogeneous viscoelastic beams; Schapery [69] used this principle for the calculation of stress intensity factors (SIF) in non-homogeneous viscoelastic medium. More recently Sladek et al. [4, 70] have used the correspondence principle based solution scheme for analysis of viscoelastic FGM solids using the Petrov-Galerkin boundary integral method. Recently Chang et al. [71] used the correspondence principle for evaluating thermal stresses in polymeric films with graded interlayers.

Research by Paulino and Jin [72] and Mukherjee and Paulino [73] demonstrated the conditions pertaining to material non-homogeneity whereby the elastic-viscoelastic correspondence principle could not be used for solving viscoelastic problems. They have provided the conditions for the description of constitutive models of materials for which correspondence principle is rendered invalid. Jin [74] has reiterated these findings regarding the limitations of correspondence principle for non-homogeneous viscoelastic materials. Further details on limitation of correspondence principle in context with non-homogeneous viscoelastic materials are discussed in Chapter 4.

2.7 MODELING OF ASPHALT CONCRETE PAVEMENTS

Asphalt concrete pavement systems have been traditionally analyzed by means of layered elastic approach [9]. Several layered elastic analysis programs have been offered such as Kenlayer from University of Kentucky [9, 75], JULEA developed by Uzan [76, 77], BISAR from Shell Bitumen [78], WESLEA developed originally at US Army Corps of Engineers and most recently MNLAYER by Khazanovich and Wang [79]. Most of these programs rely on a layered approach for simulation of the non-homogenieites in the asphalt concrete. Alkasawneh et al. [80] have extended layered elastic approach to

account for temperature variation in the pavement structure through a graded approach. However the use of layered elastic analysis approach has several limitations such as assumption of non-realistic boundary conditions, lack of viscoelasticity in simulation of asphalt concrete, difficulty in simulating coupled thermo-mechanical analysis etc.

Finite-element analysis of asphalt concrete pavements has also been widely used. Axysymmetric analysis program Illi-Pave developed by Elliot and Thompson [81] was one of the pioneering works in this field. Recently a variety of pavement distresses have been studied using finite-element analysis. For example Dave et al. [22], Baek and Al-Qadi [38], Ling et al. [82] have studied reflective cracking, Mun et al. [83] studied fatigue cracking and Novak et al. [84] studied rutting in asphalt concrete pavements and overlays. As with layered elastic analysis a limited amount of finite-element studies consider the non-homogeneities such as aging and temperature variation. Buttlar et al. [39, 85], Kim and Buttlar [36], and Myers et al. [86] have all considered effects of aging and temperature variation through the depth of asphalt concrete pavement in numerical simulations. Among these studies only Buttlar et al. [39] have utilized smoothly graded modeling approach. As mentioned earlier they used the GIF elements proposed by Kim and Paulino [65] and their results reinforce the superiority of graded approach in comparison with the traditional layered approach. Song et al. [19, 20, 87] have simulated the crack propagation in asphalt concrete using cohesive zone modeling approach. Their work has shown that the use of viscoelastic bulk properties yield better agreement between numerical and experimental results. The natural extension to these previous studies would be incorporation of time and spatial dependence in the simulation of asphalt concrete pavements which would require a graded viscoelastic analysis technique, as presented herein.

2.8 SUMMARY

Through the background information obtained from literature review on modeling of FGMs, analysis of viscoelastic FGMs, asphalt concrete material behavior and analysis of asphalt concrete pavements, following key points could be summarized in context of the this research:

- In order to accurately capture the key responses of flexible (asphalt) pavement it is important to model asphalt concrete as a viscoelastic material.
- Asphalt concrete layers exhibit significant property gradients due to aging and temperature variations, these gradients should be included in the analysis of pavement systems.
- The graded finite-element analysis approach is better suited and more efficient for simulation of asphalt pavements with consideration of aging and thermal gradients. Other effects can naturally be included in the formulation.
- A finite element formulation for graded viscoelastic analysis can be developed using either correspondence principle or time-integration approach.

Based on the above shown summary, the following research was conducted:

- Development of viscoelastic finite element analysis procedure with generalized isoparametric formulation (GIF).
- Implementation and verification the finite element analysis code with (a) correspondence principle, and (b) time-integration schemes.
- Simulation of viscoelastic FGM boundary value problems using the analysis codes developed through this research:
    - Beam (property gradients and temperature induced gradients)
    - Radially graded viscoelastic body with stationary crack
    - Asphalt pavements (aging property gradients and simulation of graded interfaces)

CHAPTER 3 – VISCOELASTIC CHARACTERIZATION OF ASPHALT CONCRETE

3.1 INTRODUCTION

This chapter describes the testing and analysis procedures used in the viscoelastic characterization of asphalt mixtures. The Indirect Tension Test is frequently used in the evaluation of asphalt materials due to its convenience for capturing both viscoelastic properties and tensile strength. The indirect tensile testing mode is a very practical configuration for testing of asphalt concrete, as Hot Mix Asphalt (HMA) samples are often cylindrical in shape. When samples are taken from the field, a core barrel is utilized, producing cylindrical specimens, as illustrated in Figure 3-1. In addition, the laboratory equipment used to produce HMA samples uses a cylindrical shaped mold during compaction. During the Strategic Highway Research Program (SHRP), in the mid-1990's, a test protocol was developed for evaluating creep and strength properties of HMA mixtures [43] in indirect tension. The test was, somewhat arbitrarily, dubbed with the acronym "IDT" during the SHRP program. Both properties are measured on the same sample, with the non-destructive creep test run before the destructive strength test.

3.2 MOTIVATION AND BACKGROUND

This is especially the case when crushing failures occur under the narrow loading strips prior to or in exclusion of the desired tensile failure, which is assumed to occur along a vertical plane spanning between the loading strips. The IDT setup developed for HMA uses a 19 mm wide loading strip on the top and bottom of the testing specimen (c.f. Figure 3-2). With the increased use of finer aggregate gradations and polymer modified asphalt binders in HMA mixtures, the IDT results can be suspect, particularly at testing temperatures above 0°C because of excessive deformations and crushing under the

narrow loading heads during the creep and strength testing. Figure 3-3 illustrates one such example from the current study.

Figure 3-1: Field Core Sample Procurement (inset: Cored Sample)

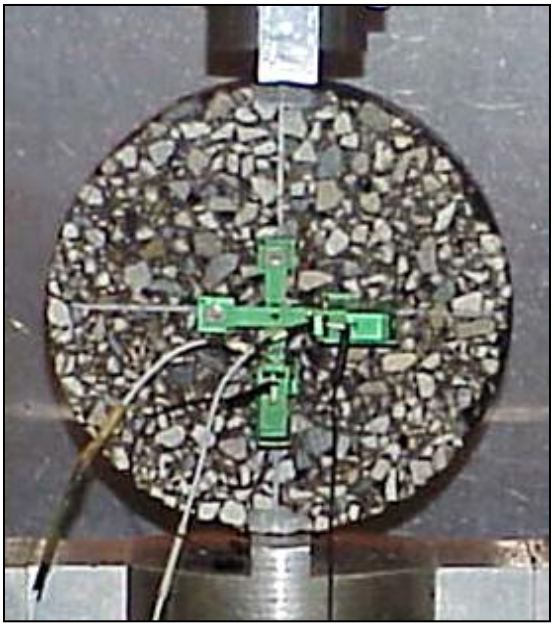

Figure 3-2: Indirect Tensile Creep and Strength Test Setup (AASHTO T-322)

Figure 3-3: Crushing Under the Loading Head

Wagoner et al. [16] briefly discussed this problem for an HMA interlayer mixture manufactured with heavily modified polymer asphalt binder and fine aggregate gradation, specially designed to reduce reflective cracking of HMA overlay pavements. One solution to this crushing problem is to increase the contact area between the loading heads and sample.

Towards this end, it is important to identify a test geometry that minimizes the material damage near the loading heads while providing sufficient tension in the middle of specimen for a global tensile failure. In the area of rock mechanics, the idea of a flattened Brazilian disc specimen has been studied [88, 89]. This testing configuration increases the surface area between the loading heads and sample; thereby reducing localized crushing and increasing the predominance of failure in tension within the sample. In place of the traditional 150-mm diameter, 50-mm thick, cylindrical specimen, Dave et al. [90] introduced a new specimen configuration for strength testing of HMA. In place of the loading heads at the top and bottom, the specimen was trimmed to produce flat planes with parallel faces, creating a "flattened-IDT." Figure 3-4 show the flattened IDT geometry.

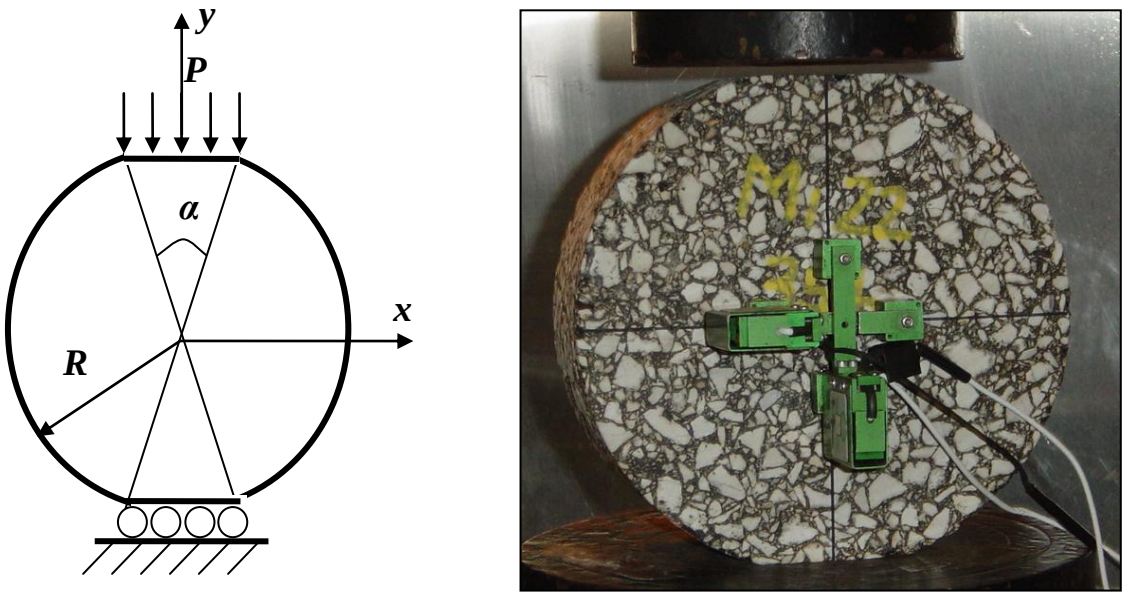

Figure 3-4: Flattened IDT Specimen Geometry (left: Test Schematics; right: Flattened IDT test setup)

A closed-form solution does not appear to exist, which considers the exact specimen geometry and loading condition present in the flattened IDT arrangement. Three-dimensional (3D) viscoelastic FE simulations were employed by Dave et al. [90] in an effort to optimize specimen geometry. The central angle α formed by the flattened faces was utilized to describe the extent of flattening. The stress contours showing vertical stresses (y-Direction) obtained from FE simulations for regular and flattened geometry are shown in Figure 3-5. The ratio of peak compressive stresses under the loading head and the peak tensile stresses near the middle of specimen for varying degree of flattening (angle α) are plotted in Figure 3-6. The first iteration of this study showed that $\alpha = 50°$ provides maximum ratio between the peak tensile stresses and peak compressive stresses. A follow-up study is currently underway to further improve on the flattened IDT geometry by means of laboratory testing of additional samples as well as more FE simulations. The viscoelastic characterizations from the follow-up study are presented later in this chapter.

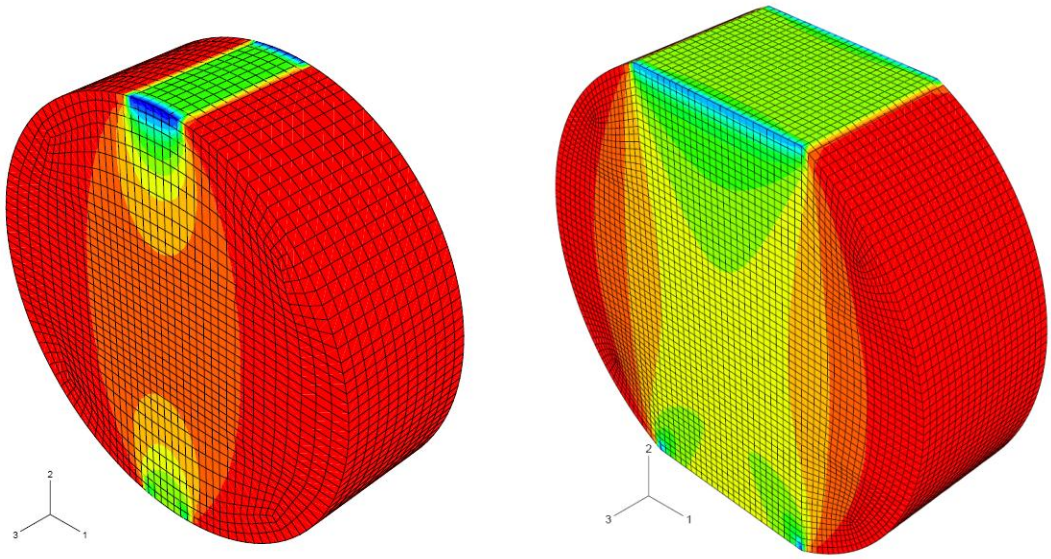

Figure 3-5: Stress Contours in Vertical (y) Direction (left: regular IDT, right: flattened IDT)

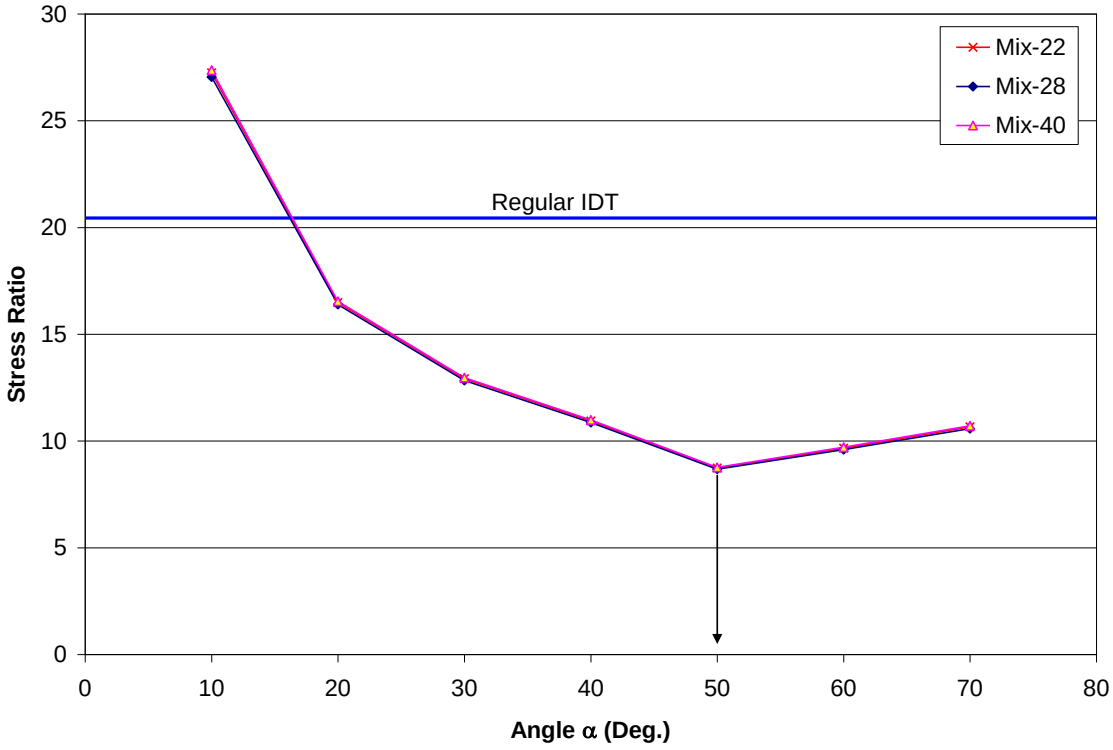

Figure 3-6: Ratio of Peak Compressive and Tensile Stresses

The extraction of viscoelastic properties and tensile strength of material in the current AASHTO T-322 test specifications rely on solution of bi-axial stress states and application of corrections for bulging and gage point rotations as described by Buttlar and Roque [43]. There is scope for improvement to the current analysis procedure due to following factors:

- Current analysis procedure assumes constant Poisson's ratio during the duration of test. Hilton [91] has demonstrated the lack of consistent definition for Poisson's ratio for viscoelastic theories and furthermore shown the significant variation of so called "elastic Poisson's ratio" during the course of creep tests.
- The creep compliance is evaluated for the current analysis procedure with assumption of point load applications and top and bottom of specimen. In other words, the analysis ignores the width of the loaded area.
- In case, the flattened IDT geometry is consistently utilized for determination of tensile strength, it is important to develop analysis procedure for extraction of creep properties for same geometry. This is important as typically same specimens are first tested for viscoelastic characterization through non-destructive creep tests and thereafter for strength tests.

3.3 INDIRECT TENSILE CREEP TEST DATA ANALYSIS

In context of motivations described in the previous section a viscoelastic solution for biaxial indirect tensile creep test is developed and discussed in this section. The elastic solution for the cylindrical diametral compression is presented in first section, the subsequent section extends the elastic solution for viscoelastic problems.

3.3.1 Elastic Solution

For the IDT geometry, an elastic solution has been initially proposed by Hertz [92]. This solution provides the peak tensile and compressive stresses for the specimen loaded with point loads on top and bottom as shown in equation (3.1).

$$\sigma_{tensile} = \frac{2P}{\pi DL}$$
$$\sigma_{compressive} = -\frac{6P}{\pi DL} \tag{3.1}$$

where, P is the imposed load, D is the specimen diameter, and L is the specimen length.

Hondros [93] provided the stress fields for cylindrical bodies in diametral compression (refer to Figure 3-7),

$$\sigma_{xx}(x,0) = \frac{2P\left(-ArcTan\left[\frac{\left(1-\frac{x^2}{R^2}\right)Tan\left(\frac{\alpha}{2}\right)}{1+\frac{x^2}{R^2}}\right]+\frac{\left(1-\frac{x^2}{R^2}\right)Sin(\alpha)}{1+\frac{x^4}{R^4}+\frac{2x^2Cos(\alpha)}{R^2}}\right)}{a\pi L}$$
$$\sigma_{yy}(0,y) = \frac{-2P\left(ArcTan\left[\frac{\left(1+\frac{y^2}{R^2}\right)Tan\left(\frac{\alpha}{2}\right)}{1-\frac{y^2}{R^2}}\right]+\frac{\left(1-\frac{y^2}{R^2}\right)Sin(\alpha)}{1+\frac{y^4}{R^4}-\frac{2y^2Cos(\alpha)}{R^2}}\right)}{a\pi L} \tag{3.2}$$

where, a is the width of loading strip. Using the plane-stress conditions, the elastic stress-strain conditions are written as,

$$\varepsilon_{xx} = \frac{1}{E}\left(\sigma_{xx} - \nu\sigma_{yy}\right)$$
$$\varepsilon_{yy} = \frac{1}{E}\left(\sigma_{yy} - \nu\sigma_{xx}\right) \tag{3.3}$$

For the IDT test setup (c.f. Figure 3-2Figure 3-2) the displacements near the center of specimen are measured by means of clip on extensometer gages. The horizontal and vertical displacements are related to the strains as follows:

$$u_x = \int_{-GL/2}^{GL/2} \varepsilon_{xx}(x,0)dx$$
$$u_y = \int_{-GL/2}^{GL/2} \varepsilon_{yy}(0,y)dy \tag{3.4}$$

Using equations (3.2), (3.3), and (3.4) the displacements are rewritten as,

$$I_1 = \frac{L}{P}\int_{-GL/2}^{GL/2} \sigma_{xx}(x,0)\,dx; \quad I_2 = \frac{L}{P}\int_{-GL/2}^{GL/2} \sigma_{yy}(x,0)\,dx$$
$$I_3 = \frac{L}{P}\int_{-GL/2}^{GL/2} \sigma_{xx}(0,y)\,dy; \quad I_4 = \frac{L}{P}\int_{-GL/2}^{GL/2} \sigma_{yy}(0,y)\,dy \tag{3.5}$$

where, I_j ($j = 1,2,3,4$) are dimensionless factors that depend on specimen geometry and gage length, GL.

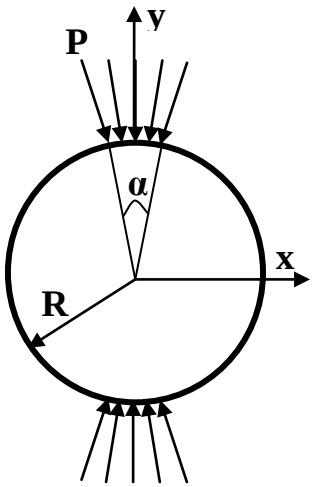

Figure 3-7: Geometry and Boundary Conditions for the Hondros Solution

3.3.2 Viscoelastic Solution

Hondros solution (elastic) could be extended to viscoelastic solution by means of the correspondence principle. Chapter 4 provides in-depth review of the correspondence principle and the theory of viscoelasticity.

The elastic material constants E and ν could be transformed to viscoelastic material quantities, creep compliances $J(t)$ and $M(t)$:

$$E \to \frac{3}{2\,s\,J(s)+s\,M(s)};\quad \nu \to \frac{J(s)-M(s)}{2\,J(s)+M(s)} \tag{3.6}$$

The symbol tilde $(\sim)$ represents the Laplace transformation of time dependent quantities and s is the transformation variable.

Taking Laplace transformation of equation (3.5) and using viscoelastic material quantities (equation (3.6)) provides the viscoelastic solution in Laplace space,

$$u_x(s) = \frac{P(s)}{L}\left[\left(\frac{2}{3}I_1 - \frac{1}{3}I_2\right)s\,J(s) + \left(\frac{1}{3}I_1 + \frac{1}{3}I_2\right)s\,M(s)\right]$$

$$u_y(s) = \frac{P(s)}{L}\left[\left(\frac{2}{3}I_4 - \frac{1}{3}I_3\right)s\,J(s) + \left(\frac{1}{3}I_3 + \frac{1}{3}I_4\right)s\,M(s)\right]$$

Simplifying, (3.7)

$$u_x(s) = \frac{P(s)}{L}\left[K_1\,s\,J(s) + K_2\,s\,M(s)\right]$$

$$u_y(s) = \frac{P(s)}{L}\left[K_3 s\,J(s) + K_4\,s\,M(s)\right]$$

Inverse Laplace transformation provides the viscoelastic solution,

$$\begin{aligned} u_x(t) &= \frac{K_1}{L}\int_0^t P(t-t')\frac{\partial J(t)}{\partial t'}dt' + \frac{K_2}{L}\int_0^t P(t-t')\frac{\partial M(t)}{\partial t'}dt' + \frac{K_1}{L}J_0P(t) + \frac{K_2}{L}M_0\,P(t) \\ u_y(t) &= \frac{K_3}{L}\int_0^t P(t-t')\frac{\partial J(t)}{\partial t'}dt' + \frac{K_4}{L}\int_0^t P(t-t')\frac{\partial M(t)}{\partial t'}dt' + \frac{K_3}{L}J_0P(t) + \frac{K_4}{L}M_0\,P(t) \end{aligned} \tag{3.8}$$

For creep tests, the load is imposed as,

$$P(t) = P_0H(t);\, H(t) = \text{Heavyside Function} \tag{3.9}$$

Using load description, equation (3.9) and solving convolution integrals in equation (3.8), the final relationship between the displacements and material properties are obtained as,

$$\begin{aligned} u_x(t) &= \frac{K_1}{L}P_0\,J(t) + \frac{K_2}{L}P_0\,M(t) \\ u_y(t) &= \frac{K_3}{L}P_0\,J(t) + \frac{K_4}{L}P_0\,M(t) \end{aligned} \tag{3.10}$$

The above shown set of equations could be used in conjunction with statistical methods to extract the creep compliances, $J(t), M(t)$, from the lab measured displacements, $u_x(t), u_y(t)$.

3.4 TESTING AND ANALYSIS

For this study, regular and flattened IDT specimens are tested. Two degrees of flattening, α =35° and 50° is explored at this stage. For comparison, Figure 3-8 shows regular and 50° flattened IDT specimens side-by-side. Notice the metal gage points glued near the center of the specimens, used for mounting the displacement gages.

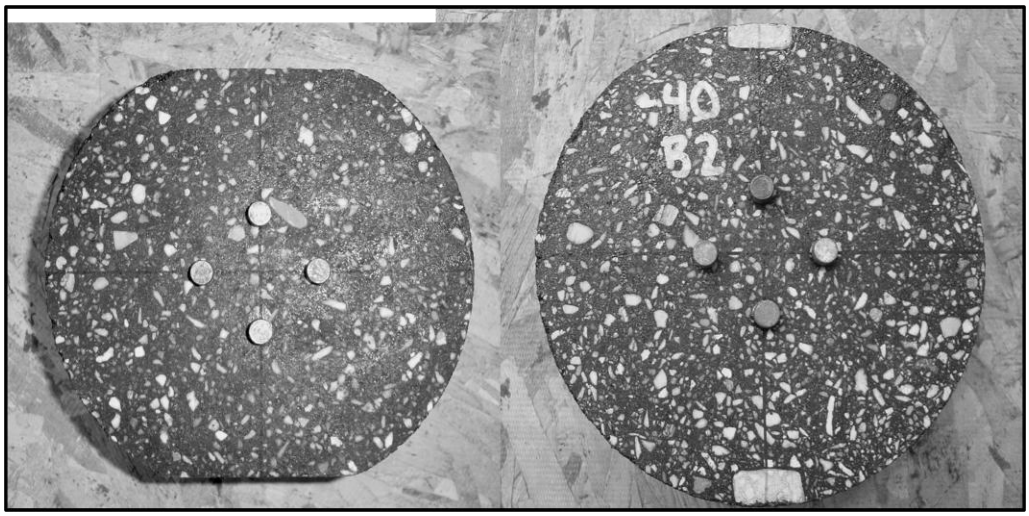

Figure 3-8: 50° Flattened (left) and Standard (right) IDT Test Specimens

The creep tests are performed for 1000 seconds at three test temperatures, 0, -10, and -20°C, following the AASHTO T322 procedure. Three replicates are tested, with displacement gages mounted in both horizontal and vertical directions on specimen faces. Compliances are calculated using the viscoelastic solution outlined in previous section, and time-temperature superposition is performed to generate creep-compliance master curves. Finally, a generalized Kelvin model is fit to the master-curve.

3.4.1 Material Details

The first step in the experimental plan is the selection and testing of three HMA mixtures in the regular IDT configuration. The three HMA mixtures are chosen in an attempt to elicit differing amounts of crushing failure, which is thought to be related to maximum aggregate size and binder stiffness. Therefore, one mixture is designed to have a large aggregate structure and is combined with a relatively stiff asphalt binder. It is anticipated that this mixture, labeled Mix-22, will not exhibit significant crushing during strength testing in the AASHTO T322 IDT test. The second mixture is designed to have a small aggregate structure and a semi-stiff binder. It is anticipated that this mixture, termed Mix-28, will experience a moderate level of crushing during the regular IDT strength test. The third mixture used a small aggregate structure with a soft binder. It is anticipated that this mixture, labeled Mix-40, will experience significant crushing during the regular IDT test. Table 3.1 and Table 3.2 summarize aggregate and binder characteristics for the three mixes used in this study.

Table 3.1: Aggregate Structure

	Nominal Maximum Aggregate Size	Aggregate Structure
Mix-22	9.5 mm	Large
Mix-28	4.75 mm	Small
Mix-40	4.75 mm	Small

Table 3.2: Binder Characteristics

	Binder Type	Binder Characteristics
Mix-22	PG64-22	Stiff
Mix-28	PG58-28	Semi-Stiff
Mix-40	PG58-40	Soft

3.4.2 Data Analysis

The AASHTO procedure describes the limit for linearity criteria of asphalt concrete as 500 microstrains. More recent work by Airey and Rahimzadeh [94] and Masad and Papagiannakis [95] suggest a linear viscoelastic limit for asphalt mixtures as low as 100 microstrains. These criteria were visited during the data analysis, since the validity of elastic-viscoelastic correspondence principle is limited to linear viscoelastic conditions. Test results for Mix-22 and Mix-28 showed that the peak strain response near the center of the test specimens were limited to 100-microstrains or lower in most instances. For tests performed at 0°C at very long loading times (> 500 seconds) a level of 200 microstrains was reached. In the case of Mix-40, the strains exceeded 500 microstrains at a test temperature of 0°C. As the test data obtained for Mix-40 at 0°C was beyond the range of linearity, it was excluded from further analysis.

3.4.3 Results

The creep compliance master-curves for Mix-22, Mix-28 and Mix-40 are presented in Figure 3-9, Figure 3-10, and Figure 3-11 respectively. Note that the markers represent the test data and the lines represent the generalized Kelvin model representing the mastercurve. All mastercurves are plotted at a reference temperature of -20°C.

The creep compliances from regular rand flattened IDT are also placed on unity plots, as shown in Figure 3-12, Figure 3-13, and Figure 3-14. In general, good agreement was found between the two testing approaches, suggesting that the flattened IDT arrangement may be a viable alternative to the standard IDT testing arrangement described in AASHTO T-332. Notice that the flattened IDT results for Mix-22 with $\alpha =$ 35° show significant deviation from regular and the 50° flattened tests. The extent of deviation for this set of results make them suspect and at this point further testing is needed to verify the results. The results for other two mixtures indicate that the 35° flattened IDT yields results closer to regular IDT and the degree of variation is within anticipated experimental variation.

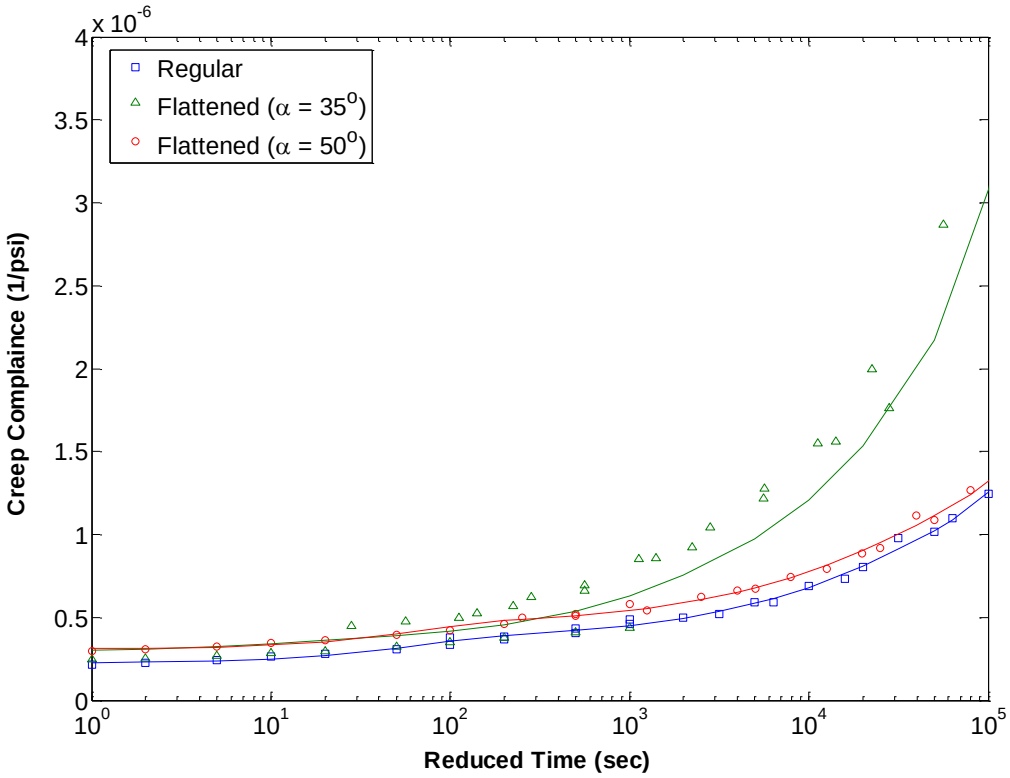

Figure 3-9: Mix-22 Creep Compliance Mastercurve (reference temperature = -20°C)

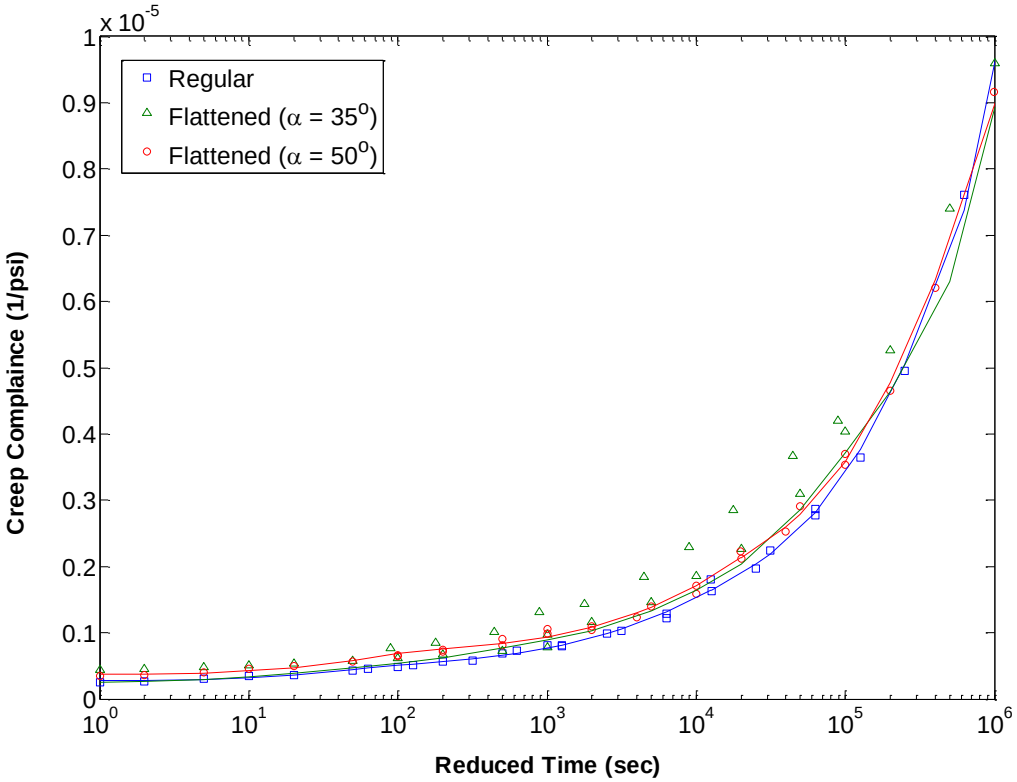

Figure 3-10: Mix-28 Creep Compliance Mastercurve (reference temperature = -20°C)

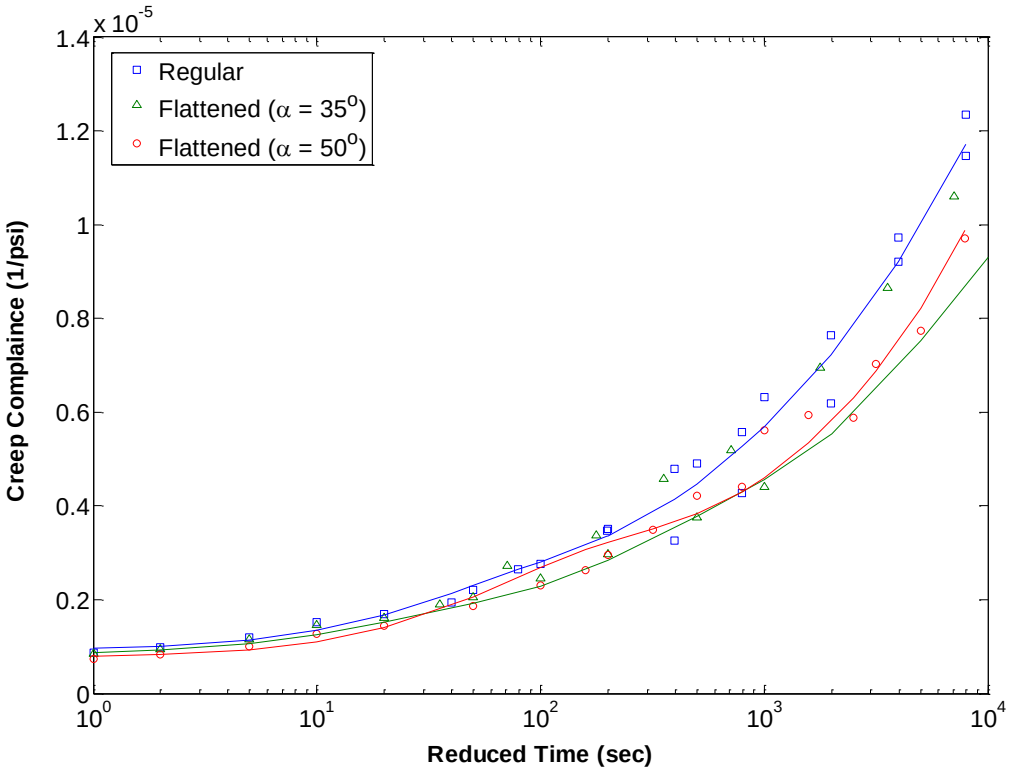

Figure 3-11: Mix-40 Creep Compliance Mastercurve (reference temperature = -20°C)

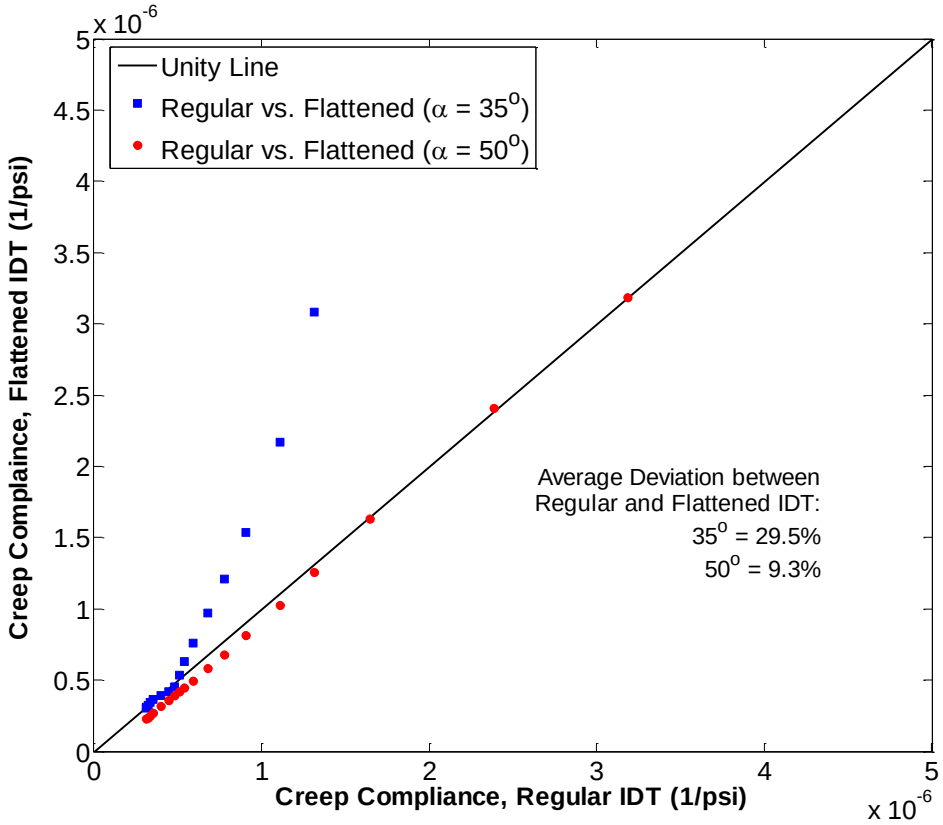

Figure 3-12: Comparison of Mix-22 Regular and Flattened Creep Compliances

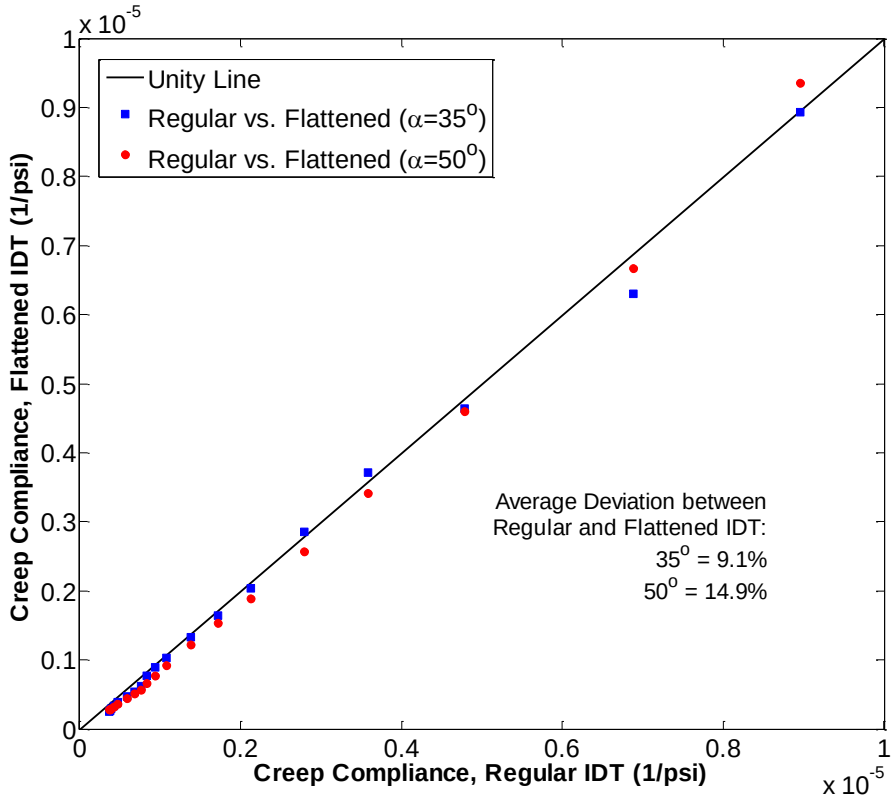

Figure 3-13: Comparison of Mix-28 Regular and Flattened Creep Compliances

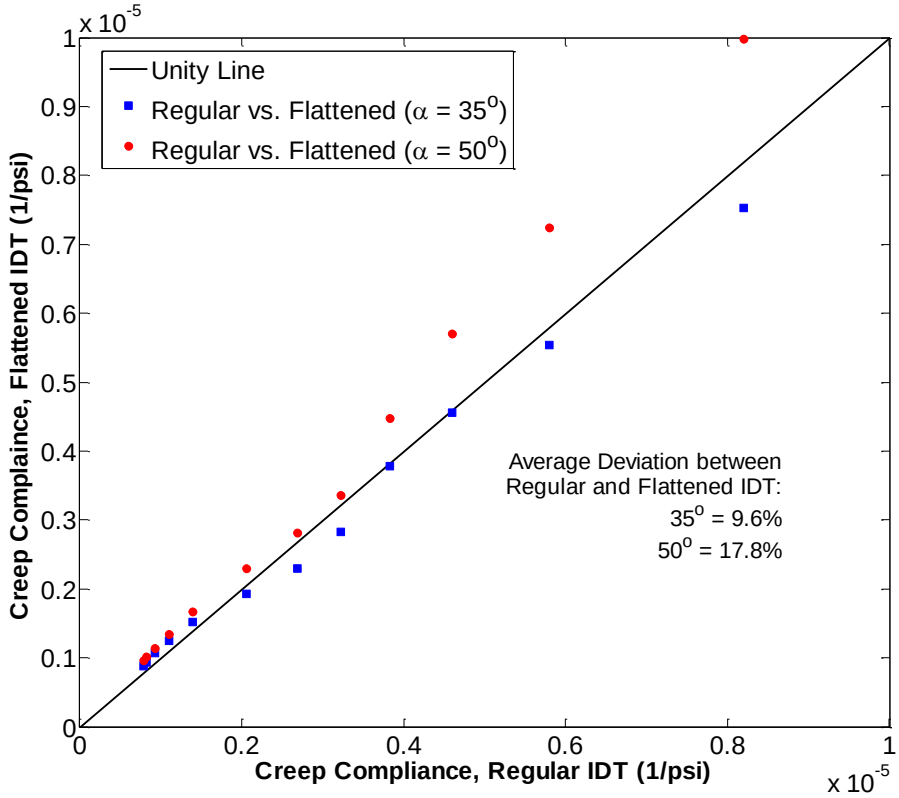

Figure 3-14: Comparison of Mix-40 Regular and Flattened Creep Compliances

More work is currently underway to further develop and validate this method. It is hoped that through improved analysis and addition experimental validation, the flattened IDT arrangement will serve as a versatile test for obtaining creep compliance and tensile strength of a broad range of asphalt-aggregate mixtures.

3.5 SUMMARY

Creep testing of three asphalt concrete mixtures is performed using the AASHTO T322 test protocol on regular cylindrical test specimens as well as for the flattened geometry. The Hondros solution is extended for viscoelastic problem through use of correspondence principle. Test data is analyzed for both configurations based on the extension of Hondros solution. For analysis of the flattened IDT geometry, it was assumed that the Hondros solution will provide enough accuracy to assess the feasibility of the proposed testing configuration.

Comparison of regular and flattened IDT results shows variations ranging from 9% to 32%. The 32% variation is for the Mix-22 with 35° flattened IDT, the significant variation between this set and the regular and 50° flattened IDT tests are considered suspect at this point and further testing is necessary. Apart from this one set, the range of variation between regular and 35° flattened IDT is between 9.1 and 9.6%. For 50° flattened IDT the range of variation from regular IDT is 9.3 to 17.8%. These ranges of variability are well within the typical testing variability for the creep tests on asphalt concrete. The sources of variation between the creep compliances determined from regular and flattened IDT specimens could include the assumptions made in the data analysis, e.g., the applicability of the Hondros solution for the flattened geometry, as well as testing and measurement variability associated with testing of asphalt mixtures with relatively small specimen dimensions.

Based on this limited study it can be inferred that the flattened IDT geometry may be a viable alternative to the current AASHTO procedure for low temperature viscoelastic characterization of asphalt concrete material, and especially advantageous when indirect

tensile strength testing is required. A follow up study is currently underway to further optimize the extent of flattening [96].

CHAPTER 4 – FUNCTIONALLY GRADED VISCOELASTIC FINITE ELEMENT ANALYSIS USING CORRESPONDENCE PRINCIPLE

4.1 INTRODUCTION

This chapter discusses the basic viscoelastic constitutive relationships, limitations of correspondence principle in regard with material non-homogeneity, finite-element formulation using correspondence principle, numerical integral transforms, implementation and verification, and examples showing comparison with the layered approach.

4.2 VISCOELASTIC CONSTITUTIVE RELATIONSHIPS

The basic stress-strain relationships for viscoelastic materials have been presented by, among other authors, Hilton [97] and Christensen [98]. The constitutive relationship for quasi-static, linear viscoelastic isotropic materials is given as:

$$\begin{aligned}\sigma_{ij}(x,t) = 2\int_{t'=-\infty}^{t'=t} G\left(x,\xi(t)-\xi(t')\right)\left(\varepsilon_{ij}(x,t')-\frac{1}{3}\delta_{ij}\varepsilon_{kk}\right)dt' \\ + \int_{t'=-\infty}^{t'=t} K\left(x,\xi(t)-\xi(t')\right)\delta_{ij}\varepsilon_{kk}\,dt'\end{aligned} \tag{4.1}$$

where σ_{ij} are stresses, ε_{ij} are strains at any location x. The parameters G and K are the shear and bulk relaxation moduli, δ_{ij} is the Kronecker delta, and t' is the integration variable. Subscripts $(i, j, k, l = 1, 2, 3)$ follow Einstein's summation convention. The reduced time ξ is related to real time t and temperature T through the time-temperature superposition principle:

$$\xi(t) = \int_0^t a\left(T\left(t'\right)\right)dt' \tag{4.2}$$

For a non-homogeneous viscoelastic body in quasi-static condition, assume a boundary value problem with displacement u_i on volume Ω_u, traction P_i on surface Ω_σ and body force F_i, the equilibrium and strain-displacement relationships (for small deformations) are as shown in Equation (4.3),

$$\sigma_{ij,j} + F_i = 0, \;\; \varepsilon_{ij} = \frac{1}{2}\left(u_{i,j} + u_{j,i}\right) \tag{4.3}$$

repectively, where, u_i is displacement and $\left(\bullet\right)_{,j} = \partial\left(\bullet\right)/\partial x_j$.

4.3 ELASTIC-VISCOELASTIC CORRESPONDENCE PRINCIPLE (CP)

4.3.1 Introduction

The concept of equivalency between transformed viscoelastic and elastic boundary value problems can be found in Read [99]. This technique been extensively utilized by researchers to analyze variety of non-homogeneous viscoelastic problems including, but not limited to, beam theory [68], finite-element analysis [100], and boundary element analysis [70].

Using correspondence principle one obtains the Laplace transform of the stress-strain relationship described in Equation (4.1) as,

$$\sigma_{ij}\left(x,s\right) = 2G\left(x,\tilde{\xi}\left(s\right)\right)\varepsilon_{ij}\left(x,s\right) + K\left(x,\tilde{\xi}\left(s\right)\right)\delta_{ij}\,\varepsilon_{kk}\left(x,s\right) \tag{4.4}$$

where s is the transformation variable and the symbol tilde (~) on top of the variables represents transformed variable. The Laplace transform of any function $f\left(t\right)$ is given by,

$$L\left[\, f\left(t\right)\right] = \tilde{f}\left(s\right) = \int_0^\infty f\left(t\right) Exp\left[-st\right]dt \tag{4.5}$$

Equilibrium (Equation (4.3)) for the boundary value problem in the transformed form becomes,

$$\begin{aligned}\tilde{\sigma}_{,j}(x,s) = 2\tilde{G}(x,s)\tilde{\varepsilon}_{,j}{}^{d}(x,s) + 2\tilde{G}_{,j}(x,s)\tilde{\varepsilon}^{d}(x,s) \\ + \tilde{K}(x,s)\tilde{\varepsilon}_{,j}(x,s) + \tilde{K}_{,j}(x,s)\tilde{\varepsilon}(x,s)\end{aligned} \tag{4.6}$$

where superscript d indicates the deviatoric component of the quantities.

Notice that the transformed equilibrium equation for a non-homogeneous viscoelastic problem has identical form as an elastic non-homogeneous boundary value problem.

4.3.2 Limitation of CP for Non-Homogeneous Viscoelastic Problems

Mukherjee and Paulino [73] demonstrated the limitation and inapplicability of correspondence principle for certain class of non-homogeneous viscoelastic material models. They have broadly classified the non-homogeneous viscoelastic materials into two categories based on the structure of constitutive models: (a) Separable models, and (b) Inseparable models.

Separable Model: The separable models are characterized by their time and space dependent portions; whereas the material parameters have either spatial or time dependence, but not both. In essence the functional form for these types of models would be as follows:

$$G(x,t) = G(x)\, f(t) \tag{4.7}$$

Inseparable Model: The inseparable models have material parameters that are simultaneously dependent on both space and time. Thus the separation of the constitutive properties as shown in Equation (4.7) is not possible.

Paulino and Jin [72] and Mukherjee and Paulino [73] concluded that in order for successful application of CP following equivalencies must exist:

Elastic Formulation ≡ Transformed Viscoelastic Formulation

$$G(x) \equiv s\tilde{G}(x,s); K(x) \equiv s\tilde{K}(x,s); \qquad (4.8)$$
$$G_{,i}(x) \equiv s\tilde{G}_{,i}(x,s); K_{,i}(x) \equiv s\tilde{K}_{,i}(x,s)$$

In case of separable models due to separation of the spatial and time dependent parts, equivalency is established between the elastic terms $G_{,i}(x), K_{,i}(x)$ and transformed viscoelastic terms $G_{,i}(x)\tilde{f}(s), K_{,i}(x)\tilde{g}(s)$. However the equivalency in-general is inconsistent in case of inseparable class of models because the spatial dependence of $G_{,i}(x)$ and/or $K_{,i}(x)$ could be quite different from that of $\tilde{G}_{,i}(x,s)$ and/or $\tilde{K}_{,i}(x,s)$.

4.3.3 CP for Non-Separable Models

The restrictions and failure of correspondence principle shown by Paulino and Jin [72] and Mukherjee and Paulino [73] are too strict and can be relaxed to some extent. Christensen [98] briefly mentioned this by explaining that for using transformation method, while using inertia terms, the equivalency could still be established however, in this case the equivalency is not between elastic solution and transformed viscoelastic solution, but it is between transformed elastic solution and transformed viscoelastic solution. Recently, Khazanovich [79] showed correspondence between elastic solutions and operator-transformed viscoelastic problems using Volterra operators in conjunction with Laplace transforms. This modified transformation allows the correspondence principle to be valid for broader types of functionally graded viscoelastic material models. Hilton [101] also discussed that the conditions on separable model can be relaxed.

The use of CP for inseparable models can be demonstrated by redefining the elastic constants as $G(x,s)$ and $K(x,s)$ instead of $G(x)$ and $K(x)$. Thus the equivalencies shown in Equation (4.8) is now be described as,

Elastic Formulation ≡ Transformed Viscoelastic Formulation

$$G(x,s) \equiv s\tilde{G}(x,s); K(x,s) \equiv s\tilde{K}(x,s); \qquad (4.9)$$
$$G_{,i}(x,s) \equiv s\tilde{G}_{,i}(x,s); K_{,i}(x,s) \equiv s\tilde{K}_{,i}(x,s)$$

In light of these equivalencies the definitions for separable and inseparable models could changed, whereby for a series type model, say generalized Maxwell model, the separable and inseparable forms of relaxation functions are given as shown below [101].

Separable Form:

$$G(x,t)=\sum_{h=1}^{n}G_h(x)Exp\left[-\frac{t}{\tau_h(x)}\right] \tag{4.10}$$

Inseparable Form:

$$G(x,t)=\sum_{h=1}^{n}G_h(x)Exp\left[-\frac{t}{\tau_h(x,t)}\right] \tag{4.11}$$

Using the above shown revised separable and inseparable forms of generalized Maxwell model the failure of CP for the inseparable model can be shown. The material non-homogeneity is assumed to have exponential variation with space. The relaxation moduli for these models are assumed to have following forms.

Separable Model:

$$E(x,t)=\sum_{h=1}^{n}E_h(x)Exp\left[-\frac{t}{\tau_h(x)}\right]=\sum_{h=1}^{n}E_h(x)Exp\left[-g_h(x)t\right] \tag{4.12}$$

where, dashpot relaxation time, $\tau_h(x)=1/g_h(x)=\eta_h(x)/E_h(x)$; spring coefficient, $E_h(x)=E_hExp[a_hx]$; and dashpot viscosity, $\eta_h(x)=\eta_hExp[a_hx]$

Inseparable Model:

$$E(x,t)=\sum_{h=1}^{n}E_h(x)Exp\left[-\frac{t}{\tau_h(x,t)}\right]=\sum_{h=1}^{n}E_h(x)Exp\left[-g_h(x,t)t\right] \tag{4.13}$$

where, dashpot relaxation time, $\tau_h(x,t)=1/g_h(x,t)=\eta_h(x,t)/E_h(x)$; E_h,η_h and a_h are the material properties and $f(t)$ is any function of time. The length scale of inhomogeneity is $1/a_h$.

In order to evaluate the equivalencies (Equation (4.9)) $\tilde{E}(x,s)$ and $\tilde{E}_{,i}(x,s)$ for each of the above shown models is evaluated.

Separable model,

$$\tilde{E}(x,s)=\sum_{h=1}^{n}\frac{E_h(x)}{s+g_h(x)} \tag{4.14}$$

$$\tilde{E}_{,i}(x,s)=\sum_{h=1}^{n}\left[\frac{\left(E_h(x)\right)_{,i}}{s+g_h(x)}-\frac{E_h(x)\left(g_h(x)\right)_{,i}}{\left(s+g_h(x)\right)^2}\right] \tag{4.15}$$

Inverse Laplace transform of Equation (4.15) yields,

$$E_{,i}(x,t)=\sum_{h=1}^{n}\left(E_h(x)\right)_{,i}Exp\left[-g(x)t\right]-E_h(x)\left(g_h(x)\right)_{,i}tExp\left[-g(x)t\right]=\frac{\partial}{\partial x}E(x,t) \tag{4.16}$$

Inseparable model, assume that $f(t)=t$,

$$\tilde{E}(x,s)=\sum_{h=1}^{n}\frac{E(x)}{\sqrt{g_h(x)}}Exp\left[\frac{s^2}{4g_h(x)}\right]\int_0^{\frac{s}{2\sqrt{g_h(x)}}}Exp\left[-t^2\right]dt \tag{4.17}$$

As seen from equation (4.17) for an inseparable model where the dashpot properties have a very simple dependence on time $\left(f(t)=t\right)$ the analytical Laplace transform is non-existent, leading to non-applicability of CP. Notice that the failure is imposed purely in form of mathematical limitations. In case of the separable model, the CP can be applied by using revised equivalencies from equation (4.9) and the transformed viscoelastic quantities from equations (4.14) and (4.16).

4.4 SELECTION OF MATERIAL MODEL

For the research proposed in this study the Prony series models (Generalized Maxwell model) was selected to represent constitutive relationship of asphalt concrete. The selection of Prony series model was based on following factors.

4.4.1 Applicability to Material

Prony series models have been used most extensively to represent the viscoelastic material behavior of asphalt concrete at low and moderate temperatures. Buttlar et al. [43] showed that the Prony series models provide very good fit to the laboratory test data. A number of studies conducted at University of Illinois and elsewhere over the period of last decade have further reinforced the applicability of Prony series models to asphalt concrete properties [11, 16, 43].

4.4.2 Flexibility of Model

Prony series models are highly flexible in the sense that they are capable of capturing a range of viscoelastic materials due to their series type of structure. Hence depending on the complexity of material behavior the number of material parameters can be adjusted. In case of asphalt concrete it is common practice to use ten parameters (Example, Five unit generalized Maxwell model) as this many parameters have shown to capture the material properties. The use of highly customized model that may only be applicable to asphalt concrete type material was also non-preferable as the applications of the current research are not limited to field of asphalt concrete.

4.4.3 Compatibility with Current Research

As described earlier the goal of this research is to develop graded viscoelastic finite-element analysis formulation using both correspondence principle and time-integration schemes. It is important to choose a model that is compatible with this proposed research, for example the sigmoidal model may not be the model of choice while using correspondence principle, as the analytical Laplace transform of the model involves higher order mathematics.

4.4.4 Other Factors

In addition to the factors discussed above other reasons for using Prony series models include:

- Access to extensive data base of Prony series parameters for various asphalt concrete types (binder grades, aggregate types, aging levels, mix types etc.) within the research group of author.
- Availability of Prony series models in commercial software such as *ABAQUS* that is useful to verify the implementation as well as allow for future customizations.
- Familiarity of author with use of this type of model.

4.5 VISCOELASTIC FGM FINITE ELEMENT FORMULATION

The derivation of finite element formulations using variational principle is described by many authors, including in textbooks by Cook et al. [102] and Reddy [103]. The variational principle for quasi-static linear viscoelastic materials under isothermal conditions can be found in Gurtin [104]. Taylor et al. [105] extended it for thermo-viscoelastic boundary value problem,

$$\begin{aligned}\pi = &\int_{\Omega_u}\int_{t'=-\infty}^{t'=t}\int_{t''=-\infty}^{t''=t-t'}\frac{1}{2}C_{ijkl}\left[x,\xi_{ijkl}\left(t-t''\right)-\xi'_{ijkl}\left(t'\right)\right]\frac{\partial\varepsilon_{ij}\left(x,t'\right)}{\partial t'}\frac{\partial\varepsilon_{kl}\left(x,t''\right)}{\partial t''}dt'\,dt''\,d\Omega_u \\ &-\int_{\Omega_u}\int_{t'=-\infty}^{t'=t}\int_{t''=-\infty}^{t''=t-t'}C_{ijkl}\left[x,\xi_{ijkl}\left(t-t''\right)-\xi'_{ijkl}\left(t'\right)\right]\frac{\partial\varepsilon^{*}{}_{ij}\left(x,t'\right)}{\partial t'}\frac{\partial\varepsilon^{*}{}_{kl}\left(x,t''\right)}{\partial t''}dt'\,dt''\,d\Omega_u \\ &-\int_{\Omega_\sigma}\int_{t''=-\infty}^{t''=t}P_i\left(x,t-t''\right)\frac{\partial u_i\left(x,t''\right)}{\partial t''}dt''\,d\Omega_\sigma = 0\end{aligned} \quad (4.18)$$

where Ω_u is the volume of body, Ω_σ is the surface on which tractions P_i are prescribed, u_i are the displacements and C_{ijkl} are space and time dependent material constitutive properties, ε_{ij} are the mechanical strains and ε^{*}_{ij} are the thermal strains while ξ_{ijkl} is the reduced time related to real time t and temperature T through time-temperature superposition principle of equation (4.2). The first variation provides the basis for the FE formulation,

$$\delta\pi = \int_{\Omega_u} \int_{t'=-\infty}^{t'=t} \int_{t''=-\infty}^{t''=t-t'} \left\{ \begin{array}{l} C_{ijkl}\left[x, \xi_{ijkl}\left(t-t''\right) - \xi'_{ijkl}\left(t'\right)\right] \\ \dfrac{\partial}{\partial t'}\left(\varepsilon_{ij}\left(x,t'\right) - \varepsilon^{*}{}_{ij}\left(x,t'\right)\right)\dfrac{\partial \delta\varepsilon_{kl}\left(x,t''\right)}{\partial t''} \end{array} \right\} dt'\, dt''\, d\Omega_u$$
$$- \int_{\Omega_\sigma} \int_{t''=-\infty}^{t''=t} P_i\left(x, t-t''\right)\frac{\partial \delta u_i\left(x,t''\right)}{\partial t''} dt''\, d\Omega_\sigma = 0 \tag{4.19}$$

The element displacement vector u_i is related to nodal displacement degrees of freedom q through the shape functions N_{ij},

$$u_i\left(x,t\right) = N_{ij}\left(x\right) q_j\left(t\right) \tag{4.20}$$

Differentiation of equation (4.20) yields the relationship between strain ε_i and nodal displacements q_i and derivatives of shape functions B_{ij},

$$\varepsilon_i\left(x,t\right) = B_{ij}\left(x\right) q_j\left(t\right) \tag{4.21}$$

Equations (4.19), (4.20) and (4.21) provides the equilibrium equation for each finite element,

$$\int_0^t k_{ij}\left(x, \xi\left(t\right) - \xi\left(t'\right)\right)\frac{\partial q_j\left(t'\right)}{\partial t'} dt' = f_i\left(x,t\right) + f_i^{th}\left(x,t\right) \tag{4.22}$$

where k_{ij} is the element stiffness matrix, f_i is the mechanical force vector and $f^{th}{}_i$ is the thermal force vector, which are described as follows

$$k_{ij}\left(x,t\right) = \int_{\Omega_u} B_{ik}^T\left(x\right) C_{kl}\left(x, \xi\left(t\right)\right) B_{lj}\left(x\right) d\Omega_u \tag{4.23}$$

$$f_i\left(x,t\right) = \int_{\Omega_\sigma} N_{ij}\left(x\right) P_j\left(x,t\right) d\Omega_\sigma \tag{4.24}$$

$$f_i^{th}\left(x,t\right) = \int_{\Omega_u} \int_{-\infty}^{t} B_{ik}\left(x\right) C_{kl}\left(x, \xi(t) - \xi\left(t'\right)\right)\frac{\partial \varepsilon^{*}{}_l\left(x,t'\right)}{\partial t'} dt'\, d\Omega_u \tag{4.25}$$

$$\varepsilon^{*}{}_{l}\left(x,t\right)=\alpha\left(x\right)\Delta_{T}\left(x,t\right) \tag{4.26}$$

where α is the coefficient of thermal expansion and Δ_T is the temperature change with respect to initial conditions.

On assembly of the individual finite element contributions for the given problem domain, the global equilibrium equation can be obtained as,

$$\int_{0}^{t} K_{ij}\left(x,\xi\left(t\right)-\xi\left(t^{'}\right)\right)\frac{\partial u_{j}\left(t^{'}\right)}{\partial t^{'}}dt^{'}=F_{i}\left(x,t\right)+F_{i}^{th}\left(x,t\right) \tag{4.27}$$

where K_{ij} is the global stiffness matrix, U_i is the global displacement vector and F_i and $F^{th}{}_{i}$ are the global mechanical and thermal force vectors respectively. The solution to the problem requires solving the convolution shown above to determine nodal displacements.

Hilton and Yi [100] have utilized the CP-based procedure for implementing the FE formulation. However the previous research efforts were limited to use of conventional finite elements, while in the current dissertation graded finite elements have been utilized to efficiently and accurately capture the effects of material non-homogeneities. Graded elements with GIF (described in Chapter 2) are used herein.

Using the elastic-viscoelastic CP, the functionally graded viscoelastic finite element problem could be deduced to have a functional form similar to that of elastic problems. Laplace transform of the global equilibrium shown in equation (4.27) is,

$$\tilde{K}_{ij}\left(x,s\right)\tilde{u}_{j}\left(s\right)=\tilde{F}_{i}\left(x,s\right)+\tilde{F}_{i}^{th}\left(x,s\right) \tag{4.28}$$

Notice that the Laplace transform of hereditary integral (equation (4.27)) led to an algebraic relationship (equation (4.28)), this is major benefit of using CP as the direct integration for solving hereditary integrals will have significant computational cost. As discussed in a previous section, the applicability of correspondence principle for viscoelastic FGMs imposes limitations on functional form of constitutive model. With this knowledge it is possible to further customize the finite-element formulation for the generalized Maxwell model. Material constitutive properties for generalized Maxwell model is given as,

$$C_{ij}(x,t) = \sum_{h=1}^{n} \left(C_{ij}(x) \right)_h Exp\left[-\frac{t}{\left(\tau_{ij}\right)_h} \right] \quad \text{(no sum)} \tag{4.29}$$

where $\left(C_{ij}\right)_h$ are the elastic contributions (spring coefficients) and $\left(\tau_{ij}\right)_h$ are the viscous contributions from individual Maxwell units, commonly called relaxation times.

For the generalized Maxwell model, the global stiffness matrix K of the system can be re-written as,

$$K_{ij}(x,t) = K_{ij}^{0}(x) Exp\left(-\frac{t}{\tau_{ij}} \right) = K_{ij}^{0}(x) K_{ij}^{t}(t) \quad \text{(no sum)} \tag{4.30}$$

where K^{0}_{ij} is elastic contribution of stiffness matrix and K^{t} is the time dependent portion.

Using (4.28) and (4.30) the problem description can be summarized as,

$$K_{ij}^{0}(x) \tilde{K}_{ij}^{t}(s) \tilde{U}_{j}(s) = \tilde{F}_{i}(x,s) + \tilde{F}_{i}^{th}(x,s) \quad \text{(no sum)} \tag{4.31}$$

4.6 FINITE ELEMENT IMPLEMENTATION

The finite-element formulation described in a previous section is implemented for solving two dimensional plane and axisymmetric problems. The implementation is coded in the commercially available software *Matlab*®. Primary reason for selection of *Matlab*® is the availability of in-built robust equation solver and ease of programming. The code is provided in the Appendix-A. The implementation of the analysis code is divided into five major steps as shown in Figure 4-1.

.

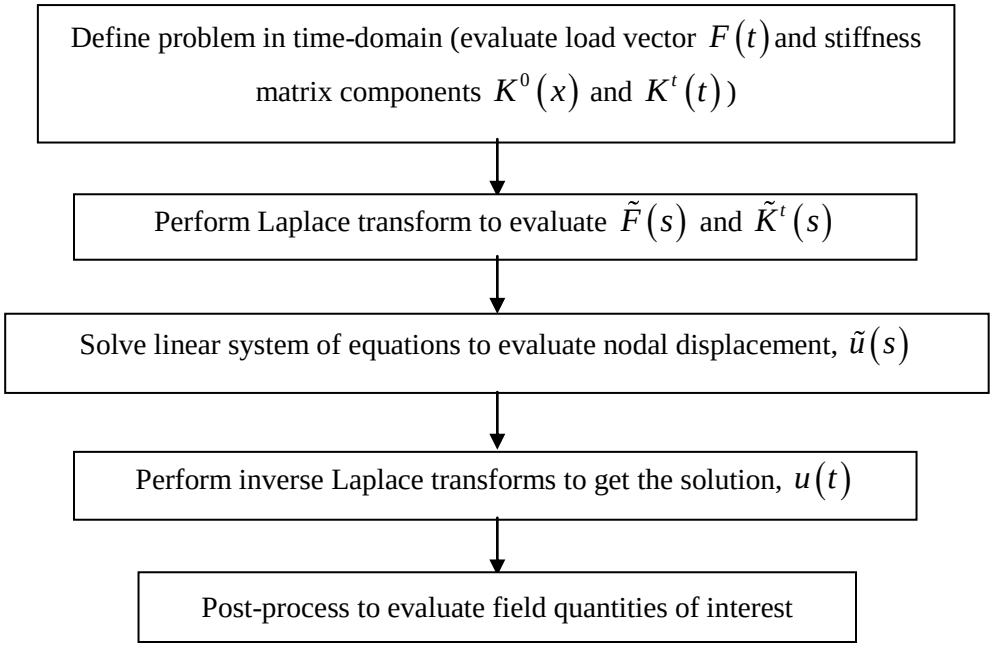

Figure 4-1: Outline of Finite Element Analysis Procedure

4.6.1 Numerical Integral Transform

For the generalized Maxwell model the Laplace transform of the time-dependent portion of stiffness matrix, $K_{ij}^t(t)$ is directly (and exactly) determined using the analytical transform (equation (4.32)).

$$\tilde{K}_{ij}^t(s) = \sum_{h=1}^{n} \frac{(\tau_{ij})_h}{(\tau_{ij})_h s + 1} \tag{4.32}$$

In the current implementation the Laplace transform of quantities other than stiffness matrix are performed using trapezoidal rule with assumption that the quantities are piecewise linear functions of time. Thus, for a given time dependent function $F(t)$, the Laplace transform $\tilde{F}(s)$ is estimated as,

$$\tilde{F}(s) = \sum_{i=1}^{N-1} \frac{1}{s^2 \Delta t} \left\{ \begin{array}{l} s\Delta t \left(F(t_i) Exp[-st_i] - F(t_{i+1}) Exp[-st_{i+1}] \right) \\ + \Delta F \left(Exp[-st_i] - Exp[-st_{i+1}] \right) \end{array} \right\} \tag{4.33}$$

where Δt is the time increment, N is total number of increments and ΔF is the change in function F for the given increment.

The inverse Laplace transform is of greater importance in the current problem as the problem is ill posed due to absence of function description on the imaginary plane. Several researchers have extensively studied this problem and proposed numerical techniques for numerical Laplace inversion. In general the methods are proposed for the set of problems where they provide most reliable results; hence it is important to select a technique that suits well to the problem at hand. Narayanan and Beskos [106, 107] have provided comprehensive comparison of various numerical inversion techniques. In case of boundary integral methods researchers have preferred use of Stehfest algorithm [108, 109] however in case of finite-element simulations this method could prove quite expensive and also distributes the evaluated functions over both real and imaginary portions of time domain. In the current study three numerical inversion techniques are studied, fast fourier transform (FFT) based method proposed by Durbin [110], Weeks' method based on Laguerre functions [111, 112] and collocation method proposed by Schapery [113, 114]. The key motivation for using FFT based inversion technique is the availability of FFT algorithm in *Matlab*®. The other two methods are selected based on recommendations from Narayanan and Beskos [106, 107] and Yi [115].

Initial trials for different functions of time (linear, exponential, logarithmic and power) are used as test functions to evaluate the suitability of each of the inversion techniques. The preliminary results indicate that the collocation method is the most efficient in sense of available accuracy for the cost of computation. The Weeks' method is the second best option and the FFT based algorithm is the last choice. FFT based algorithms are in general preferable for oscillatory type of time functions and hence for the selected test functions they did not perform well. Another benefit to using collocation method is its flexibility in making selection of the inversion parameters.

The approximate inverse transform of function $\tilde{f}(s)$ in collocation method is given by following series form,

$$f(t) = \sum_{i=1}^{n} g_i Exp[-\alpha_i t] \tag{4.34}$$

where g_i is related to $\tilde{f}(s)$ through,

$$s\,\tilde{f}(s) = \sum_{j=1}^{n} g_i \left(1 + \frac{\alpha_j}{\alpha_i}\right)^{-1} \quad (i = 1, 2, \cdots, n) \tag{4.35}$$

It is apparent from equations (4.34) and (4.35) that the selection of appropriate function for parameter α is critical. Cost and Becker [116] have shown that α should be selected in such a way that the exponential function shown in equation (4.34) is centered at the desired location on the $\log t$ scale. While Schapery [117] recommended selection of α that are centered at any point on $\log s$ scale. A functional form for α is determined by combining the recommendations by Schapery [117] (Exponential term) and Cost and Becker [116] (Power term).

$$\alpha_i = iExp\left[\frac{s}{a}\right] + (n-i)10^{a+\frac{ib}{n}} \tag{4.36}$$

where a and b depend on region of interest on the $\log t$ scale and other symbols are same as those shown in previous equations.

For the current implementation the numerical inverse transform is compared with exact inversion using generalized Maxwell model (c.f. equation (4.29)) as the test function. The results, shown in Figure 4-2, compare the exact analytical inversion with the numerical inversion results. The numerical inversion was carried out using 20 and 100 collocation points. With 20 collocation points the average relative error in the numerical estimate is 2.7%, whereas with 100 collocation points, the numerical estimate approaches the exact inversion.

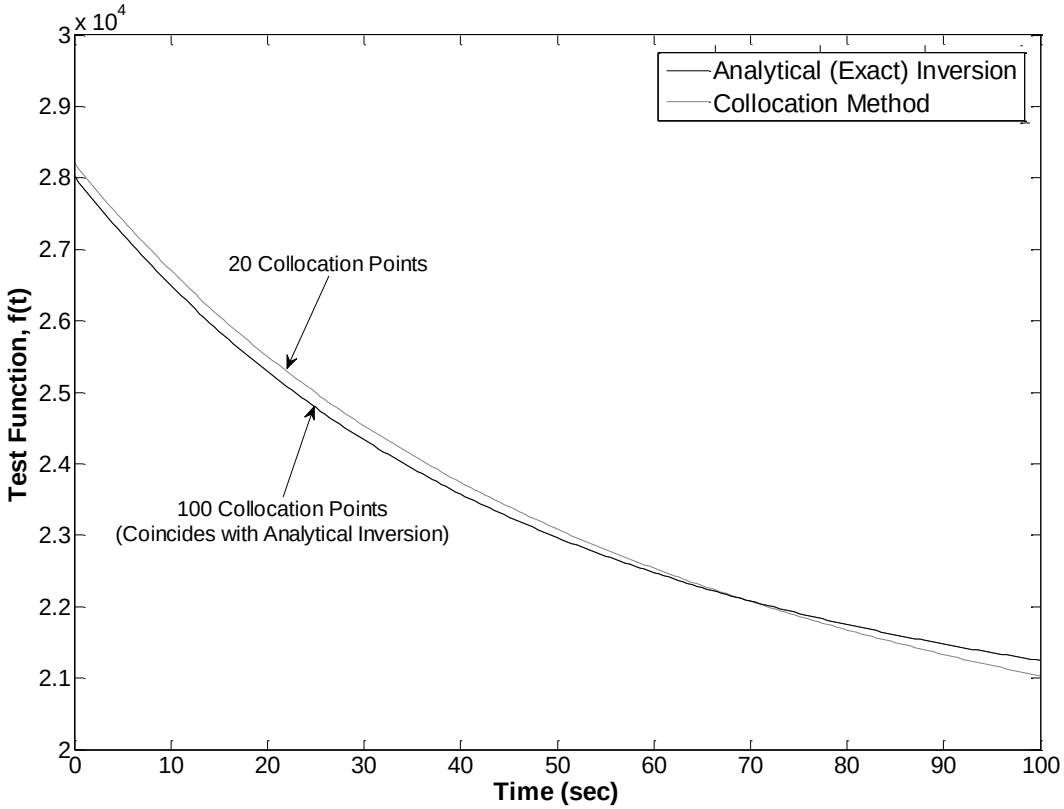

Figure 4-2: Numerical Laplace Inversion using Collocation Method

4.7 VERIFICATION EXAMPLES

In order to verify the present formulation and its implementation a series of verifications were performed. The verification was divided into two categories: (a) verification of the implementation of GIF elements to capture material non-homogeneity, and (b) verification of the viscoelastic portion of the formulation to capture time and history dependent material response.

4.7.1 Verification of Graded Elements

A series of analyses were performed to verify the implementation of the graded elements. The verifications were performed for fixed grip, tension and bending (moment) loading conditions. The material properties were assumed to be elastic with exponential spatial variation. The numerical results were compared with exact analytical solutions available in the literature [65]. The comparison results for fixed grip loading, tensile loading and bending were performed. The results for all three cases show a very close

match with the analytical solution verifying the implementation of the GIF graded elements. Comparison for the bending case is presented in Figure 4-3.

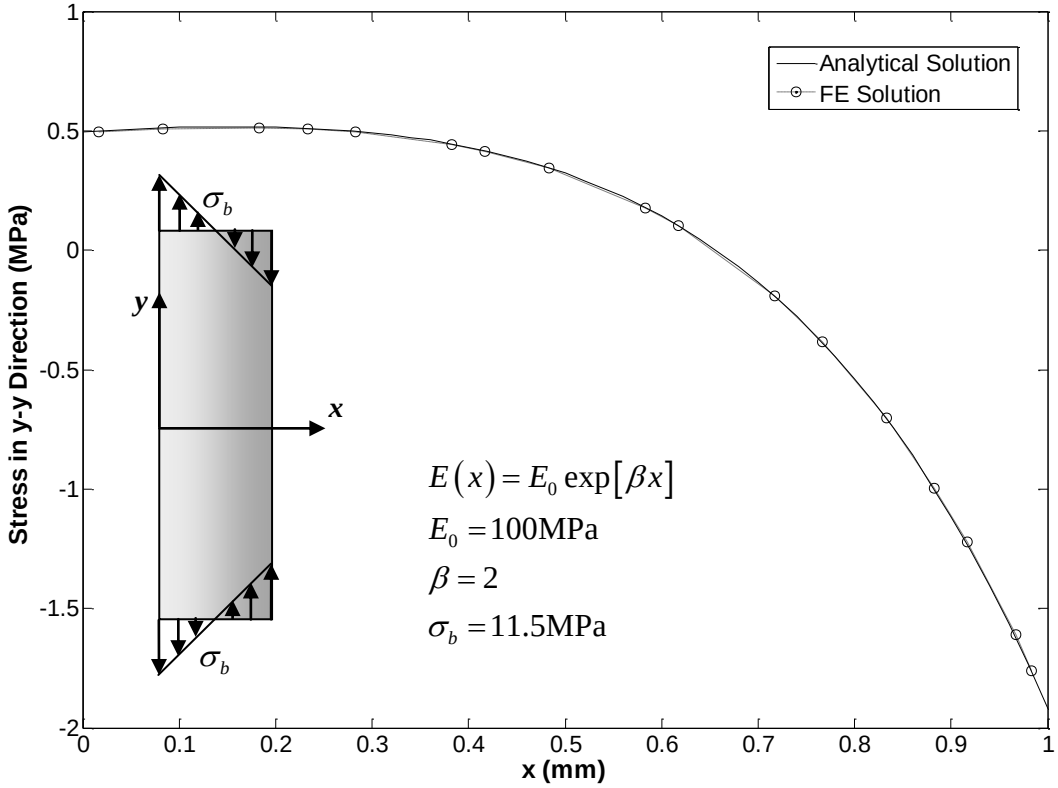

Figure 4-3: Comparison of Exact (line) and Numerical Solution (circular markers) for Bending of FGM Bar (insert illustrates the boundary value problem along with material gradation)

4.7.2 Verification of Viscoelastic Analysis

Verification results for the implementation of the correspondence principle based viscoelastic functionally graded analysis were performed and are provided. The first verification example represents a functionally graded viscoelastic bar undergoing creep deformation under a constant load. The analysis is conducted for the Maxwell model. Figure 4-4 compares analytical and numerical results for this verification problem. The analytical solution [73] was utilized for this analysis. It can be observed that the numerical results are in very good agreement with the analytical solution.

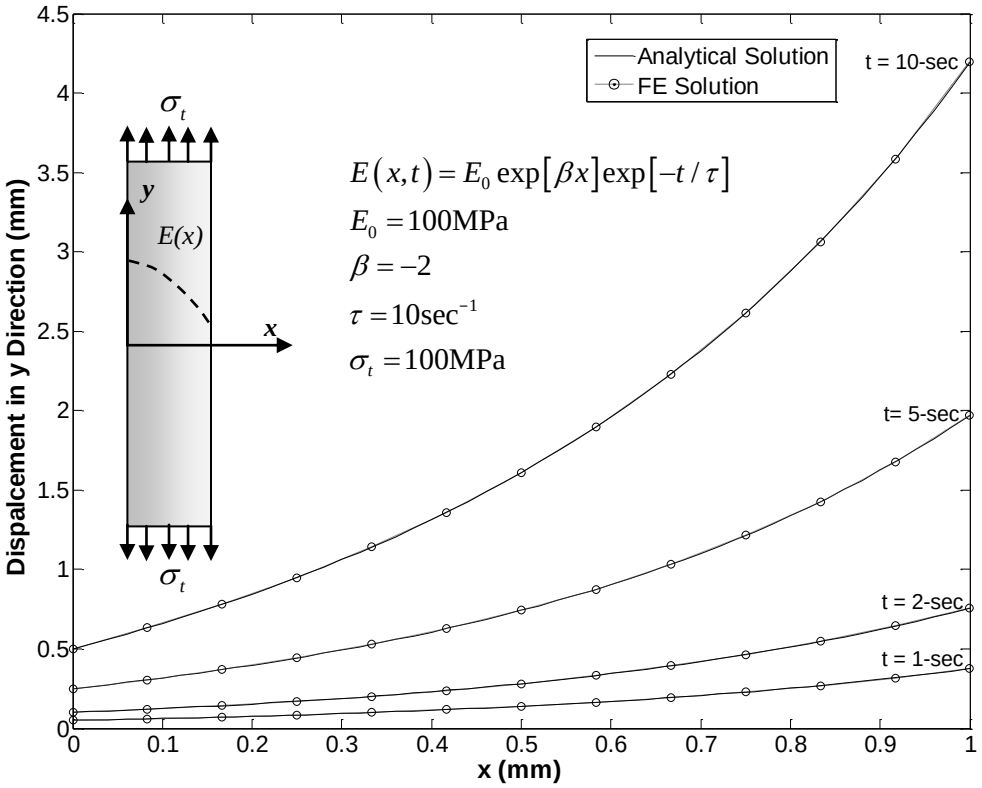

Figure 4-4: Comparison of Exact and Numerical Solution for the Creep of Exponentially Graded Viscoelastic Bar

The second verification example is simulated for fixed grip loading of an exponentially graded viscoelastic bar. The numerical results are compared with the available analytical solution [73] for a viscoelastic FGM. Figure 4-5 compares analytical and numerical results for this verification problem. Notice that the results are presented as function of time, and in this boundary value problem the stresses in y-direction are constant over the width of bar. Excellent agreement between numerical results and analytical solution further verify the veracity of the viscoelastic graded finite-element formulation derived herein and its successful implementation.

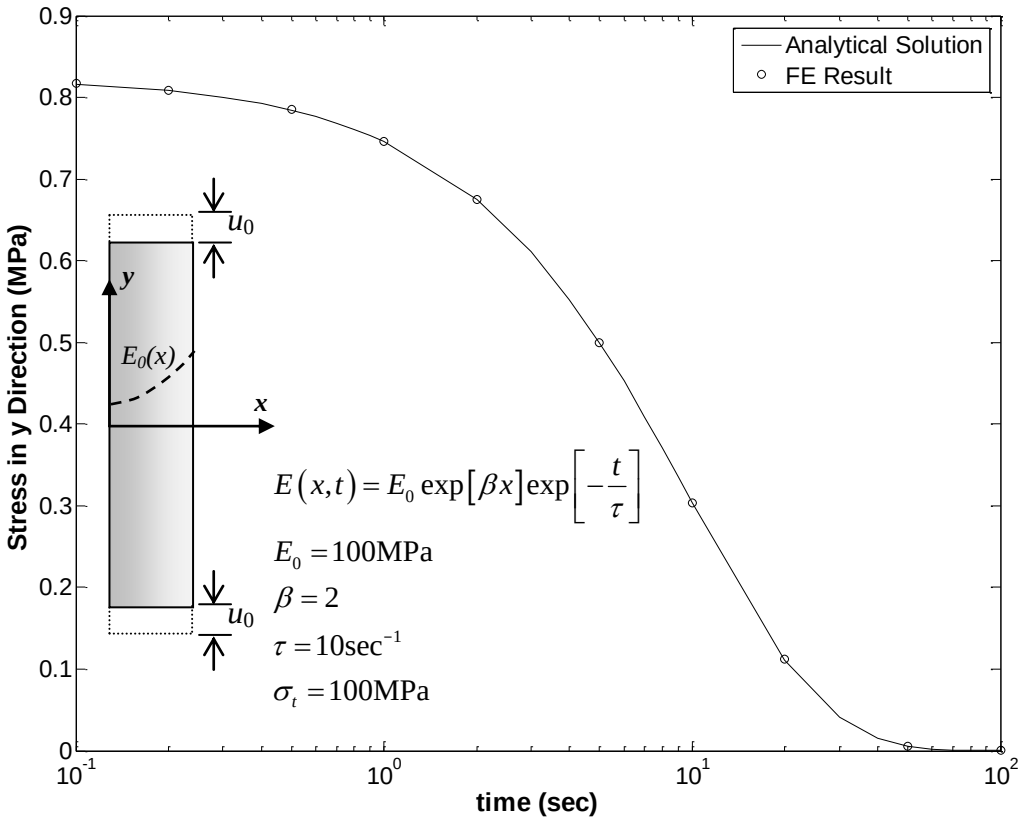

Figure 4-5: Comparison of Exact and Numerical Solution for the Relaxation of Exponentially Graded Viscoelastic Bar

4.8 COMPARISONS WITH COMMERCIAL SOFTWARE

In this section an example utilizing the graded viscoelastic analysis scheme discussed in this chapter is presented. The example is for a simply supported functionally graded viscoelastic beam in a three-point bending configuration. In order to demonstrate the benefits of the graded analysis approach, comparisons are made with analysis performed using commercially available software (ABAQUS®). In the case of ABAQUS® simulations, the material gradation is approximated using a layered approach and different refinement levels.

4.8.1 Boundary Conditions

Figure 4-6 shows the geometry and boundary conditions for the graded viscoelastic simply supported beam. A creep load, $P(t)$, is imposed at mid-span:

$$P(t) = P_0\, h(t); h(t) = \text{Heavyside Function} \tag{4.37}$$

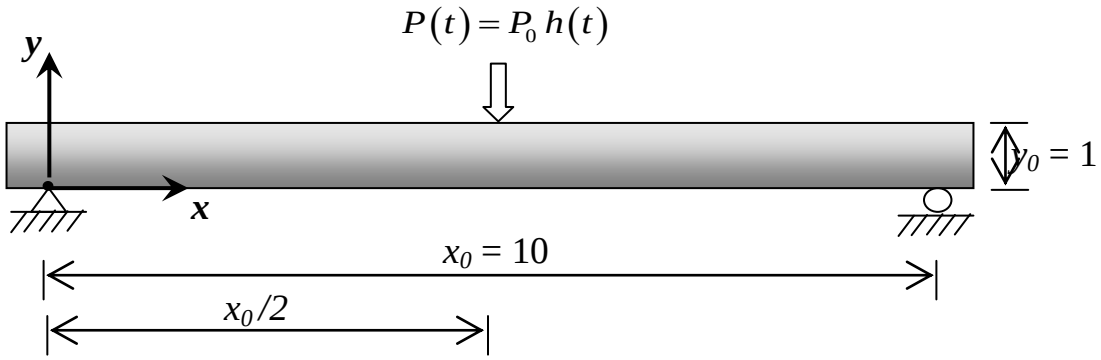

Figure 4-6: Graded Viscoelastic Beam Problem Configuration

4.8.2 Material Distribution

The viscoelastic relaxation moduli on the top ($y = y_0$) and bottom ($y = 0$) of the beam are shown in Figure 4-7. The variation of moduli is assumed to vary linearly from top to bottom as follows:

$$E(y,t) = \left(\frac{y}{y_0}\right) E_{Top}(t) + \left(\frac{y_0 - y}{y_0}\right) E_{Bottom}(t) \tag{4.38}$$

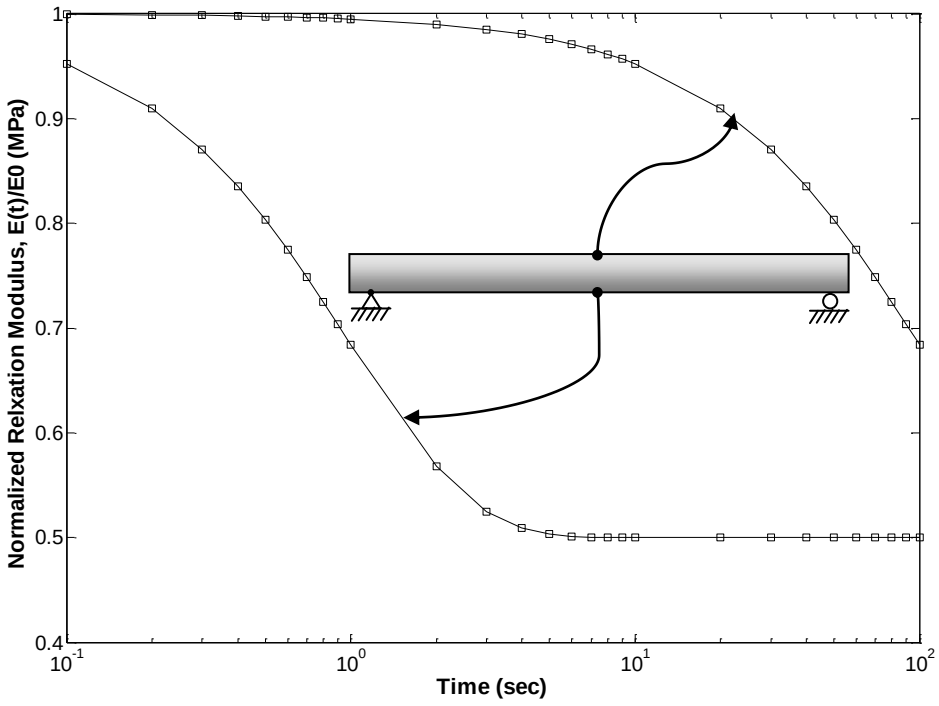

Figure 4-7: Relaxation Moduli on Top and Bottom of the Graded Beam

4.8.3 FE Models

The problem was solved using three approaches namely, (a) graded viscoelastic analysis procedure (present paper); (b) commercial software ABAQUS with different levels of mesh refinements and averaged material properties assigned in the layered manner, and (c) assuming averaged material properties for the whole beam. In the case of the layered approach using commercial software ABAQUS, three levels of discretization were utilized. A sample of the mesh discritization used for each of the simulation cases is shown in Figure 4-8. Table 4.1 presents mesh attributes for each of the simulation cases.

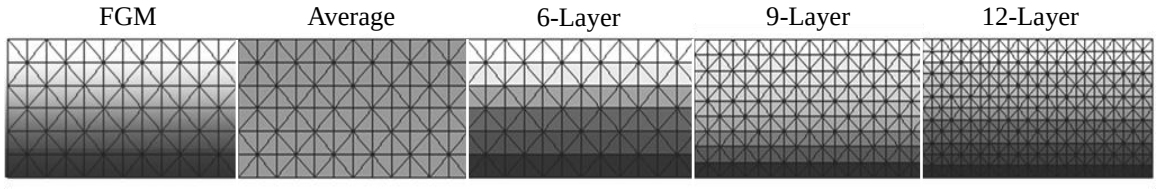

Figure 4-8: Mesh Discretization for Various Simulation Cases ($1/5^{th}$ beam span shown for each case)

Table 4.1: Mesh Attributes for Different Analysis Options

Simulation Case	Number of Elements	Number of Nodes	Total Degrees of Freedom
FGM/Average/6-Layer	720	1573	3146
9-Layer	1620	3439	6878
12-Layer	2880	6025	12050

4.8.4 Results and Discussions

The parameter selected for comparing the various analysis options is the mid span deflection for the beam problem discussed earlier (c.f. Figure 4-6). The results from all four simulation options are presented in Figure 4-9. Due to the viscoelastic nature of the problem, the beam continues to undergo creep deformation with increasing loading time. The results further illustrate the benefit of using the graded analysis approach as a finer

level of mesh refinement is required in order for the layered approach to begin to converge with the graded approach. The results also demonstrate the drawback of using averaged properties which yield significantly poorer results when compared to graded and layered approaches. Also it is worthy to note that in the case of graded viscoelastic problems it is important to consider the results over the complete time history. In the current problem the severity of the material gradation increases with time. This effect is apparent in the results, where the deviation between graded and layered approaches increases with increasing time.

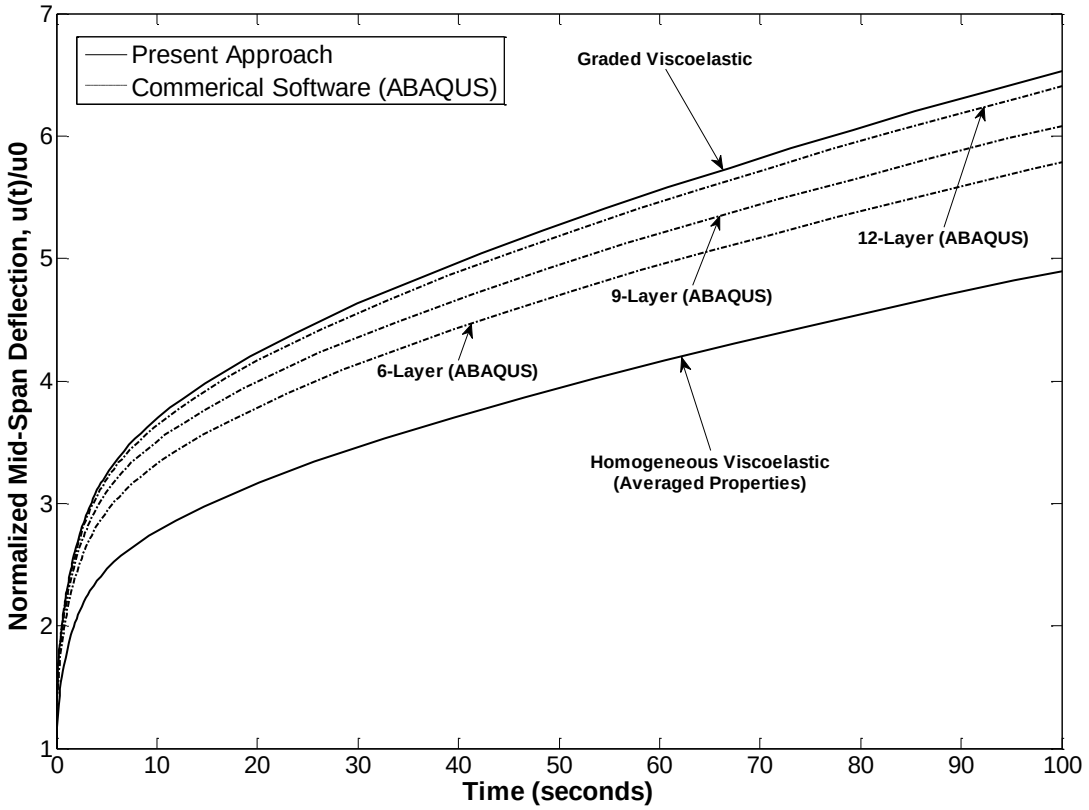

Figure 4-9: Normalized Mid-Span Deflection for the Beam

4.9 SUMMARY

A functionally graded viscoelastic finite element formulation based on correspondence principle is proposed. The formulation is implemented to solve two-dimensional plane and axi-symmetric problems. The GIF is extended for graded (non-homogeneous) viscoelastic elements. The collocation method is selected for performing

the inverse Laplace transformation. The implementation is verified for cases involving material non-homogeneities as well as viscoelastic effects.

Using these new techniques, an application example is presented. The example provided a comparison between graded, averaged homogeneous and layered approaches. Also a comparison between the predictions made using the present approach versus those made by commercially available software is provided.

CHAPTER 5 – FUNCTIONALLY GRADED VISCOELASTIC FINITE ELEMENT ANALYSIS USING TIME-INTEGRATION SCHEME

5.1 INTRODUCTION

The previous chapter described the formulation, implementation and verification of the viscoelastic FGM analysis scheme using the correspondence principle. At this point it is important to reiterate the necessity for the implementation of the time-integration-based finite element code. The key motivations for formulating and implementing the time-integration-based analyses are:

- Limitation of correspondence principle in solving certain type of boundary value problems, such as transient thermal boundary conditions;
- Excessive dependence of the analysis accuracy on the numerical integral transform methods in case of the correspondence principle, furthermore lack of a readily available technique to estimate error;
- Inverse integral transformation is not very accurate over a very wide range of time intervals, especially near the boundaries (very short and very long loading times); and
- In order to minimize the error in numerical inverse integral transform, the numerical inversion parameters need to be adjusted depending on the problem and the material properties.

This chapter describes brief overview of available time-integration schemes for viscoelastic analysis followed by description of methods of choice and finally the details on implementation and verification for the methods of choice.

5.2 TIME INTEGRATION APPROACHES

A detailed description of a functionally graded viscoelastic finite element formulation is presented in Chapter 3. The final problem description can be written in form of following convolution integral,

$$K_{ij}^{e}\left(x\right)u_{j}\left(0\right)+\int_{0}^{t}K_{ij}\left(x,\xi-\xi^{'}\right)u_{j}\left(t^{'}\right)dt^{'}=F_{j}\left(x,t\right) \tag{5.1}$$

Hopkins and Hamming [118] and Lee and Rogers [119] have performed some of the pioneering works on direct numerical integrations for solving viscoelastic problems. This preliminary work demonstrated use of Newton-Cotes expansion to ensure that complete material history is considered for predicting the results at any given time. The finite element problem described in equation (5.1) can be solved using a Newton-Cotes expansion as,

$$u_{j}\left(t_{n}\right)=\left[K_{ij}^{e}\left(x\right)+K_{ij}\left(x,\xi_{n}-\xi_{n-1}\right)\right]^{-1}\left\{\begin{array}{l}2F_{i}\left(t_{n}\right)-\left[K_{ij}\left(x,\xi_{n}\right)-K_{ij}\left(x,\xi_{n}-\xi_{1}\right)\right]u_{j}\left(0\right)\\-\sum_{m=1}^{n-1}\left[K_{ij}\left(x,\xi_{n}-\xi_{m-1}\right)-K_{ij}\left(x,\xi_{n}-\xi_{m+1}\right)\right]u_{j}\left(t_{m}\right)\end{array}\right\} \tag{5.2}$$

It is important to notice that the above solution requires storage of solutions at all time increments prior to the current increment. In past, the limitation on storage memory motivated several researchers to develop numerical methods that circumvent need for storing the previous solutions.

5.2.1 Brief Review of Time-Integration Approaches for Viscoelastic Analysis

A direct integration scheme represents the above shown expansion (Equation(5.2)) into a series of time increments where integrations are performed over each increment through approximate schemes such as trapezoidal rule or Newmark method [120]. Dubois et al. [121] proposed direct integration through incremental scheme suited for fracture analysis of viscoelastic materials. Ellsiepen and Hartmann [122, 123] utilized differential-algebraic equation form of the constitutive equations for solving linear and non-linear dynamic viscoelastic problems using diagonally implicit Range-Kutta methods for time marching schemes. Hartmann and Wensch [124] have also utilized differential-algebraic equations with Rosenbrock type numerical scheme, which are beneficial over previous

methods due to its iteration-less nature. Mesquita and Coda [125] have proposed incremental scheme for dynamic analysis of viscoelastic materials represented by Kelvin model. The disadvantage of the direct integration approaches is the high memory requirement for storage of responses from all previous iterations as well as computational times in accessing that information.

Zak [126] utilized a numerical scheme that utilizes history of one iterative step to calculate stresses in solid rocket propellant using a finite-difference formulation. The procedure is based on calculation of the increment in the material response for a given time step. Zienkiewicz et al. [127] used a similar incremental scheme in the finite-element framework to solve the linear viscoelastic problems. Taylor et al. [105] extended the similar scheme to solve thermo-mechanical problems; this was obtained through extending variational function proposed by Gurtin [104] to include the thermal strain contributions. Over the period of last three decades several researchers have proposed different types of numerical integration schemes for viscoelastic finite-element analysis. Yi and Hilton [128] proposed a recursive formulas using Newmark average acceleration method for transient dynamic response of viscoelastic composite laminates. A similar approach has been utilized for nonlinear thermo-viscoelastic analysis of laminated composite shells [129]. Several integration schemes have been proposed by modification of the recursive schemes. Another popular integration approach is the one utilized by Zocher et al. [130] called the integration point constitutive update scheme. The integration point constitutive update scheme utilizes separation of stress increments whereby linearly related stress contribution to strain increment is directly updated and the non-linear contribution is evaluated from the previous iteration. Poon and Ahmad [131] improved on the integration point constitutive update scheme for thermo-viscoelastic problems by using the time-temperature superposition relations. Yang and Han [132] have proposed a recursive integration scheme suited for non-linear viscoelastic analysis. The recursive formulation is achieved by expending all variables in form of non-linear differential-integral equation systems with boundary and initial values. This leads to a series of recurrent linear boundary value problem for which corresponding FEM based formulae were developed.

Haj-Ali and Muliana [133] proposed non-linear viscoelastic FEM procedure whereby the constitutive equations are expressed in an incremental form for each time step with assumption of a constant incremental strain rate. They proposed iterative procedure with predictor-corrector type steps combined with the recursive integration method. Similar procedure was utilized by Muliana and Khan [134] for analysis of thermo-rheologically complex viscoelastic materials and more recently by Sawant and Muliana [135] for non-linear orthotropic viscoelastic materials.

The time stepping scheme implemented in the commercial finite element analysis code *ABAQUS* was briefly explored. The Newton-Raphson time stepping scheme is utilized by *ABAQUS,* whereby the creep-strain increment in each step is evaluated and is compared against the user provided maximum value. The software assumes the iteration to be convergent as long as creep strain increment is lower than the user prescribed value.

Notice that the most of the recent integration procedures have been proposed for solving non-linear viscoelastic problems. For the analysis of linear problems these procedures revert back to one of the following categories: (a) direct integration, (b) incremental approach, or (c) recursive approach. The focus of this dissertation is limited to linear viscoelastic problems. In this dissertation the direct, incremental and recursive integration approaches were explored. The recursive scheme was chosen for further exploration and simulation of pavement systems.

5.3 ANALYSIS USING INCREMENTAL SCHEME

The incremental approach to solving viscoelastic problems involve determination of the solution increment at the current time step based on the neighboring solutions in time. Mathematically this is expressed as,

$$u(t_n) = \frac{1}{p\Delta t}\left[\sum_{m=1}^{p}(t_{n+m} - t_n)u_{n+m} + (t_n - t_{n-m})u_{n-m}\right] \tag{5.3}$$

where, solution at time, t_n is represented in terms of neighboring p solutions.

The incremental scheme proposed by Zak [126] is implemented for finite-difference analysis of an axisymmetric problem. The implementation is verified by comparing the results with analytical solution provided by Freudenthal and Shinozuka [136, 137].

5.3.1 Problem Description

The problem consists of infinitely long thick-walled viscoelastic hollow cylinder bonded inside a rigid casing. Figure 5-1 illustrates the problem geometry.

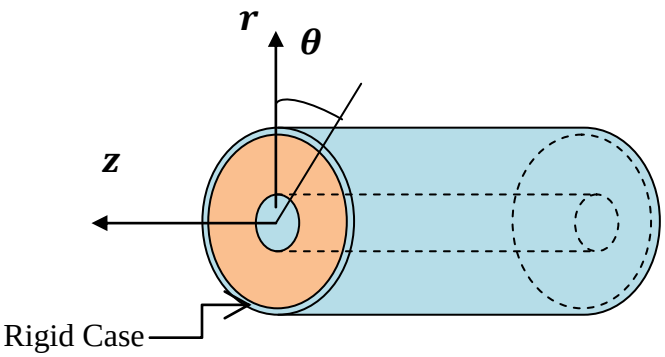

Figure 5-1: Problem Geometry

The material properties are assumed to be:

$$D(t) = \left(182.544 - 165.839\,Exp\left[-\frac{t}{11\tau}\right]\right)/K$$
$$J(t) = \left(-91.161 + 82.919\,Exp\left[-\frac{t}{11\tau}\right]\right)/K \qquad (5.4)$$

The thermal strain is imposed by means of time dependent temperature variation given as,

$$T(t) = 1 - Exp\left[-\frac{t}{\tau}\right] \qquad (5.5)$$

5.3.2 Results and Comparison with Analytical Solution

The above shown problem is analyzed for the hollow cylinder with internal and external diameters of 1 and 3 units respectively. For two levels of geometry

discretizations (number of radial partitions) and time discretizations (time steps) the radial stresses and tangential stresses are numerically calculated and compared to analytical solution. Figure 5-2 shows the comparison of numerical and analytical results for tangential stresses and Figure 5-3 shows comparison for radial stresses. The comparison shows good agreement with analytical solution.

The simulation times for this relatively simple problem with finite-difference approach were relatively high. The accuracy levels are also not as great as those obtained from the recursive and direct integration schemes (discussed later). Nonetheless the implementation of incremental scheme provided better understanding on the topic of numerical integration and provided necessary background to the author for understanding and implementing recursive scheme.

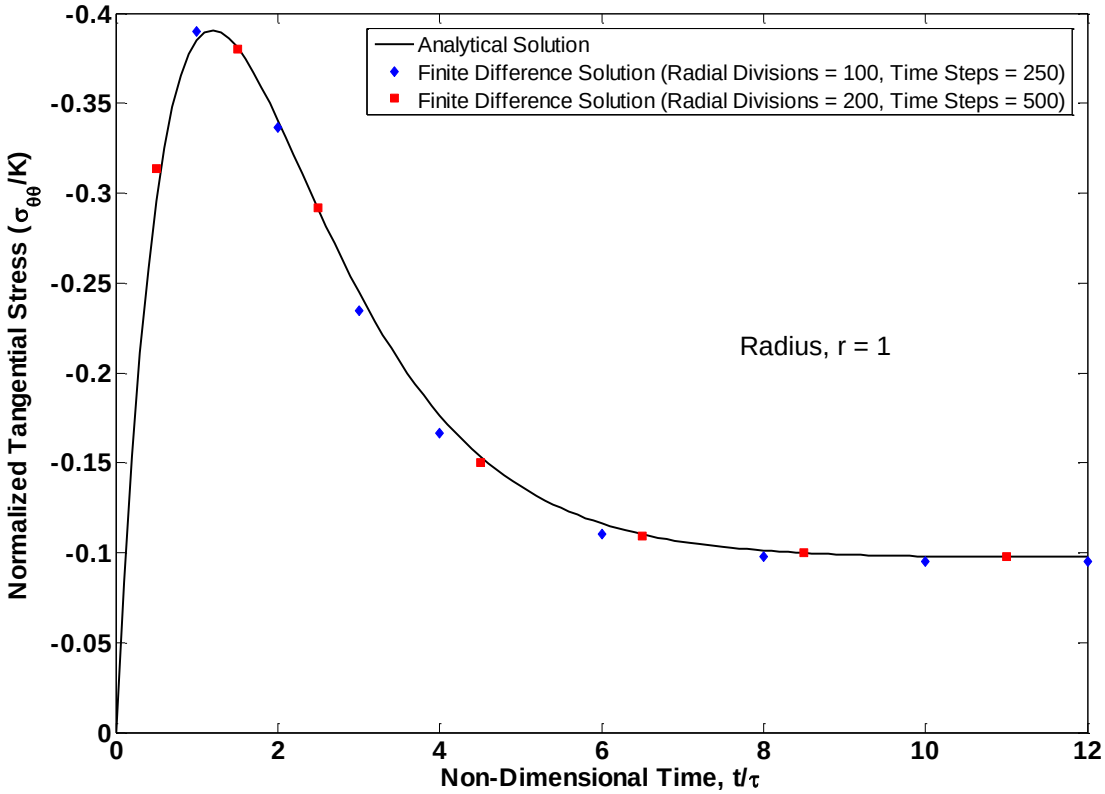

Figure 5-2: Comparison of Analytical and Numerical Evaluation of Tangential Stresses

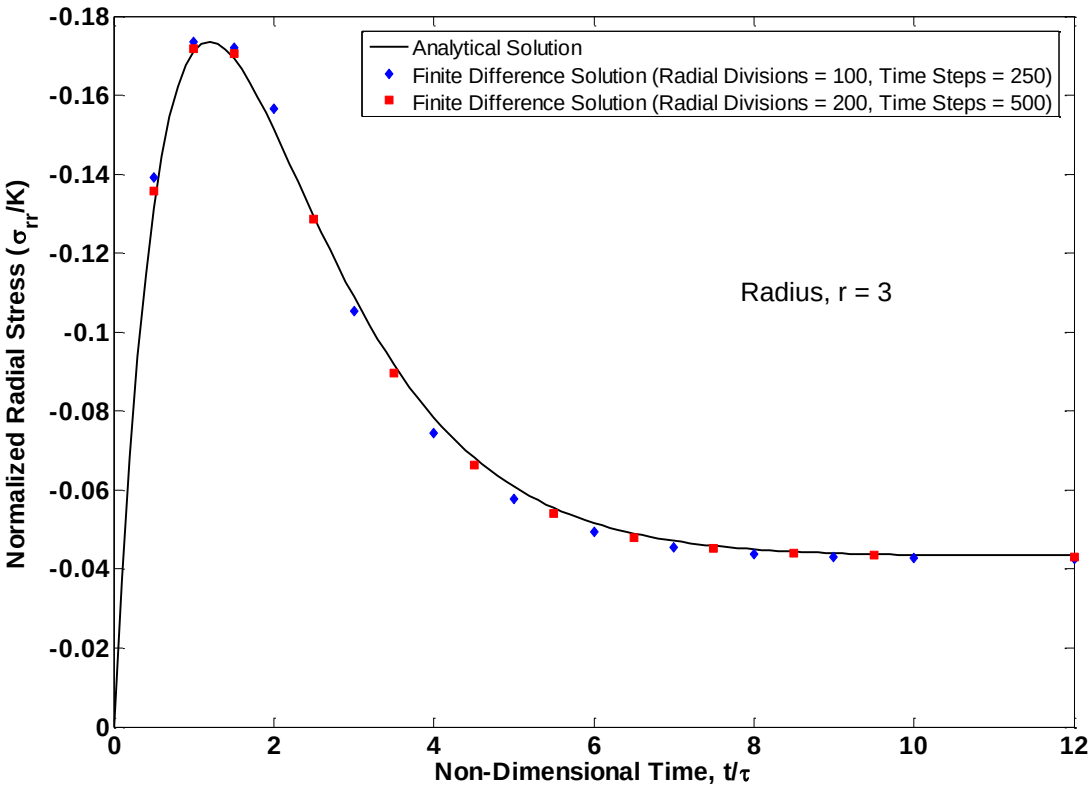

Figure 5-3: Comparison of Analytical and Numerical Evaluation of Radial Stresses

5.4 FINITE ELEMENT ANALYSIS USING RECURSIVE SCHEME

The recursive integration scheme based on the formulation by Yi and Hilton [128] is presented in this section for viscoelastic FGM problems. Comparisons between the direct integration and recursive approaches for homogeneous and FGM viscoelastic problems are made and the results are described later in this section. The subsequent sections describe more rigorous verification and validation examples.

5.4.1 Recursive Formulation

The viscoelastic FGM represented by generalized Maxwell model with h units, the kernel K_{ij} expands as,

$$K_{ij}(x,\xi) = \sum_{h=1}^{m} \left(K_{ij}^{e}(x)\right)_h \, Exp\left(-\frac{\xi - \xi'}{\left(\tau_{ij}(x)\right)_h}\right) \tag{5.6}$$

The nodal displacements and its time derivatives can be approximated as,

$$
\begin{aligned}
&u_j(t_n) = u_j(t_{n-1}) + \frac{\partial u_j(t)}{\partial t}\Delta t + \frac{\partial^2 u_j(t)}{\partial t^2}\left(\frac{\Delta t}{2}\right)^2, \quad t_{n-1} \le t \le t_n \\
&\frac{\partial u_j(t)}{\partial t} = \dot{u}_j(t_n) = \frac{u_j(t_n) - u_j(t_{n-1})}{\Delta t} \\
&\frac{\partial^2 u_j(t)}{\partial t^2} = \ddot{u}_j(t_n) = \frac{\dot{u}_j(t_n) - \dot{u}_j(t_{n-1})}{\Delta t}
\end{aligned}
\tag{5.7}
$$

Using assumptions shown in equation (5.7), the kernel form in equation (5.6) and by performing integration by parts, the viscoelastic FGM FE problem described in equation (5.1) can be expressed as,

$$
\begin{aligned}
&\left[\sum_{h=1}^{m}\left(K_{ij}^{e}(x)\right)_h \cdot \left[\left(v_{ij}^{1}(x,t_n)\right)_h \Delta t - \left(v_{ij}^{2}(x,t_n)\right)_h\right]\frac{2}{\Delta t^2}\right] u_j(t_n) = F_i(t_n) \\
&+\sum_{h=1}^{m}\left[\left[\left(K_{ij}^{e}(x)\right)_h \cdot Exp\left[-\frac{\xi(t_n)}{\left(\tau_{ij}(x)\right)_h}\right]\right]\left\{\left(v_{ij}^{1}(x,t_{n-1})\right)_h\left[u_j(t_{n-1})\frac{2}{\Delta t} + \dot{u}_j(t_{n-1})\right]\right.\right. \\
&\qquad -\frac{2}{\Delta t^2}\left(v_{ij}^{2}(x,t_{n-1})\right)_h\left[u_j(t_{n-1}) + \dot{u}_j(t_{n-1})\Delta t\right] \\
&\qquad \left.\left. -u_i(t_0) + \left(v_{ij}^{1}(x,t_0)\right)\dot{u}_j(t_0)\right\} + \left(R_i(t_n)\right)_h\right]
\end{aligned}
\tag{5.8}
$$

where,

$$
\begin{aligned}
&\left(v_{ij}^{1}(x,t_n)\right)_h = \int_0^{t_n} Exp\left[-\xi(t')/\left(\tau_{ij}(x)\right)_h\right]dt' \\
&\left(v_{ij}^{2}(x,t_n)\right)_h = \int_{t_{n-1}}^{t_n}\left(v_{ij}^{1}(x,t')\right)_h dt' \\
&\left(R_i(t_n)\right)_h = K_{ij}^{e} \cdot Exp\left[-\xi(t')/\left(\tau_{ij}(x)\right)_h\right]\cdot\left(v_{ij}^{2}(x,t_n)\right)_h \ddot{u}_j(t_{n-1}) \\
&+Exp\left[-\xi(t')/\left(\tau_{ij}(x)\right)_h\right]\left(R_j(t_{n-1})\right)_h
\end{aligned}
\tag{5.9}
$$

5.4.2 Implementation and Verification

The formulation described in previous section is implemented in the commercially available software Matlab®. The code is provided in Appendix B. The finite-element implementation is performed for solving two-dimensional (2D) planer and axisymmetric problems. A series of verification examples are simulated to ensure the accuracy of

verification and implementation. Preliminary comparisons are made between direct integration and recursive integration schemes.

The verifications are made at different levels of sophistication; the initial verifications ensure the accuracy of formulation for homogeneous viscoelastic problems. Later examples demonstrate verification for functionally graded viscoelastic boundary value problems.

Verification Example: Creep of Homogeneous Viscoelastic Bar

A viscoelastic boundary value problem simulating 100 second creep extension of a bar is simulated using recursive and direct integration methods. The computation times and solution accuracy are determined for different time step sizes.

The same boundary value problem was solved using the CP-based formulation described in Chapter 4. The computation times and error analysis for different time step sizes are plotted in Figure 5-4 and Figure 5-5. Notice that cumulative errors over the analysis period are plotted. The analysis present results as expected, with larger computation times for smaller time step sizes and lower errors for smaller time steps.

The general observation from this example shows greater computation cost for direct integration compared to recursive formulation; this is due to continuous access and computations utilizing all the previous solutions at each increment. The solution accuracy for both time integration approaches depends on time step sizes. Recursive formulation requires smaller time step sizes compared to direct integration for same level of accuracy.

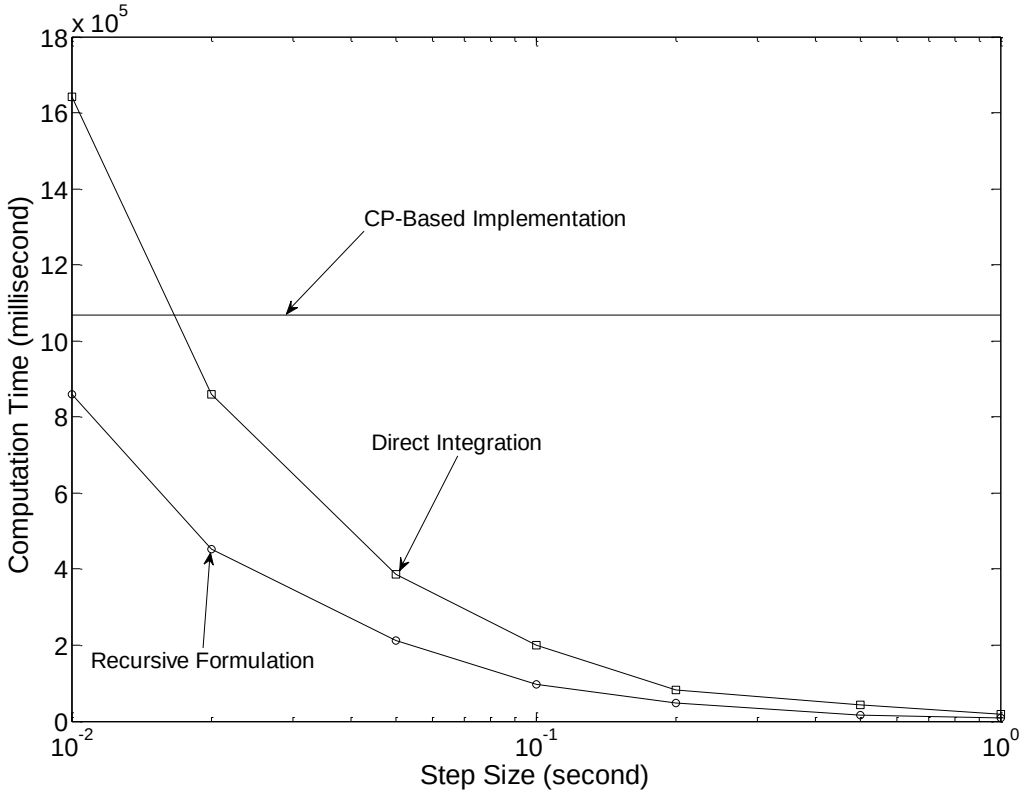

Figure 5-4: Computation Times for Different Solution Schemes

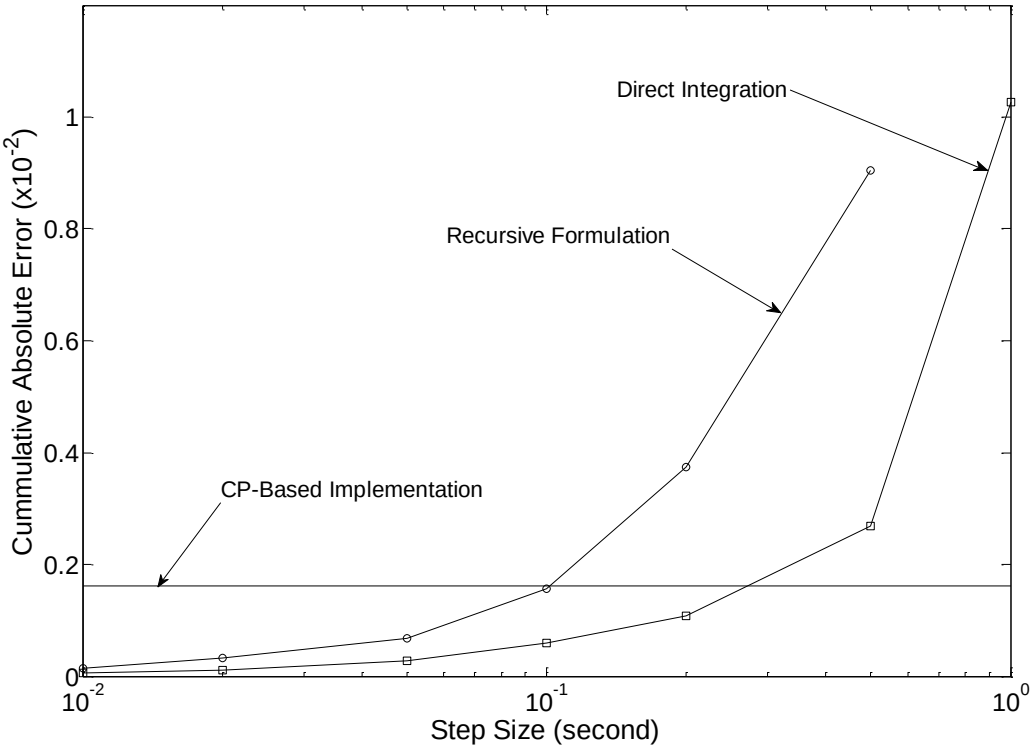

Figure 5-5: Error Analysis for Different Solution Schemes

Verification Example: Three Point Bending of Viscoelastic Beam

A viscoelastic beam in three-point bending condition is simulated using recursive FE formulation. The geometry and boundary conditions are shown in Figure 5-6, the mid-span loading condition is given as:

$$P(t) = P_0\, h(t); \quad h(t) = \text{Heavyside function} \tag{5.10}$$

The relaxation modulus for the beam is presented in Figure 5-7. FE simulations are performed using time step sizes of 0.1, 1, 2, 5, 10, and 20 seconds. The normalized mid-span deflections are presented for FE simulations along with analytical solutions in Figure 5-8. The inset in Figure 5-8 shows the evolution of error for different time step sizes. As anticipated the results converge with analytical results as the time step size reduces. The results show that the recursive formulation based implementation predicts accurate results for homogeneous viscoelastic boundary value problem when the time step size is reduced sufficiently.

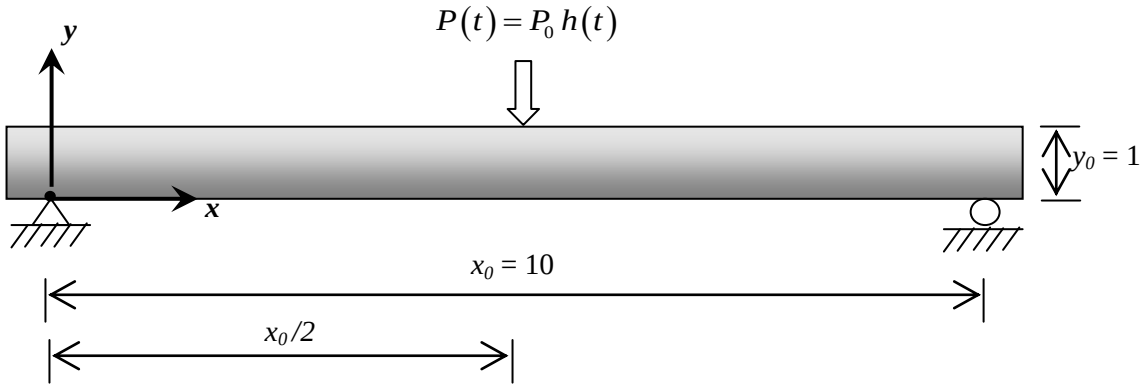

Figure 5-6: Viscoelastic Beam Problem Configuration

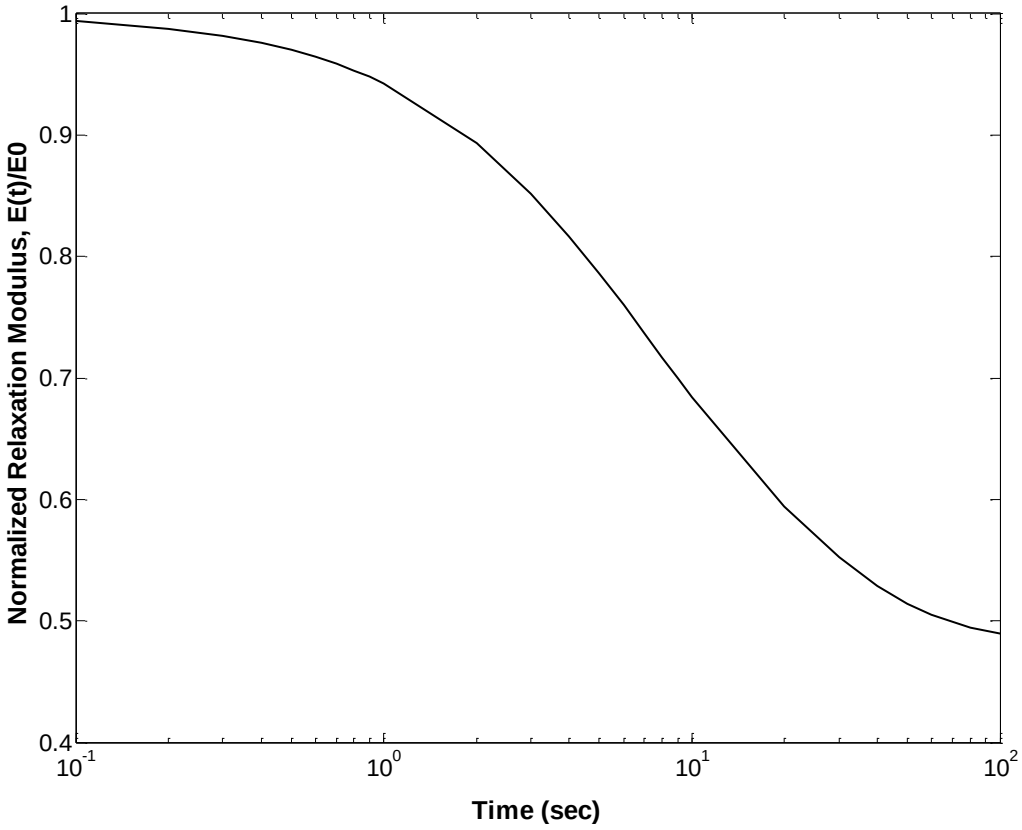

Figure 5-7: Relaxation Modulus for the Beam Bending Verification Example

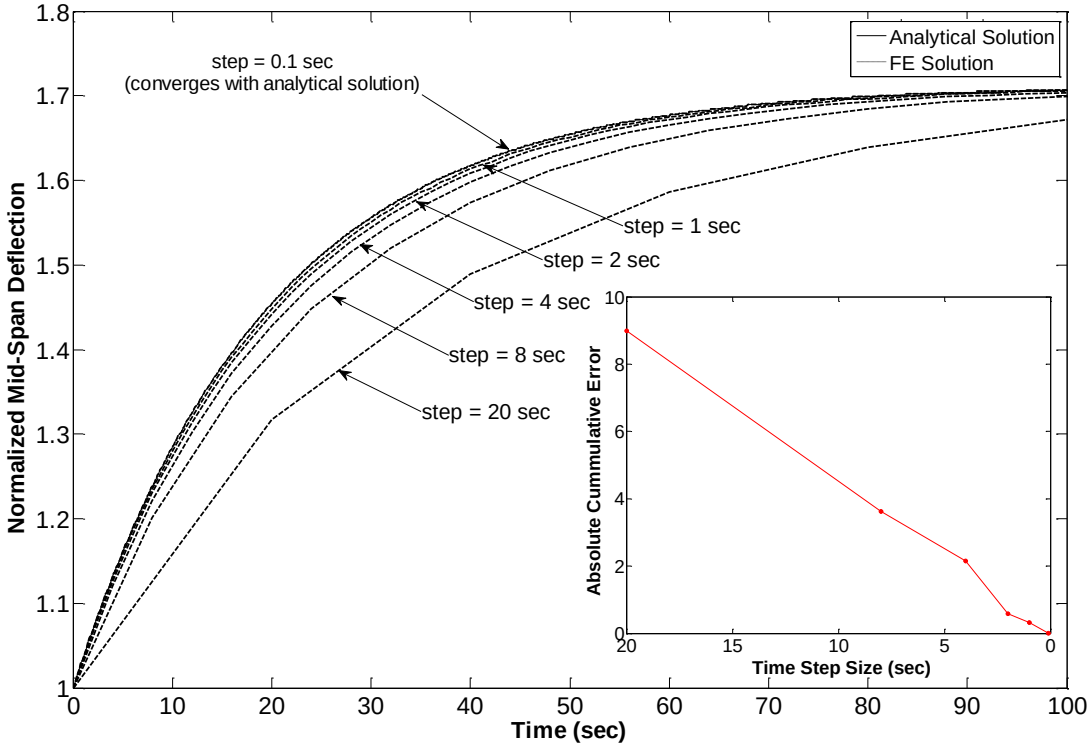

Figure 5-8: Normalized Mid-Span Deflections for the Viscoelastic Beam

Verification Example: Relaxation of Functionally Graded Viscoelastic Bar

This example demonstrates the capability of recursive FE method in predicting the response for viscoelastic FGM problem. The verification example from Mukherjee and Paulino [73] is utilized. The simulations are performed for time step sizes of 0.1, 0.2, 0.5 and 1 second. The example represents a functionally graded viscoelastic bar undergoing stress relaxation under fixed grip loading. Figure 5-9 compares numerical results with analytical solution. The results show very good agreement with analytical solution for 0.1 second time step.

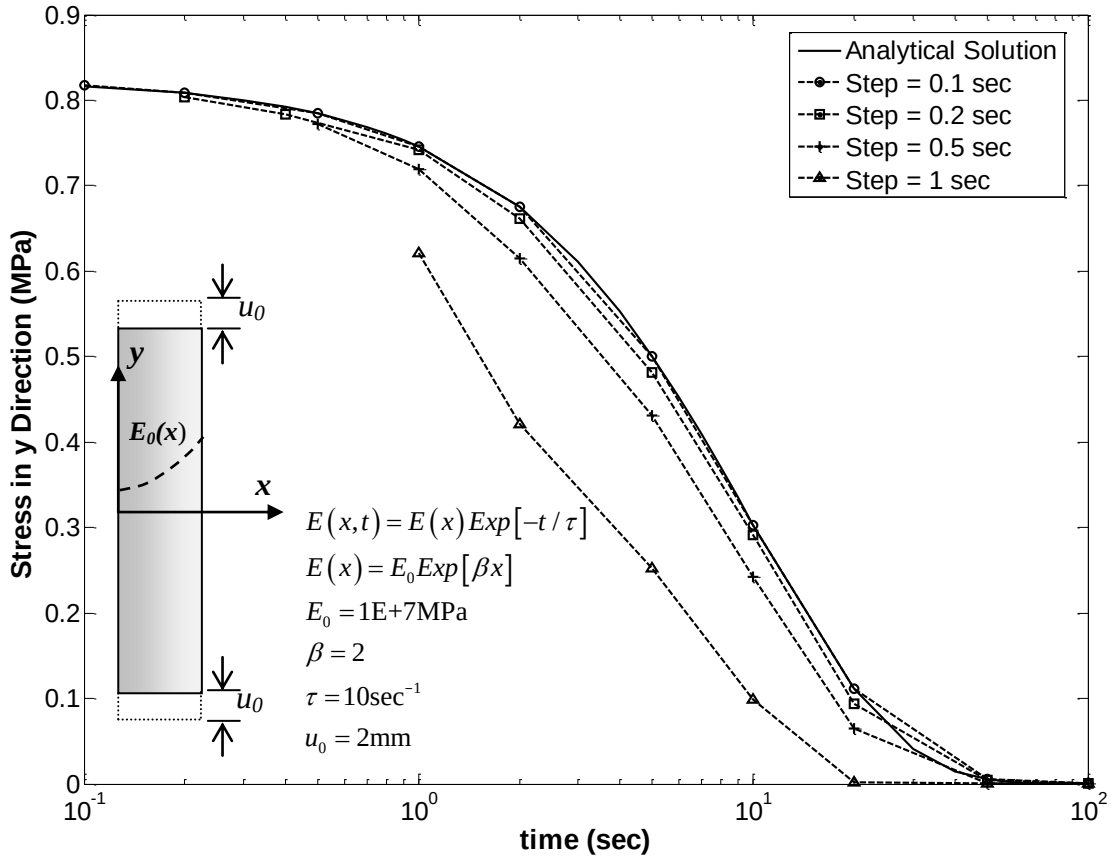

Figure 5-9: Comparison of Exact and Numerical Solution for the Exponentially Graded Viscoelastic Bar in Fixed Grip Loading

Verification Example: Creep of Functionally Graded Viscoelastic Bar

This example further verifies the prediction capability of recursive FE method for viscoelastic FGM problems. The example representing exponentially graded viscoelastic

bar undergoing creep loading is simulated. Closed form solution from Mukherjee and Paulino [73] is compared with the FE predictions. The simulations are performed using time step size of 0.1 second. Figure 5-10 compares numerical results with analytical solution at different loading times. The results show very good agreement with analytical solutions further demonstrating the veracity of the viscoelastic graded finite-element formulation presented herein and its successful implementation.

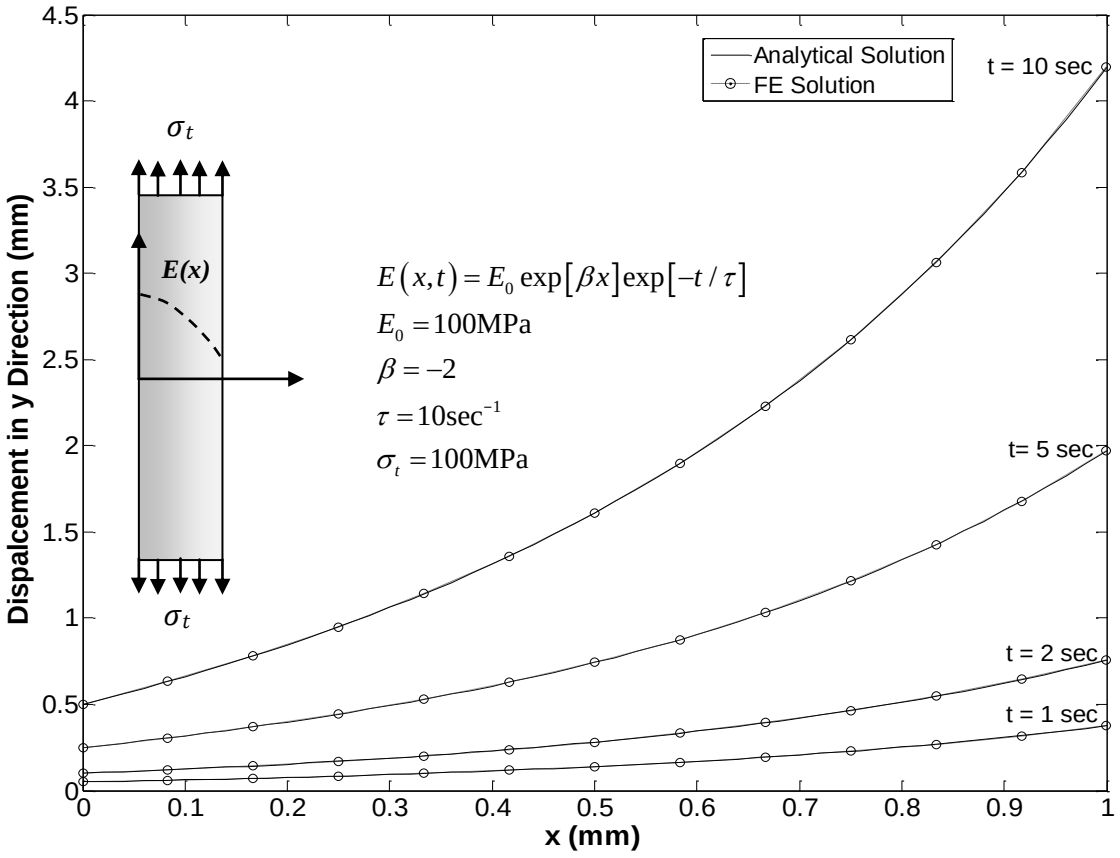

Figure 5-10: Comparison of Exact and Numerical Solution for the Exponentially Graded Viscoelastic Bar in Creep Loading

5.4.3 Comparisons with Commercial Software

In order to validate the viscoelastic FGM FE analysis using present approach and to demonstrate its strength, comparisons are made against commercial software ABAQUS®. The analysis is performed for a viscoelastic beam with temperature gradient. Temperature

induced properties gradients along the thickness (y-direction) creates material non-homogeneity. The FGM analysis is compared with layered gradations with varying degree of layer refinements. The layered analyses are performed using ABAQUS®. It is important to ensure that the present formulation is capable of capturing temperature induced property gradients as the HMA pavement systems always exhibit this type of behavior (c.f Section 2.2). The boundary conditions and temperature distribution for the beam are shown in Figure 5-11.

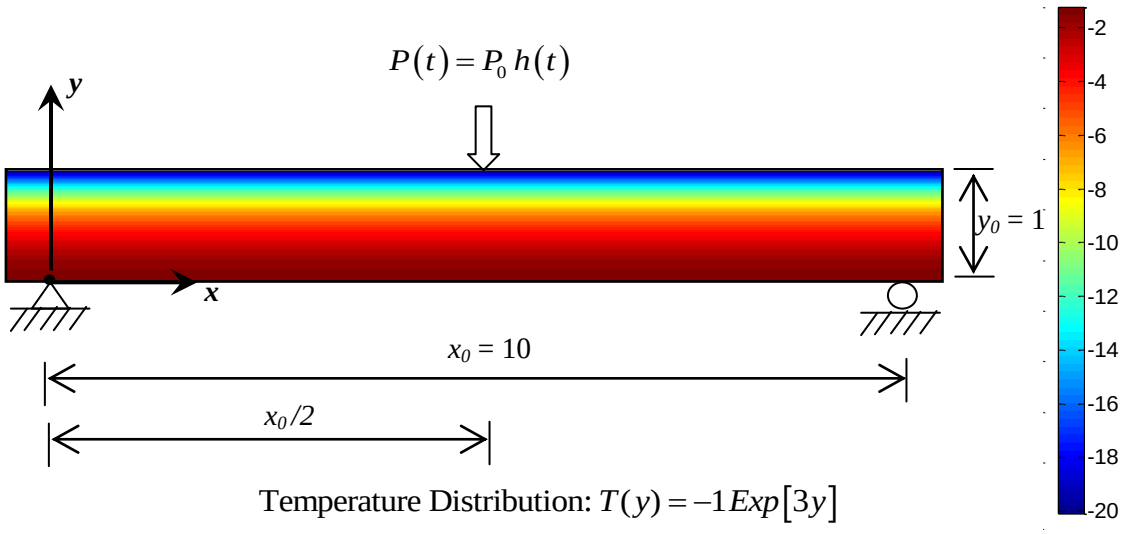

Figure 5-11: Boundary Conditions and Temperature Distribution (legend on right provides temperature in °C)

The present approach (viscoelastic FGM) is capable of accurate representation of the temperature distribution and in-turn the smoothly graded viscoelastic properties in space and time. Whereas in the case of commercial software, the lack of graded elements restrict capturing non-homogeneous properties through mesh refinement and assignment of discrete properties to each layer. For the current problem, the gradation was approximated in ABAQUS using 3, 6, 9, and 18 layers. The temperature distribution for the different simulation cases is presented in Figure 5-12. The viscoelastic properties for the material are shown in Figure 5-13. The relaxation modulus mastercurve is plotted at reference temperature of -20°C. The inset shows the time-temperature shift factors with assumption that material behaves in thermo-rheologically simple manner. The shift

factors link the thermal distribution to the material property distributions as described in Section 3.2.

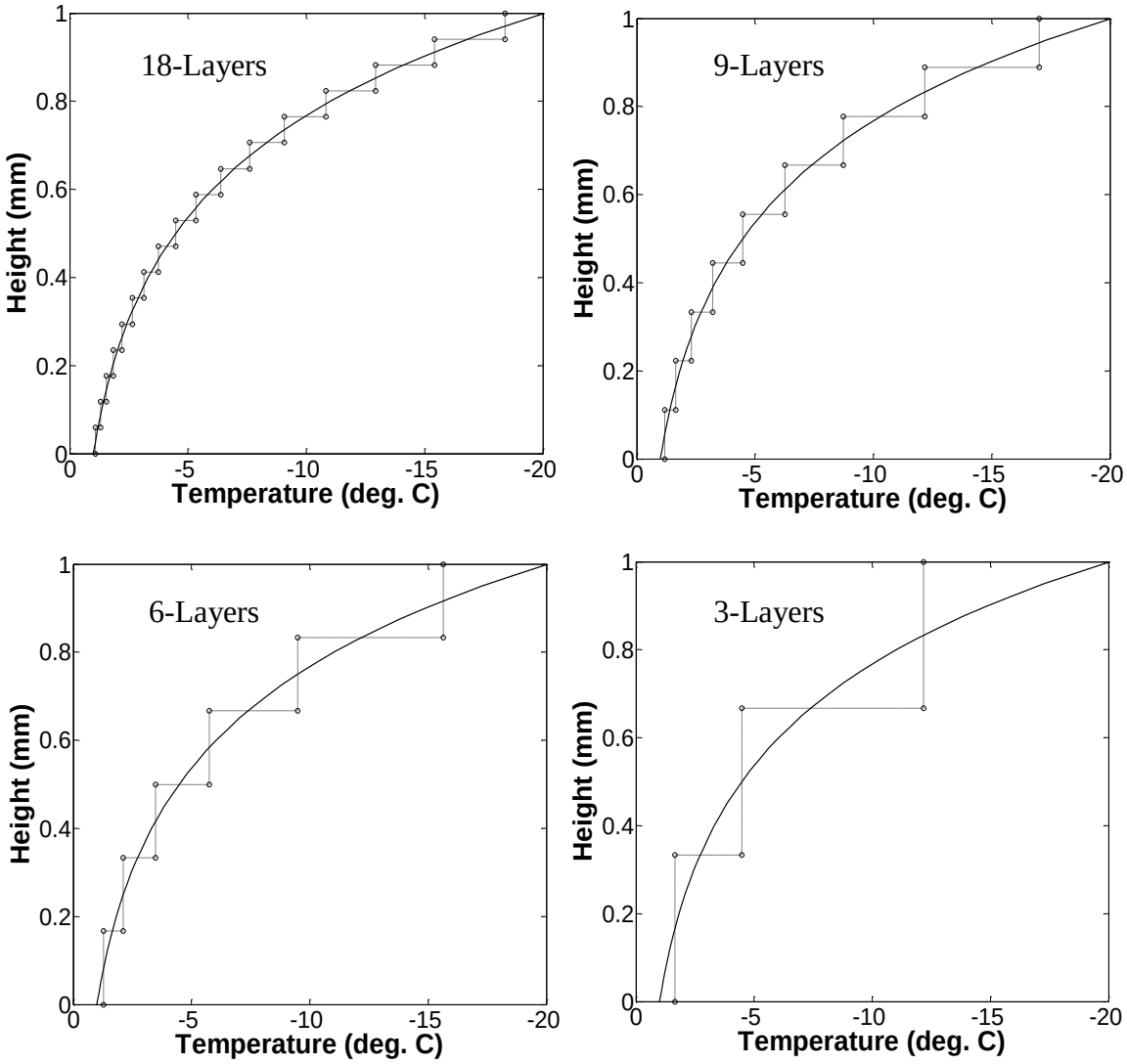

Figure 5-12: Temperature Input for Different Simulation Cases (solid line: FGM approach (present formulation), dashed line: layered approach (ABAQUS®)

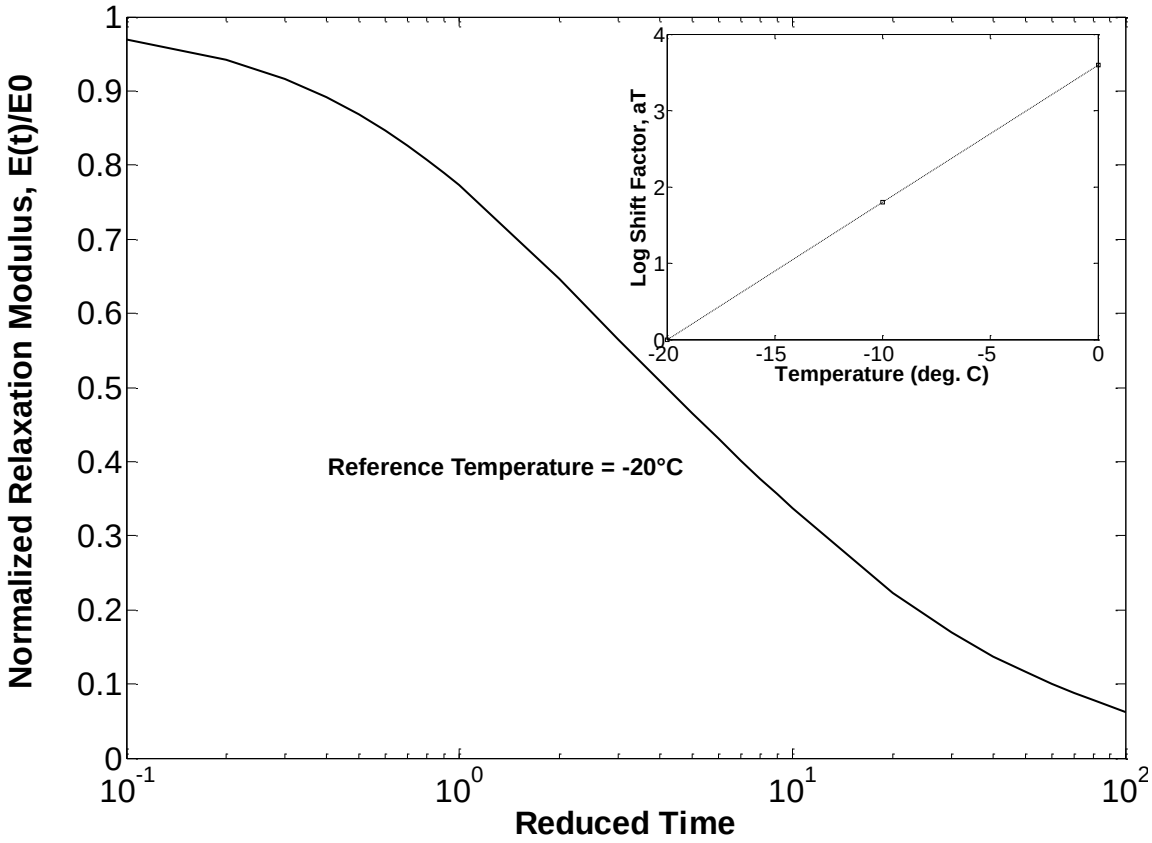

Figure 5-13: Relaxation Modulus (inset: Time temperature superposition shift factors)

The mesh structures and the mesh statistics for different simulation cases are shown in Figure 5-14. Notice that the significant difference between the number of degrees of freedom (DOF) for different simulation cases (c.f. Table 5.1). The simulation results are plotted in Figure 5-15. The results for the problem are presented in form of normalized mid-span deflections as function of time. The results clearly demonstrate the accuracy of the present formulation in capturing temperature-induced viscoelastic property gradients. With increasing mesh refinement levels the layered gradation begins to converge with the FGM results. Figure 5-16 shows the deviation of the layered approach from the viscoelastic FGM approach.

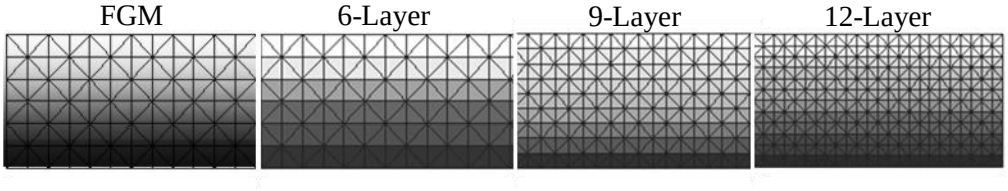

Figure 5-14: Mesh Discretization for Various Simulation Cases (1/5th beam span shown for each case)

Table 5.1: Mesh Attributes for Different Analysis Options

Simulation Case	Number of Elements	Number of Nodes	Total Degrees of Freedom
FGM/6-Layer	720	1573	3146
9-Layer	1620	3439	6878
12-Layer	2880	6025	12050

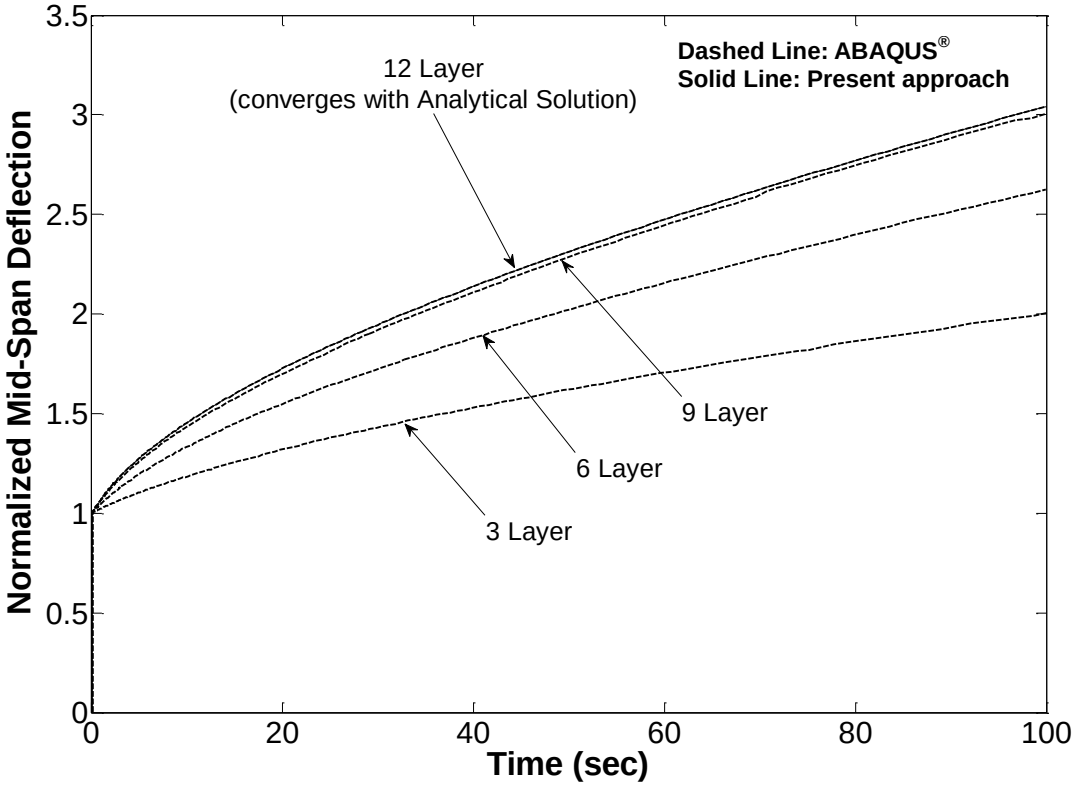

Figure 5-15: Normalized Mid-Span Deflections for Thermally Induced Graded Beam

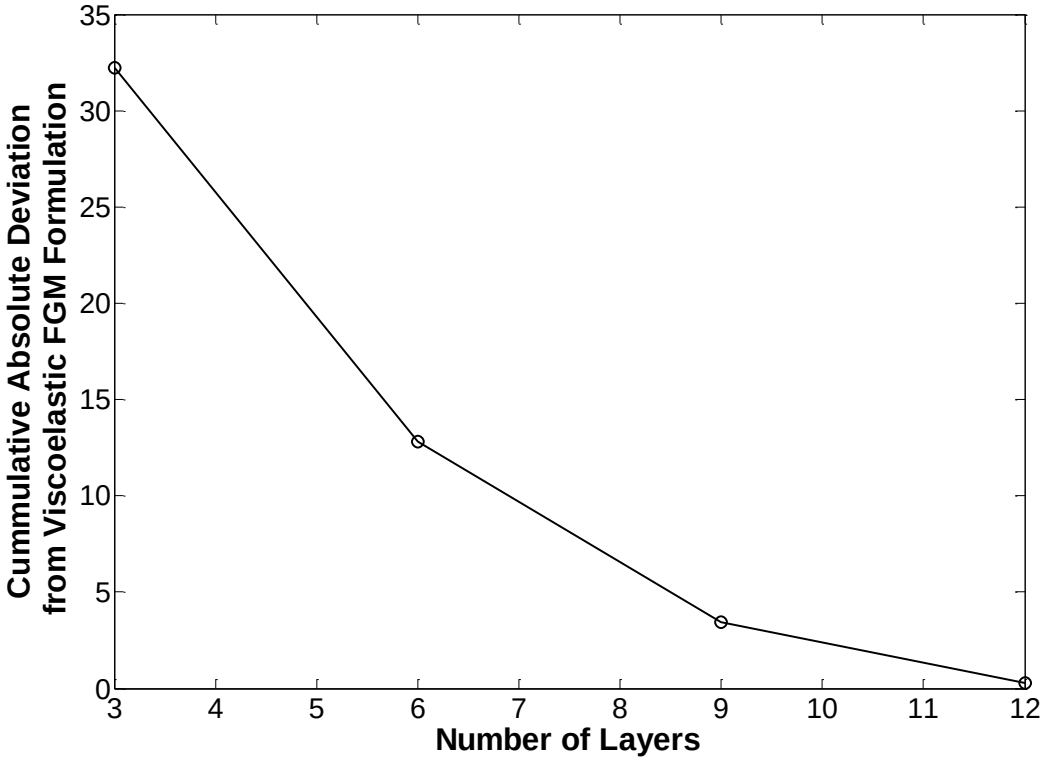

Figure 5-16: Deviation of Layered Results with FGM Results

5.5 BOUNDARY LAYER ANALYSIS OF VISCOELASTIC FGM

5.5.1 Introduction

This section describes crack-tip stress fields in radially graded viscoelastic material determined using boundary layer model. The description of boundary layer model follows.

Williams [138] presented the stationary crack tip stress and displacement fields, Eischen [139] extended them for elastic non-homogeneous bodies with continuous, differentiable and bounded material properties. The stress fields and corresponding displacements as derived by Eischen are as follows:

$$\begin{aligned} \sigma_{ij} &= \frac{K_I}{\sqrt{2\pi r}} f_{ij}^{I}(\theta) + \frac{K_{II}}{\sqrt{2\pi r}} f_{ij}^{II}(\theta) + T\delta_{i1}\delta_{j1} + O\left(r^{1/2}\right) \\ u_i &= \frac{K_I}{G_{tip}}\sqrt{\frac{r}{2\pi}} g_i^{I}(\theta) + \frac{K_{II}}{G_{tip}}\sqrt{\frac{r}{2\pi}} g_i^{II}(\theta) + O(r) \end{aligned} \tag{5.11}$$

where K_I and K_{II} are mode I and mode II stress intensity factors (SIFs), $f_{ij}(\theta)$ and $g_i(\theta)$ are angular functions for stresses and displacements, and T is the T-stress.

Marur and Tippur [140] utilized FEM for investigation of crack tip stress fields in FGMs. Kim [141] investigated crack-tip stresses in exponentially graded materials through use of boundary layer model and evaluated auxiliary fields for FGMs.

5.5.2 Problem Description and FE Mesh

Figure 5-17 shows the problem description along with angular convention. Amongst others, Eftis et al. [142] have presented the loading conditions on the outer boundary corresponding to the asymptotic stresses at the crack tip. In the current example Mode I displacement loading conditions were assumed, these are given by,

$$u_i = \frac{K_I}{G_{tip}}\sqrt{\frac{r}{2\pi}}g_i^I(\theta);$$

$$\text{where, } g_1^I(\theta) = \cos\frac{\theta}{2}\left[\frac{1}{2}(\kappa-1)+\sin^2\frac{\theta}{2}\right] \text{ and} \qquad (5.12)$$

$$g_2^I(\theta) = \sin\frac{\theta}{2}\left[\frac{1}{2}(\kappa+1)-\cos^2\frac{\theta}{2}\right]$$

The finite element model was developed with 3232 elements and 6599 nodes using 6 node plane stress triangular elements (T6). Figure 5-17 shows the FE mesh, the average element side length of $0.2\times R$ was utilized along the periphery which was reduced to $10^{-4}\times R$ at the center.

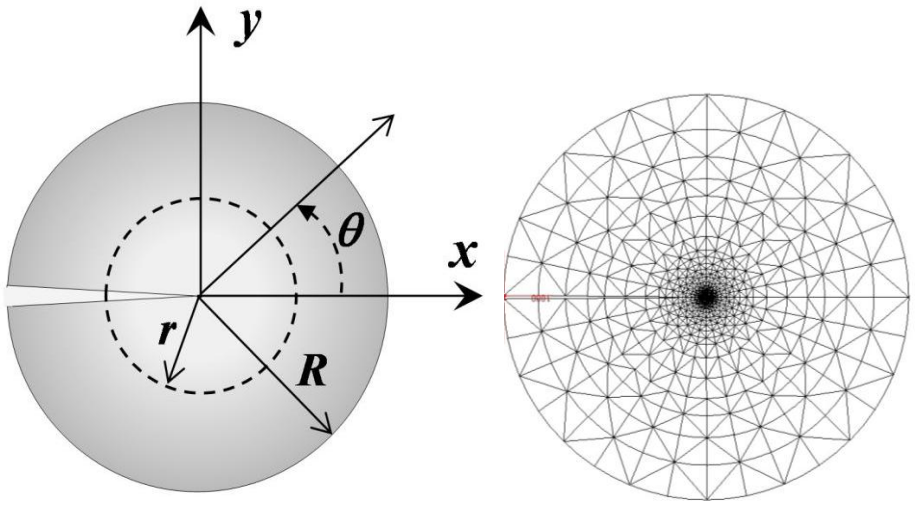

Figure 5-17: Problem Description and FE Model

5.5.3 Material Gradation

The simulations are performed for a viscoelastic FGM with radial gradations for both elastic and viscous properties. A generalized Maxwell model is utilized for representation of time and space dependent material. The functional form of the material properties and the gradation for various components of the generalized Maxwell model are shown in equation (5.13). Notice that the stiffness of material at any given time is greatest along the periphery and lowest at the center of the body. The material gradation is illustrated in Figure 5-18, the plot shows variation of relaxation modulus with time and radial distance, r. In addition to the viscoelastic FGM material two cases representing the most compliant and stiff materials are simulated, these are recovered from Equation (5.13) for $r = 0$ (compliant) and $r = R$ (stiff).

$$E(r,t) = \sum_{i=1}^{2} E_i(r) Exp\left(-\frac{t}{\tau_i(r)}\right);$$

$$E_i(r) = E_0 Exp\left(a\frac{r}{R}\right);\ \tau_1(r) = b\left(1+\frac{r}{R}\right)^c;\ \tau_2(r) = d\left(1-Exp\left(e\frac{r}{R}\right)\right) \qquad (5.13)$$

$a, b, c, d,$ and e are all scalar material constants

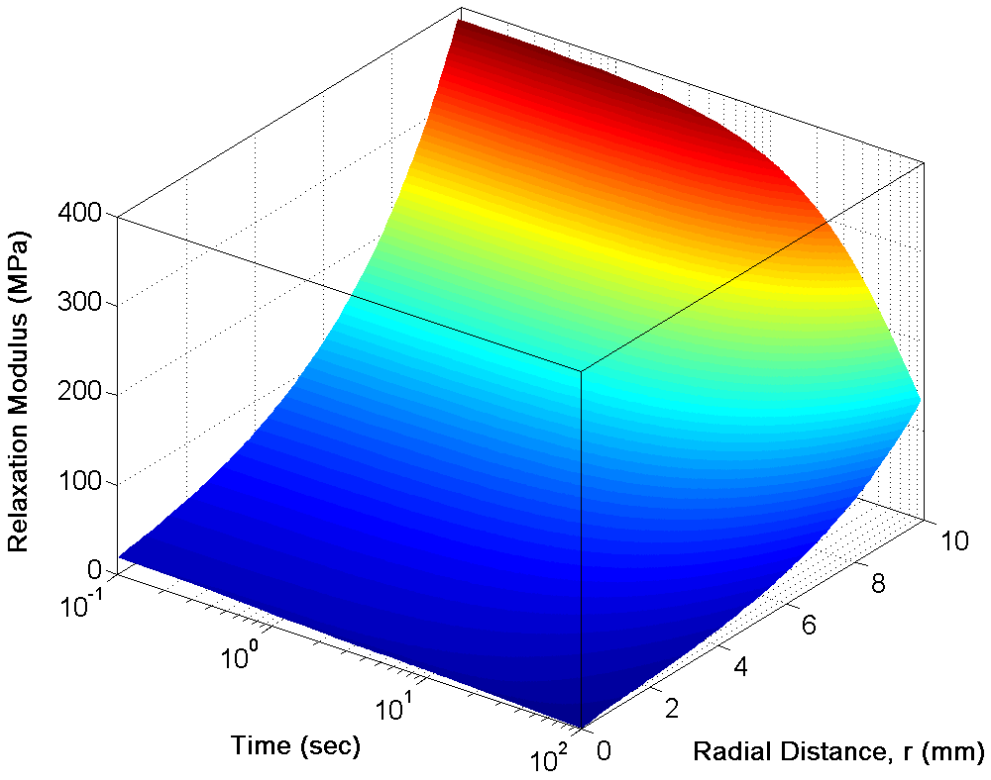

Figure 5-18: Relaxation Modulus Variation with Radial Distance and Time

5.5.4 Results

The elastic stress fields for the homogeneous cases are first visited to ensure the accuracy of the FE solutions. The results at instantaneous loading (time, t = 0) for the "stiff" material are shown in Figure 5-19. The plot shows the variation of stresses at different deflection angles. The results are shown for four radial distances and as anticipated the stresses match closely. This set of results provides confidence that the displacement boundary conditions are accurately imposed and the elastic FE analysis yield correct results.

The elastic normal and shear stress fields for both homogeneous material distributions and FGM distribution are presented in Figure 5-20. Stresses for FGM are shown for one radial distance $\left(r / R = 0.012\right)$. The elastic stresses are found to be matching with the results reported by previous researchers, such as Kim [141]. The FGM stress fields are consistently in between the "stiff" and "compliant" materials, as

expected. Notice that as the deflection angle approaches the crack $(\theta = \pi)$ the stress free conditions are recovered. In order to demonstrate the effect of radial gradation on elastic stresses, normal stresses are plotted at different radial distances for FGM along with homogeneous materials (c.f. Figure 5-21).

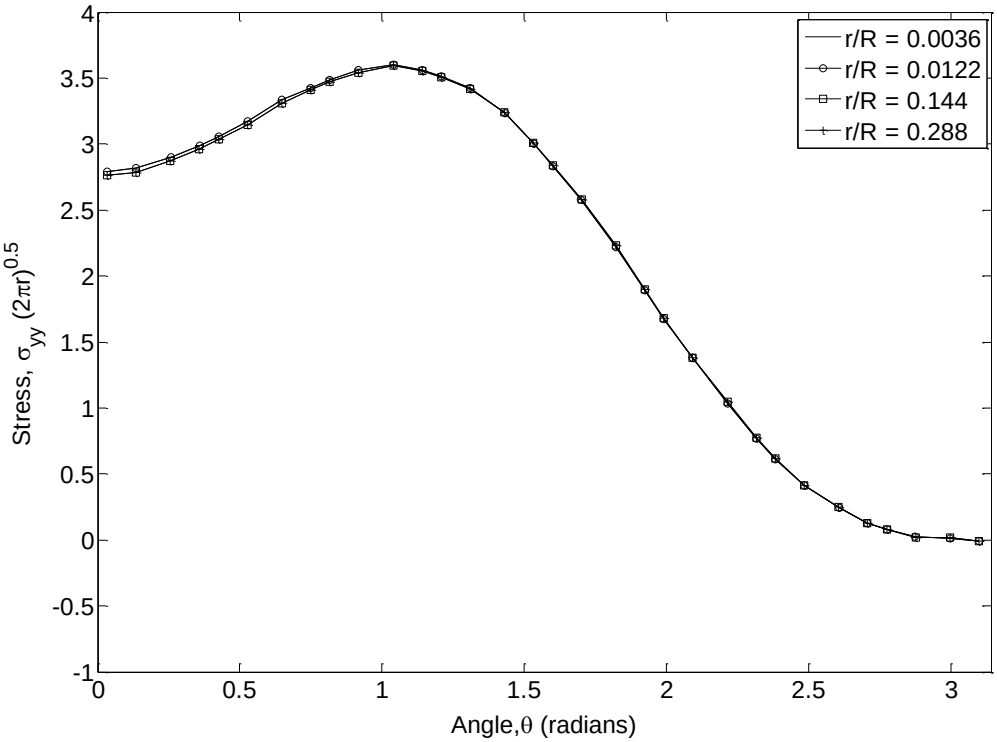

Figure 5-19: Elastic Stresses for Homogeneous "Stiff" Properties at Different Radial Distances

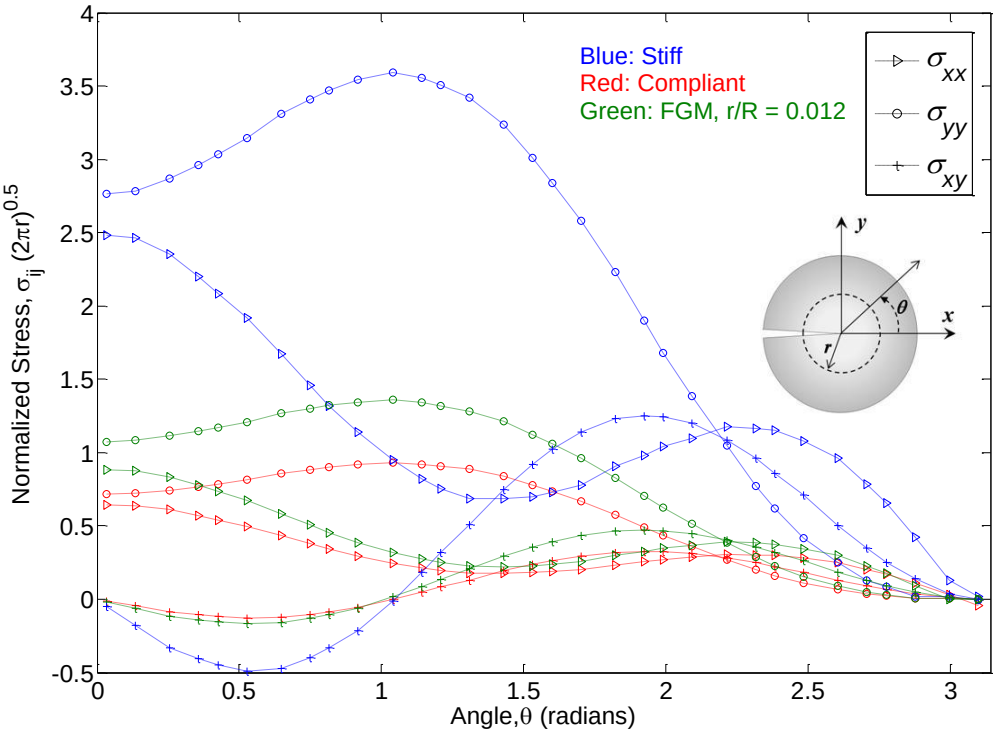

Figure 5-20: Elastic Stresses for All Material Distributions (Homogeneous and FGM)

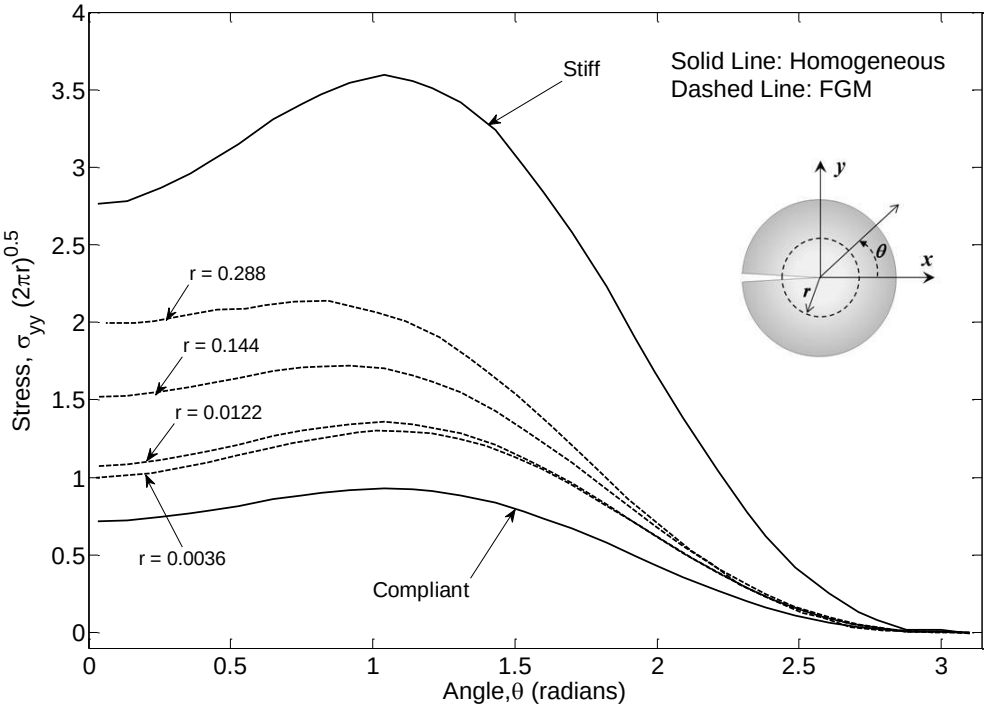

Figure 5-21: Elastic Stresses (y-Direction) for FGM (at Four Radial Distances) and Homogeneous Materials

The key motivation of this study is to demonstrate the viscoelastic stress fields for FGM. The distribution of stresses with time and deflection angles for different material distributions (homogeneous and FGM) is extracted from the FE analysis. The normal stresses (y-direction) for homogeneous and FGM conditions are shown in Figure 5-22. The results clearly demonstrate the viscoelastic stress relaxation with increasing time. In order to further explore the stress relaxation behavior, the peak normal stresses for each material type are plotted against time, as shown in Figure 5-23. It should be noted that the relaxation of stresses is not distributed evenly with time. This trend illustrates the graded nature of the time dependent material properties. If the spatial gradation of constitutive parties was limited to elastic components the plots would have shown constant deviation between different radial distances. For this example, the time effect of property gradation is most pronounced between the radial distances of r/R = 0.0122 and r/R = 0036.

The shear stresses for all material types are shown in Figure 5-24. The greatest shear stresses are observed at shortest loading times and for stiffest material properties. Stress relaxation is evident in all cases as with the normal stresses. Figure 5-25 shows the peak shear stresses for both homogeneous material distributions and at four radial distances for FGM. The relaxation behavior of stresses again demonstrates the effect of combined spatial and temporal variation in properties.

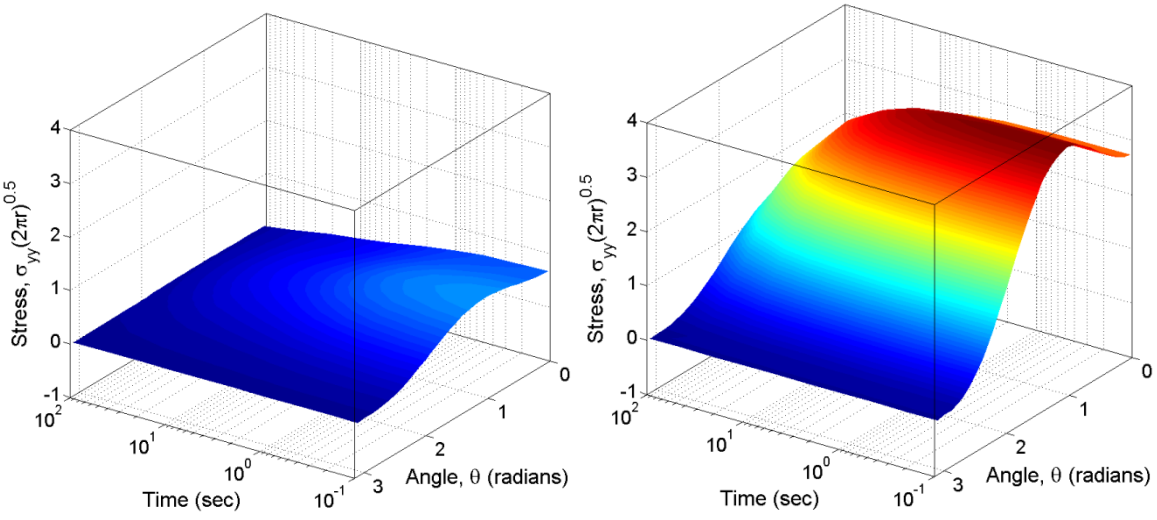

(a) Compliant Material (b) Stiff Material

(i) Homogeneous Material

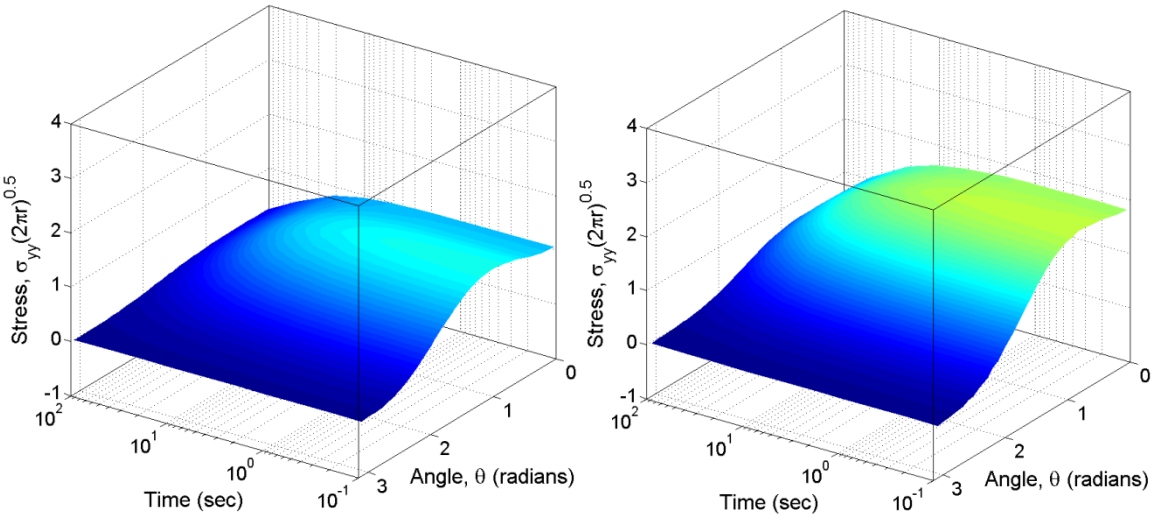

(a) r/R = 0.0122 (b) r/R = 0.288

(ii) FGM

Figure 5-22: Viscoelastic Normal Stresses (y-Direction) for All Material Distributions (Homogeneous and FGM)

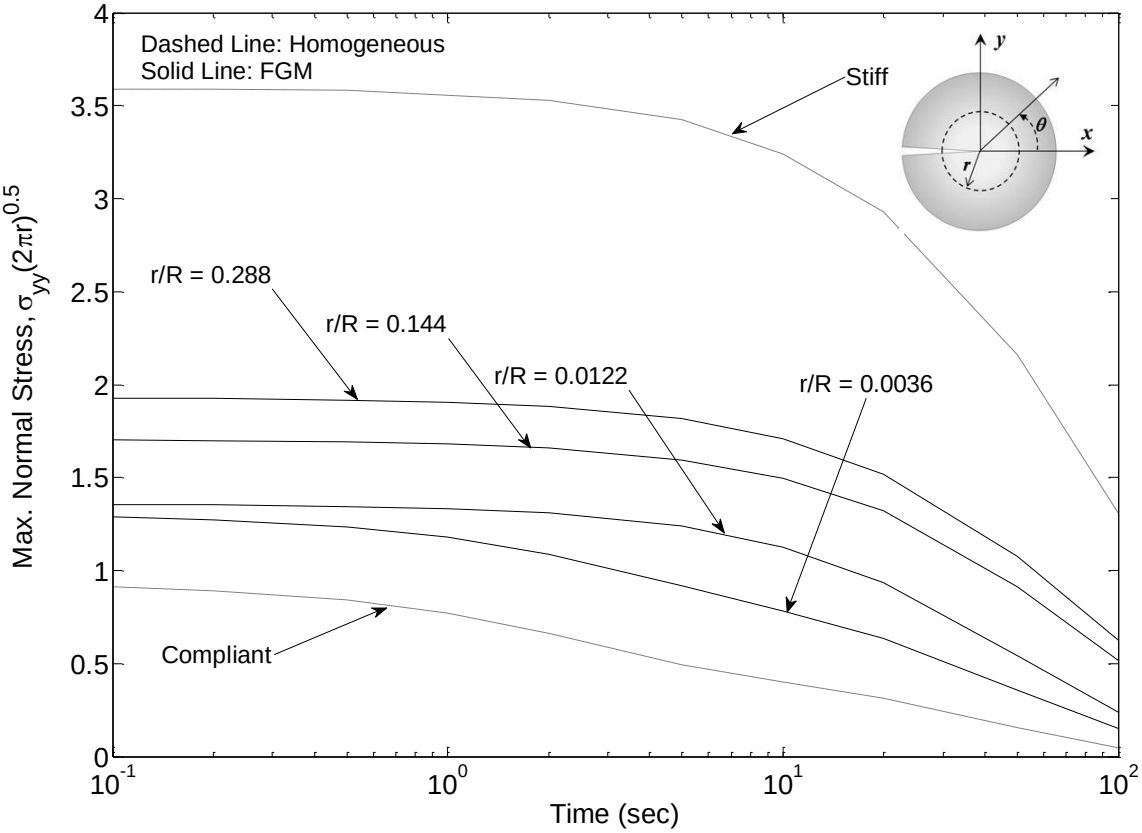

Figure 5-23: Peak Normal Stresses (y-Direction) for All Material Distributions (Homogeneous and FGM)

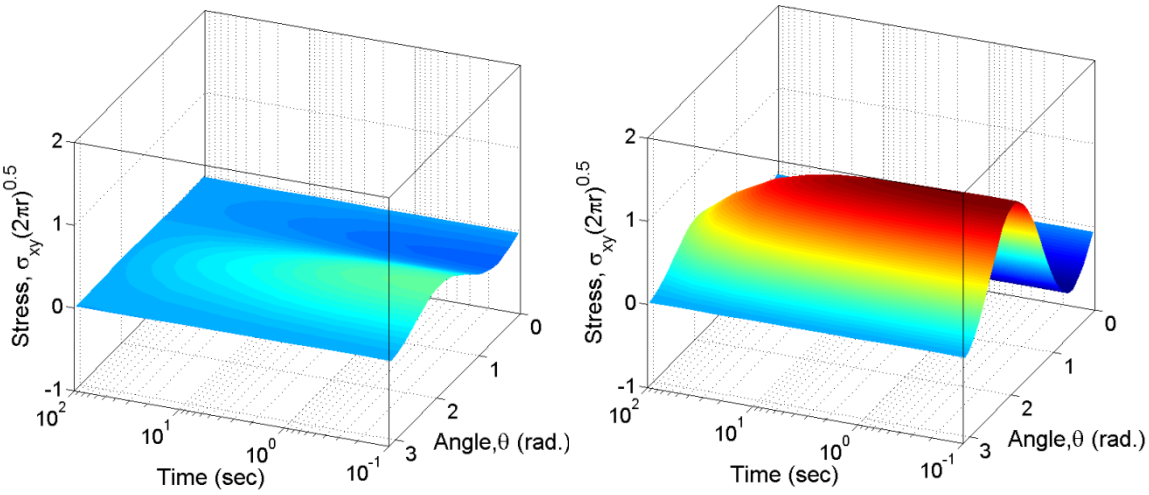

(a) Compliant Material (b) Stiff Material

(i) Homogeneous Material

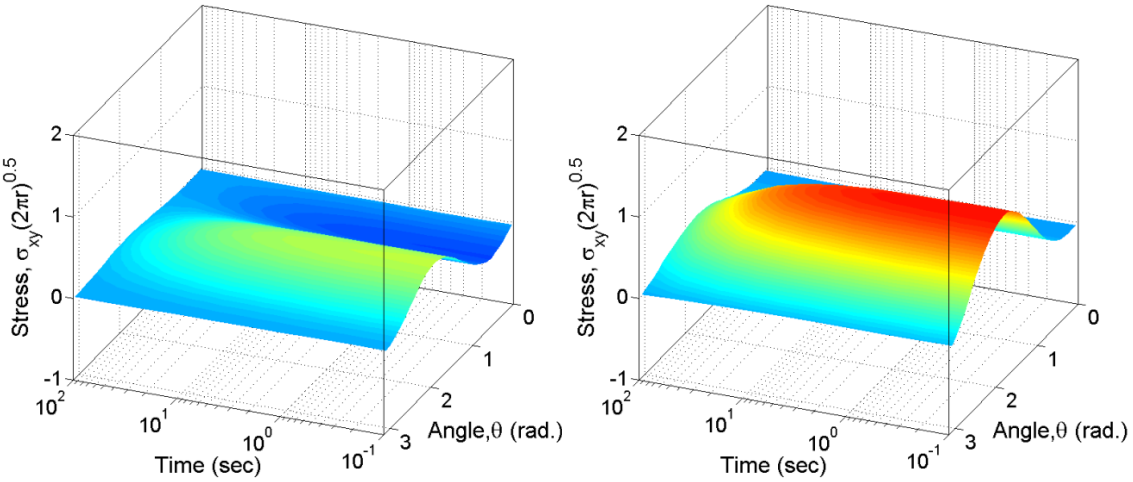

(a) r/R = 0.0122 (b) r/R = 0.288

(ii) FGM

Figure 5-24: Viscoelastic Shear Stresses for All Material Distributions (Homogeneous and FGM)

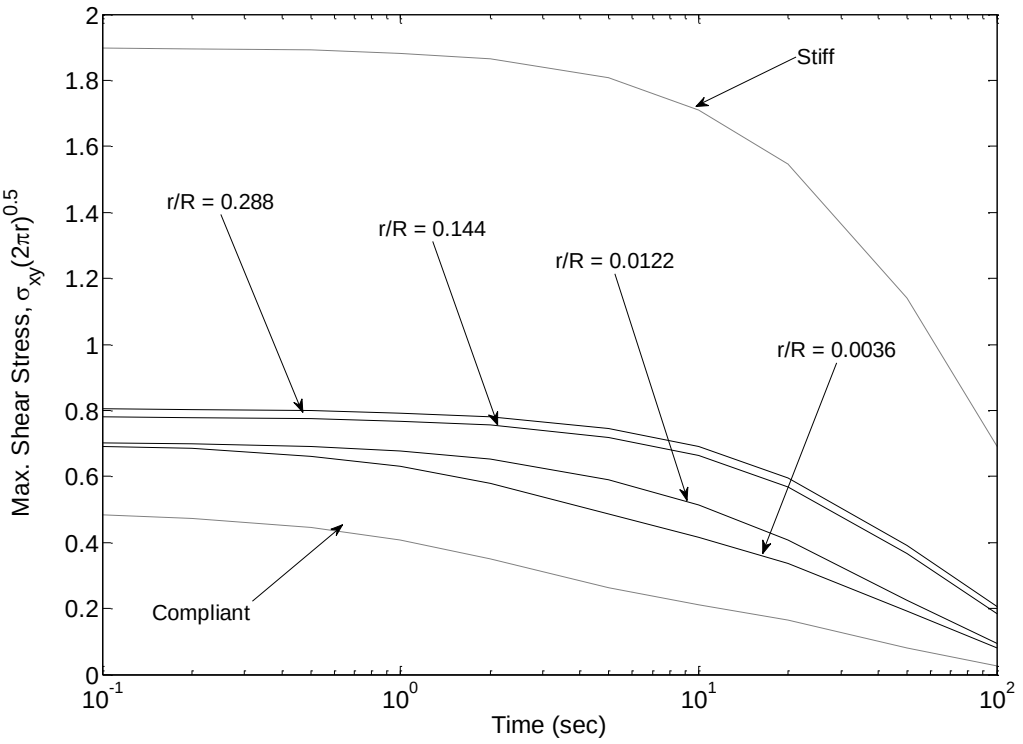

Figure 5-25: Peak Shear Stresses for All Material Distributions (Homogeneous and FGM)

5.5.5 Summary of Boundary Layer Analysis

A radially graded viscoelastic FGM in mode-I loading conditions is simulated to study the crack tip responses. The elastic stress results match the results presented by previous researchers. This further verifies the accuracy and efficiency of the GIF elements and the loading conditions for the example. The viscoelastic crack tip stresses are shown for loading times up to 100 seconds. The non-homogeneous time dependent portions of the constitutive properties are evident from the stress results.

The example presented here demonstrates that the FE formulations discussed in this chapter are capable of predicting the stationary crack fields in viscoelastic FGMs.

5.6 SUMMARY

Various time integration schemes for viscoelastic FE analysis have been explored through a survey of technical literature. Three major classes of time integration methods were identified, namely: (a) direct integration, (b) incremental schemes, and (c) recursive

schemes. The incremental scheme presented by Zak [126] was explored by means of finite difference code. The recursive formulation for non-homogenous viscoelastic finite elements is presented and implemented in form of a computer code. A series of verification examples are shown to verify the implementation for homogeneous and functionally graded viscoelastic problems. An example problem is presented demonstrating the use of proposed formulation for simulation of temperature induced viscoelastic functionally graded boundary value problem. Comparisons are made with commercial software ABAQUS® which demonstrate the accuracy and efficiency of proposed approach over conventional layered approach. The comparison example also validates the present approach for accurate analysis of temperature-induced viscoelastic FGMs, which, apart from aging, is the key source of gradation in asphalt pavements.

Boundary layer analysis for crack tip fields in viscoelastic FGM is presented. The elastic and viscoelastic stress fields are shown for homogeneous and FGM conditions. The results demonstrate the veracity of the time-integration based viscoelastic FE analysis in predicting crack tip fields. This ensures that the current formulation is capable of analyzing asphalt concrete pavements with stationary cracks.

CHAPTER 6 – CASE STUDIES: ASPHALT CONCRETE PAVEMENT SYSTEMS

6.1 INTRODUCTION

This chapter describes the applications aspects of the present research in the context of asphalt pavement systems. The preliminary section describes the relevance and implications of present research in context of analysis and design of asphalt pavements.

Three case studies illustrating the use of the formulations and finite element codes developed in Chapters 3 and 4 for analysis of asphalt concrete pavements. Pavement systems analyzed include aged conventional and full-depth asphalt pavements and overlay-interlayer system with graded interface. The analyses are performed using the research described in this dissertation as well as the conventional approaches. The results from both are compared and contrasted.

6.2 PRACTICAL IMPLICATIONS OF THE PRESENT RESEARCH

The asphalt pavement continuously undergoes property variations due to effects of aging and climatic cycling. A pavement section constructed at the University of Illinois' Advance Testing and Research Engineering Laboratory (ATREL) for study of reflective cracking is shown in Figure 6-1. Notice that on left the pavement is shown immediately following the construction, whereas picture on right shows the pavement after nineteen months. The difference in pavement surface texture and color are result of aging and climatic weathering, this demonstrates continuous variations that asphalt pavements commonly undergo.

Figure 6-1: Pavement Section at ATREL
(left: immediately after construction right: 19 months after construction)

Analysis and design of pavements based only on homogeneous properties obtained using single aging conditions and without consideration of temperature induced gradients leads to non-realistic performance predictions. The present research enables pavement designers to simulate the pavements under various climatic conditions and in-service ages.

The critical pavement distress of interest generally changes with pavement age and climatic conditions. From a mechanistic perspective, the three major distress mechanisms are commonly studied, these include: rutting or permanent deformation, load associated cracking (fatigue and reflective cracking), and non-load associated cracking (thermal and block cracking). For all of these mechanisms it is critical to consider temperature induced property gradients. In addition to this, for cracking related distresses, the aging induced gradation will play a key role.

The practical implication of the present research is to enable pavement engineers to accurately and efficiently predict pavement performance. Based on the distress mechanisms of interest, practicing engineers can select the aging levels and the choice of temperature distribution. For example, a study of thermal cracking performance will require simulation of pavements during critical cooling event with non-homogeneous

temperature distribution and aged pavement conditions. The relevance of the present research is illustrated in realm of pavement design and analysis in Figure 6-2.

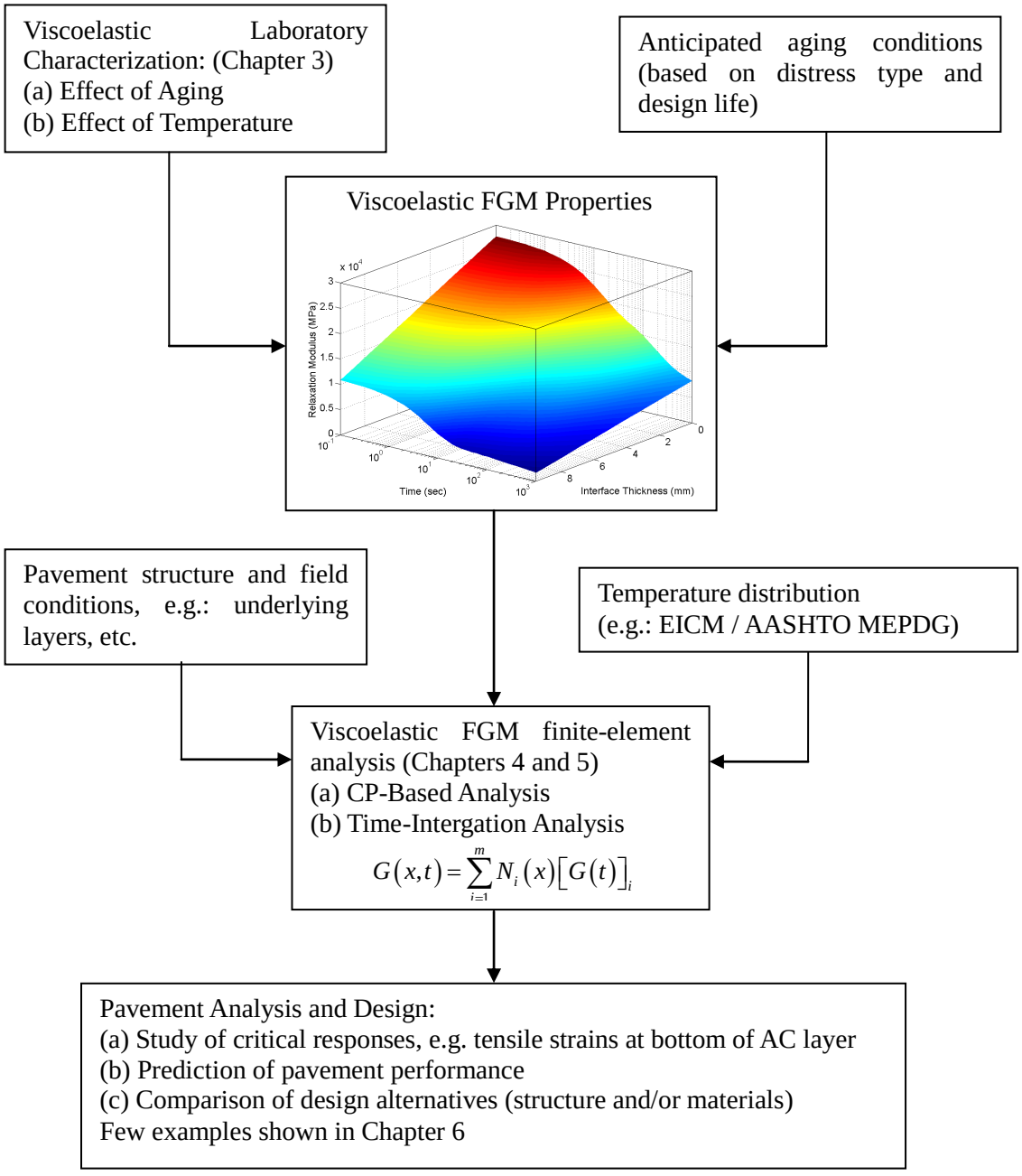

Figure 6-2: Relevance of Present Research in Context of Pavement Analysis and Design

6.3 PAVEMENT SYSTEM 1, CONVENTIONAL ASPHALT PAVEMENT

An asphalt pavement simulation example is presented in this section to illustrate the application of the CP-based graded viscoelastic finite element analysis procedure. The simulation was also conducted for the same problem using the layered approach, and results from layered and graded approaches are compared.

6.3.1 Pavement Section

A conventional asphalt pavement section was simulated. Section details are shown in Figure 6-3 along with the finite-element mesh.

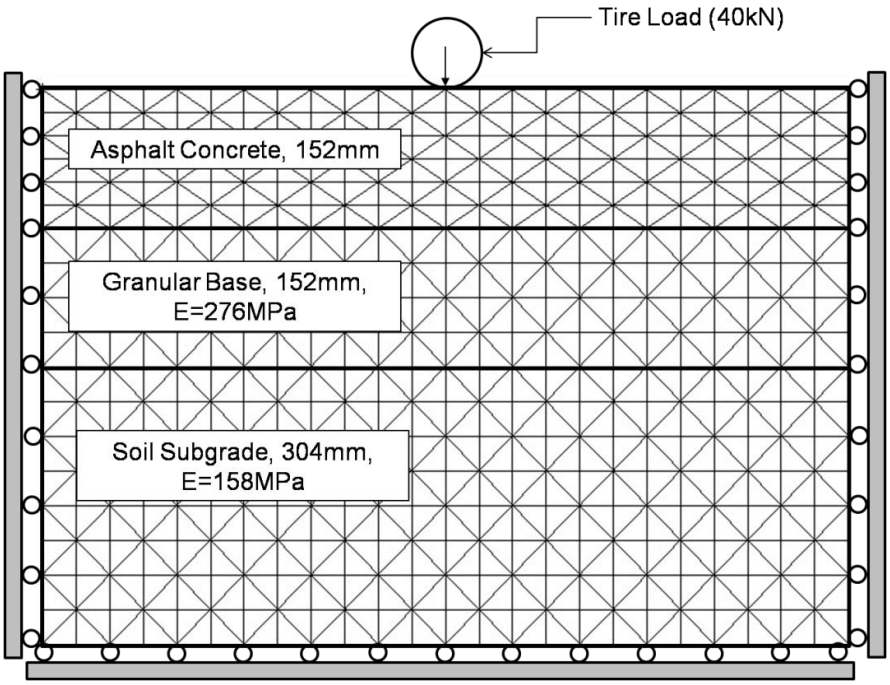

Figure 6-3: Pavement Section and FE Mesh

6.3.2 Asphalt Concrete Properties

The pavement is assumed to be highly aged, and hence the asphalt concrete layer is simulated as a graded viscoelastic material. Apeagyei et al. [34, 143] have studied the effects of antioxidant treatment on asphalt binders and mixtures. They have performed viscoelastic characterization of short-term and long-term aged asphalt mixtures. Short term and long-term aged properties from Apeagyei et al. are utilized for simulation of aged asphalt concrete pavement in this example. The shear relaxation modulus is

assumed to be varying linearly through the pavement thickness, going from a long-term aged condition on surface to a short-term aged condition on the bottom of the asphalt concrete layer. This is illustrated in Figure 6-4. The bulk modulus is assumed to be constant with time. In the case of the layered simulation, the asphalt concrete layer is divided into six layers, where each layer is assigned average properties.

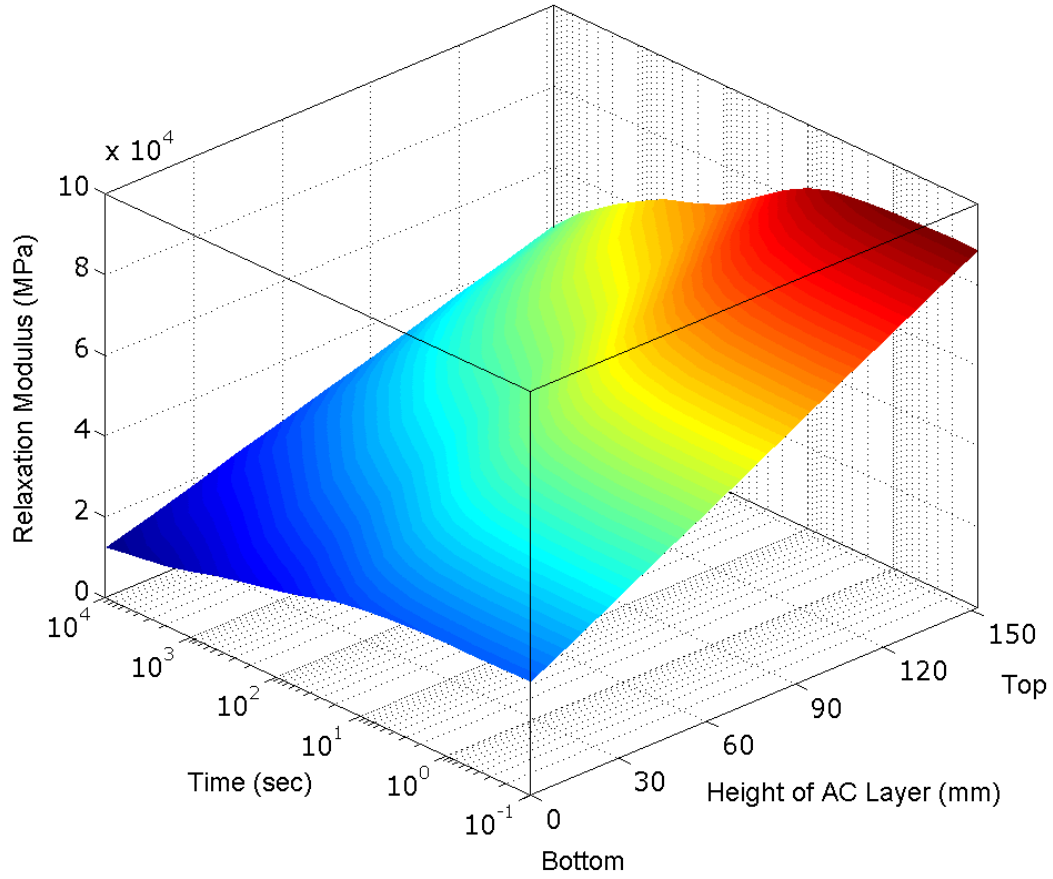

Figure 6-4: Relaxation Modulus of Asphalt Concrete (variation with height of AC layer and time)

6.3.3 Boundary Conditions

Boundary conditions for the simulation problem are given in Figure 6-3. The imposed load is applied to simulate a single 40kN (9000lb) tire with 700kPa (100psi) pressure. Contact pressure is assumed to be vertically oriented (no horizontal loading). The asphalt concrete temperature is assumed to be uniform through the thickness, with a value of -10°C.

6.3.4 Results and Discussions

In the case of asphalt pavements, stresses in the horizontal direction are often of interest to the pavement engineer, as they are taken as critical response parameters at low and intermediate temperatures. These stresses are commonly linked to fatigue cracking in pavements, which is one of the most devastating pavement damage mechanisms. The horizontal stresses directly under the tire load are compared for layered and graded viscoelastic approaches. The results are shown in Figure 6-5 for stresses at a loading time of 100 seconds. Notice that in order to exaggerate the difference between layered and graded approaches, the nodal stresses are presented for the graded approach, whereas for the layered approach, the nodal stresses are averaged in a layered fashion. Hence the discontinuities are observed at layer interfaces. It is interesting to note that the extent of tensile stresses is relatively low as compared to the compressive stresses near the surface. This trend is not unexpected for the aged pavement system, as the material closer to surface is stiffer and thus accumulates greater stresses, while unaged material near the bottom is compliant and exhibits a greater degree of stress relaxation.

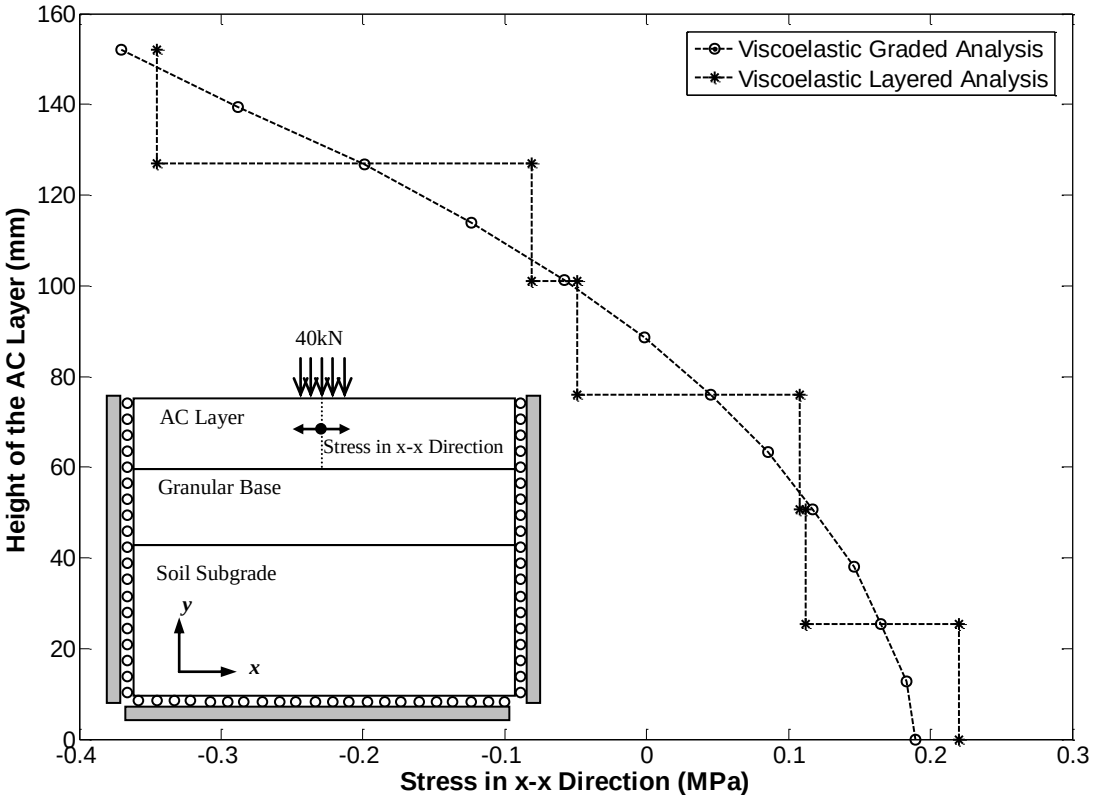

Figure 6-5: Stresses in Horizontal Direction (x-direction) directly under the Tire Load

6.4 PAVEMENT SYSTEM 2, FULL-DEPTH ASPHALT PAVEMENT

A full-depth asphalt pavement is modeled using aged, unaged, functionally graded and layered gradations. The pavement section is modeled after interstate highway I-155 near town of Lincoln, IL located in mid-western USA. This pavement has been previously studied by Buttlar et al. [39] using graded finite-element technique.

6.4.1 Pavement Section

This section of highway is constructed as a full-depth asphalt concrete pavement with lime-stabilized clay subgrade. The pavement consists of a 1.5-inch of surface course followed by 13-inches of binder course. The cross-section of the pavement is illustrated in Figure 6-6.

Figure 6-6: Full-Depth Asphalt Pavement Section (I-155, Lincoln, IL)

6.4.2 Asphalt Concrete Properties

The asphalt concrete properties for the simulations are approximated based on the laboratory test results reported by Apeagyei et al. [34, 143]. In order to simulate an aged pavement condition, it was assumed that short-term aged properties represent material at the bottom of asphalt concrete layer and long term aged properties represent material at the top of asphalt concrete layer (c.f. Figure 6-6). The variation of the material properties is chosen similarly to that predicted by the Global Aging Model [33]. Figure 6-7 shows the relaxation modulus variation with time and space (across asphalt concrete thickness).

As anticipated, the material is significantly stiffer at the pavement surface and short loading times; and conversely, most complaint near the pavement bottom at longer loading times.

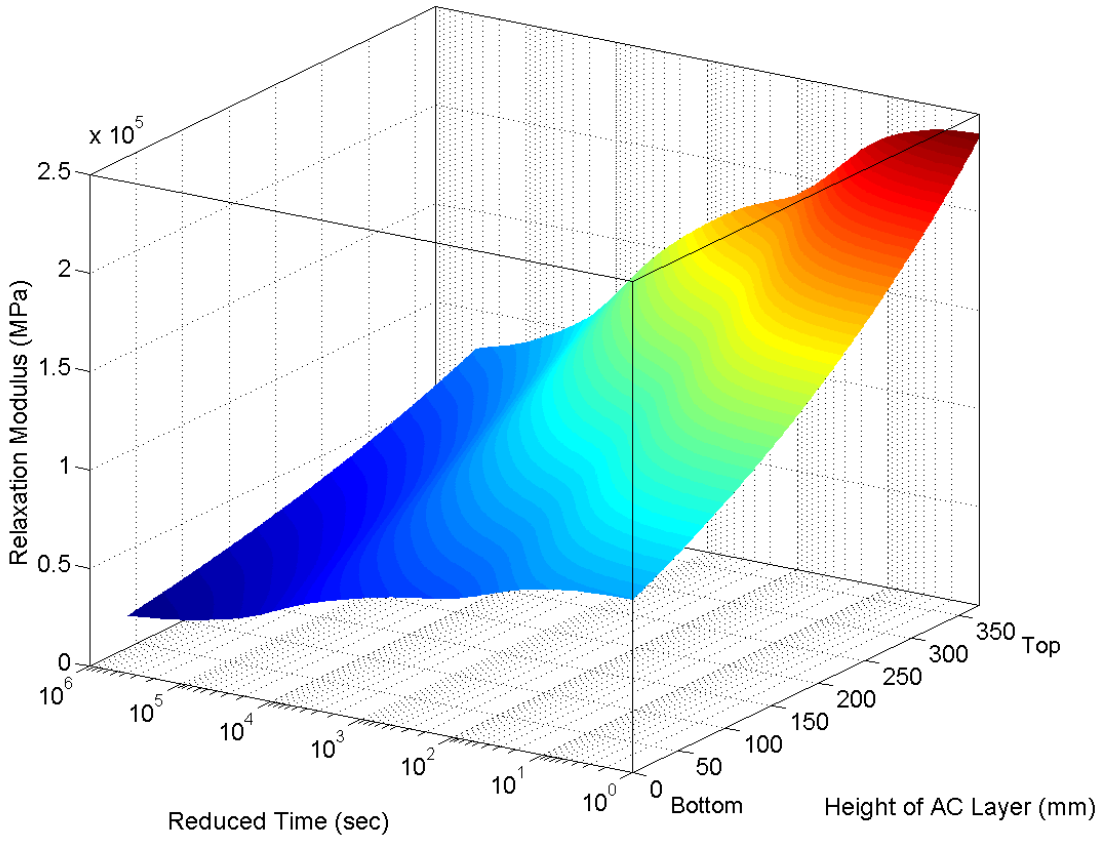

Figure 6-7: Relaxation Modulus of Full-Depth AC Pavement (variation with Height of AC Layer and Time)

As mentioned previously four material distributions are simulated. Viscoelastic FGM analysis is performed by simulating the spatial and temporal material variation which is shown in Figure 6-7, and thus this material representation is labeled as "FGM" throughout the rest of this section. Layered approximation is utilized to compare and contrast with the FGM approach; thus this representation is labeled as "Layered" and two homogeneous materials are simulated representing short term aging properties ("Unaged") and long-term aging properties ("Aged"). The "Aged" and "Unaged" properties are similar to those shown in Figure 6-7 at top (height = 375.1 mm) and

bottom (height = 0 mm) of asphalt layer respectively. For layered approximation the surface course is divided into six layers (6.35 mm each) and the base course is divided into sixteen layers (21 mm). The property gradients are significantly steep near the top of asphalt concrete, thus finer resolution is utilized near the top.

6.4.3 FE Model and Boundary Conditions

A two-dimensional axisymmetric model is used for the simulations. Two levels of mesh discretizations are utilized. Two meshes are generated; the first one is utilized for simulation of graded and homogeneous material properties (FGM, Unaged, and Aged properties), and the second one with higher refinement is utilized for performing simulations using layered approximation. The FE meshes for the full domain as well as the asphalt concrete layers are shown in Figure 6-8. The total nodal degrees of freedom for the coarser mesh are 72150, versus 129060 for the finer mesh utilized in the layered approach.

A single tire with 40 kN (9000 lb.) load and 758 kPa (100 psi) inflation pressure is simulated. The simulations are performed for quasi-static loading conditions with the loading times up to 1000 seconds. The domain extent, load and displacement boundary conditions are shown in Figure 6-9.

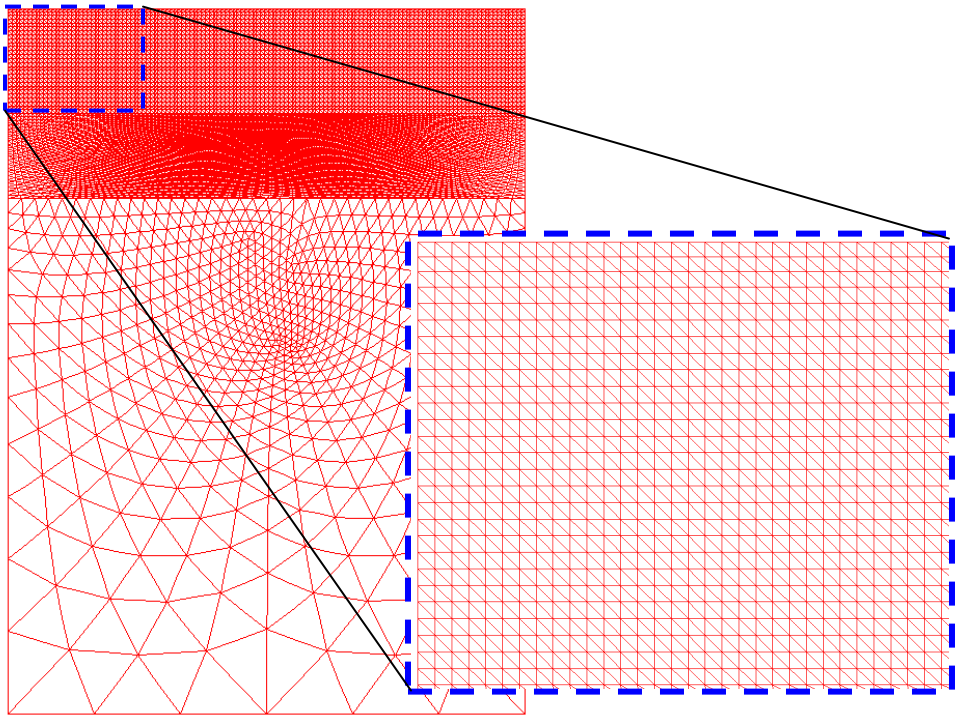

(a) Fine Mesh (AC Properties: Homogeneous and FGM), 72150 DOFs

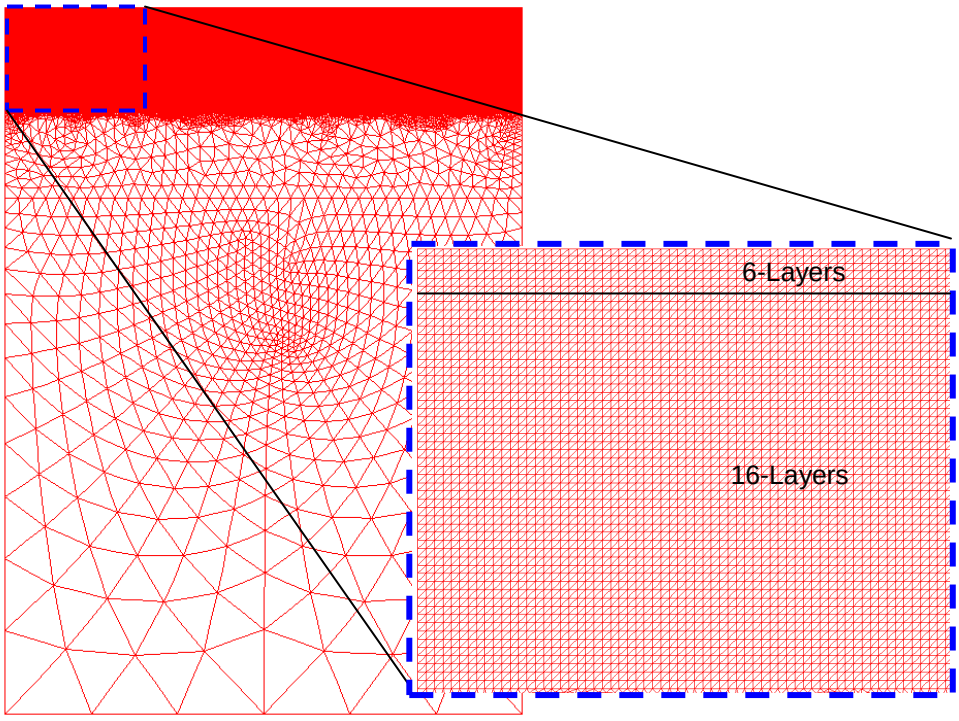

(b) Coarse Mesh (AC Properties: Layered Gradation), 129060 DOFs

Figure 6-8: FE Meshes for Full Depth AC Pavements (Inset: Region of AC Layers)

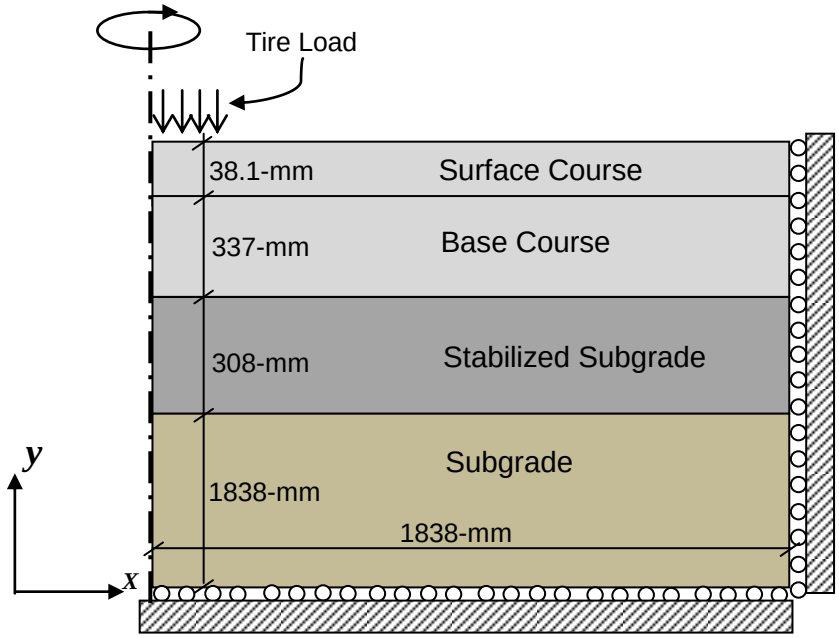

Figure 6-9: FE Model Schematic

6.4.4 Results

The pavement response parameters that are commonly utilized in analysis and design of asphalt pavements are: (1) compressive strain at the top of asphalt concrete, (2) tensile strain at the bottom of asphalt concrete, and (3) shear strain at the edge of tire load. The first two have been empirically related to pavement's permanent deformation and fatigue behaviors. The shear strain has been recently studied by several researchers to relate it with longitudinal cracking along the wheel path.

The vertical strains directly under the wheel load for different loading times are shown in Figure 6-10 for unaged material properties. The results are as anticipated with the compressive strains reaching peak value shortly under the surface and dropping off with increasing depth. The viscoelastic effect is also evident in this plot, showing increase in strains with longer loading times.

The peak compressive strains near the top of asphalt layer for each of the four material properties (unaged, aged, FGM, and layered) are shown in Figure 6-11. Similarly the peak tensile strains near the bottom of asphalt layer and peak shear stresses

at the edge of tire loading for each of the material property distributions are shown in Figure 6-12 and Figure 6-13 respectively.

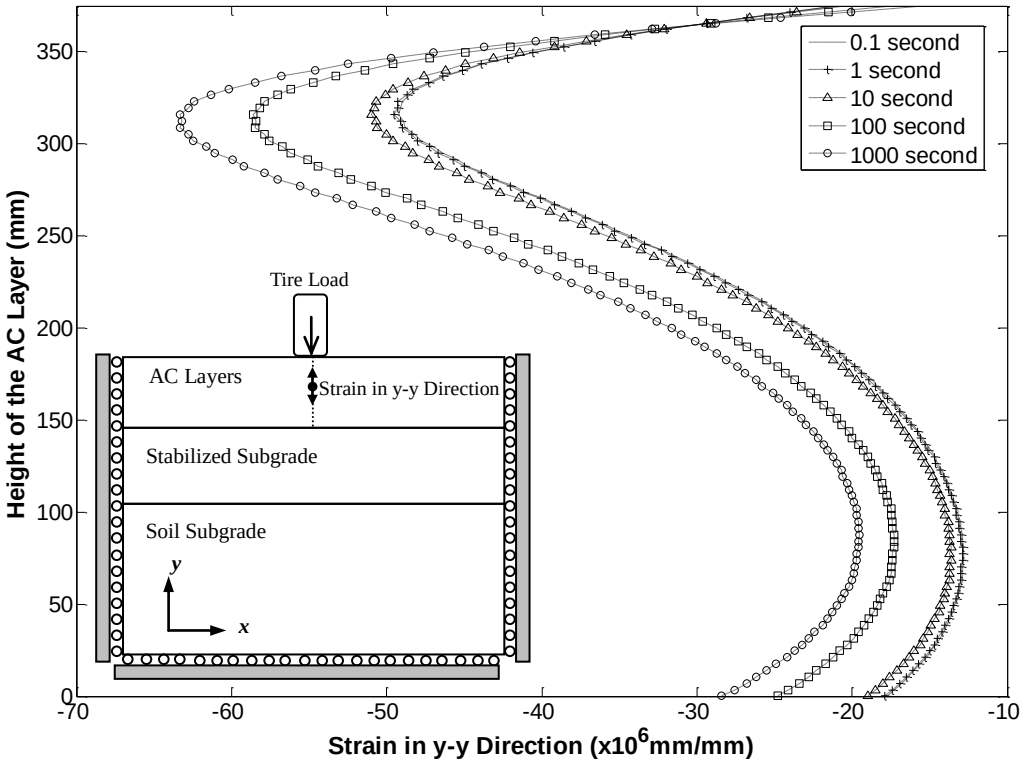

Figure 6-10: Strain in y-y Direction across AC Thickness for Unaged Conditions

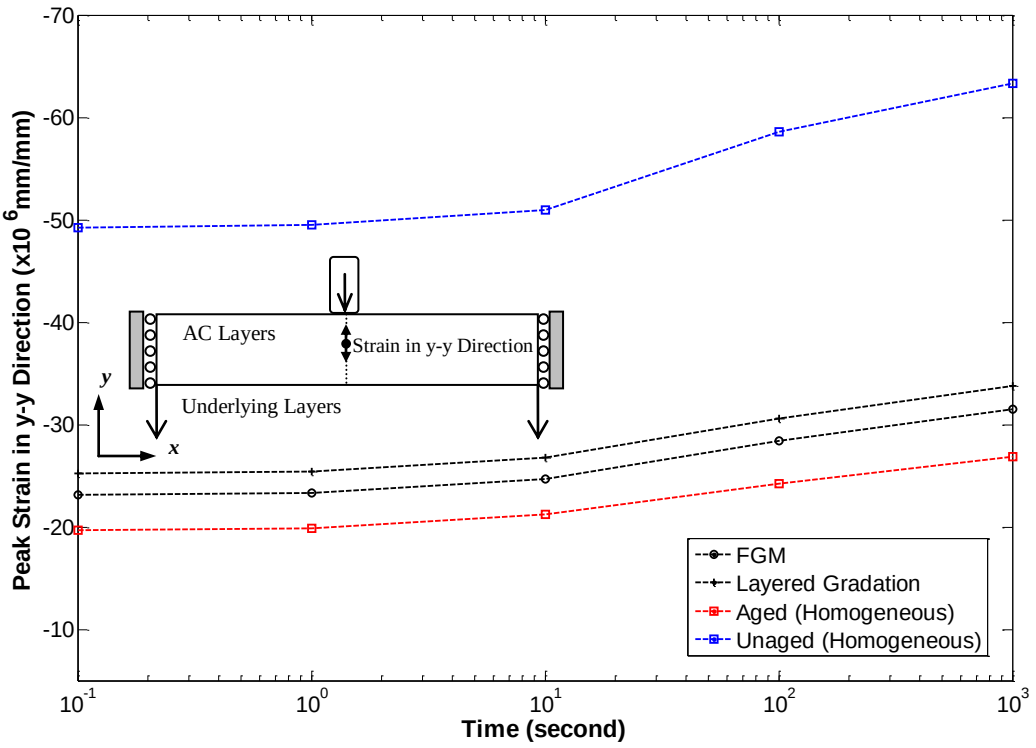

Figure 6-11: Peak Strain in Vertical (y) Direction

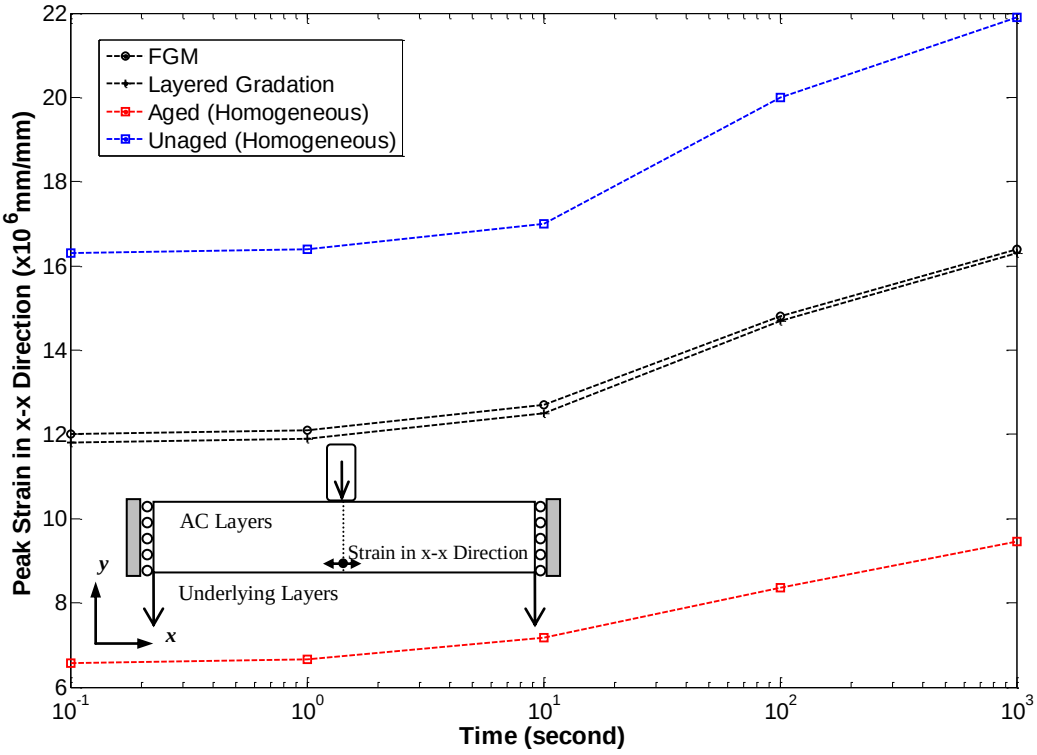

Figure 6-12: Peak Strain in Horizontal (x) Direction

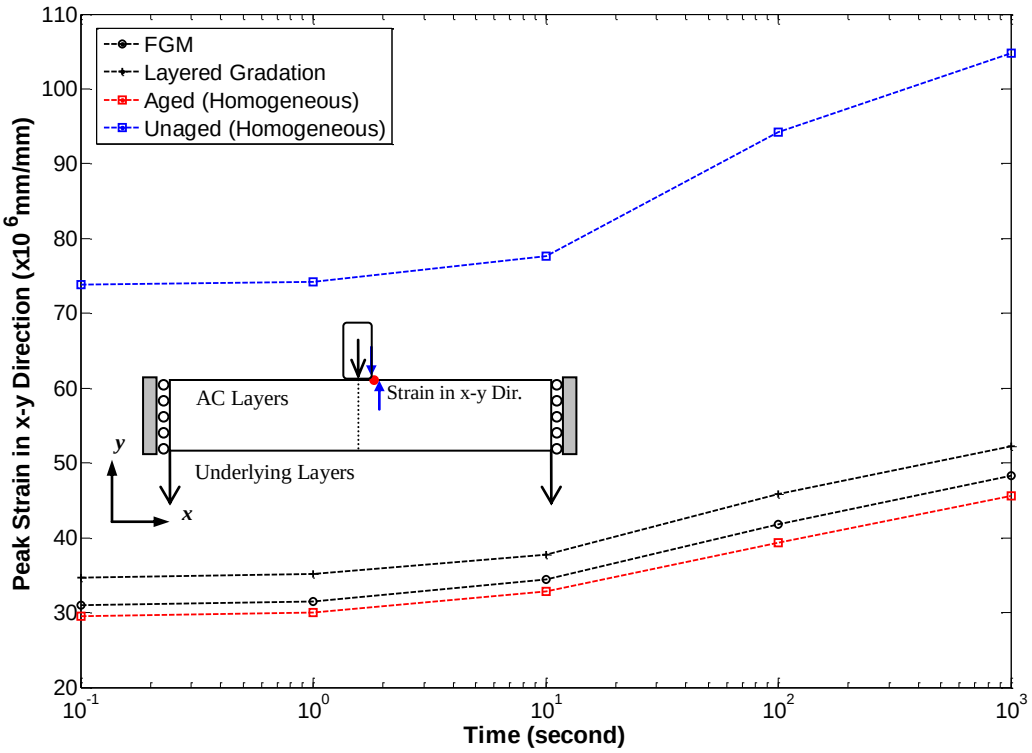

Figure 6-13: Peak Shear Strains (x-y Direction)

6.4.5 Discussion of Results

The typical responses indicate that the layered approach provides reasonable approximation compared with the graded approach. However it should be noted that significantly higher mesh refinement is utilized for the layered analysis. In addition to this, the quantities in the plots are evaluated in proximity of surface or bottom of asphalt concrete where the responses may not have been so sensitive to the material variation. The predictions from layered approaches are questionable at the interfaces of layers and this could lead to significant errors in the analysis, as illustrated by looking at a response at the interface of surface and base course within asphalt pavement. Figure 6-14 shows strains in y-y direction near the interface at 1000 second loading time. It can be observed that as much as 20% error is incurred while utilizing layered approach, whereas the graded approach provides smooth predictions without jump in the strains.

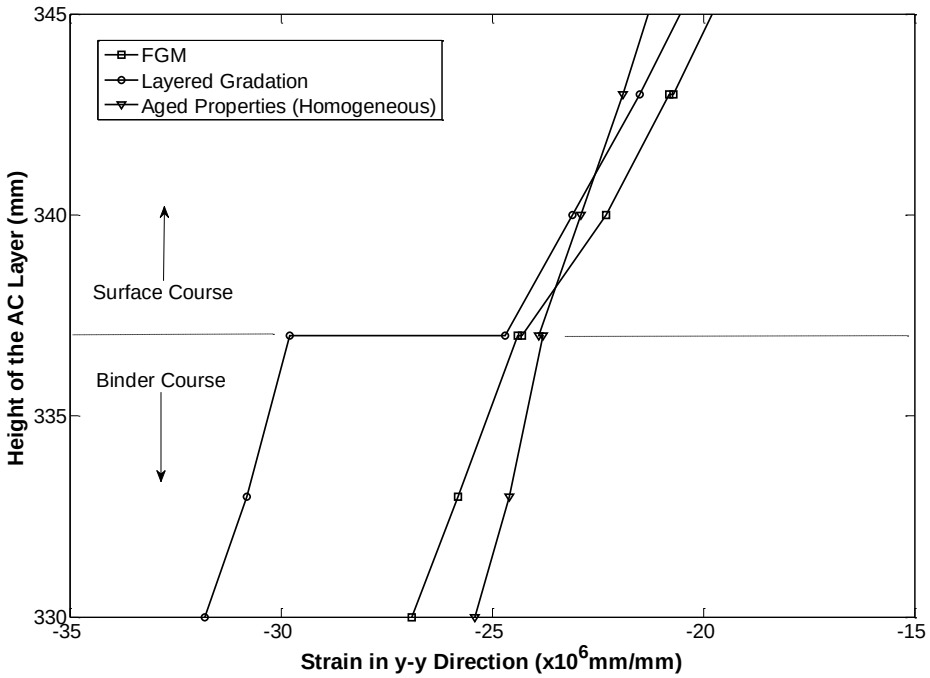

Figure 6-14: Strain in Vertical Direction at Interface of Surface and Binder Courses

The following key points can be observed from the simulation results:

- It is important to consider effects of aging in the course of analysis; the unaged predictions made using unaged properties may be significantly different from those obtained with the consideration of aging.
- The viscoelastic FGM analysis procedure developed herein provides an accurate and efficient way of analyzing asphalt pavements.
- Layered approach may provide results with significant errors in derivative quantities at the layer interfaces.
- The most severe response observed for this limited study was the high magnitude of shear strains generated at the edge of tire load.

6.5 PAVEMENT SYSTEM 3, OVERLAY-INTERLAYER SYSTEM WITH GRADED INTERFACE

6.5.1 Introduction and Motivation

A common practice in the design and construction of asphalt concrete layers in a pavement is to utilize a number of different courses ranging from 18 mm (3/4 inch) to 75 mm (3 inch) in thickness. The interfaces between these layers form a continuously graded zone of finite thickness. In the case where the asphalt pavement is constructed with the same asphalt concrete for different courses this interface does not require any special attention for modeling. In contrast, for the pavements designed and constructed with layers of significantly different properties it is critical to give due attention to the graded nature of the interface. Typical examples of pavement systems with significantly different materials include overlay–interlayer systems, surface treatments with open graded mixtures laid on top of dense graded mixtures, and special treatments that yield varying asphalt binder content through the thickness of course, such as chip seals or bonded overlays. The interfaces of different construction lifts are shown in Figure 6-15 for two asphalt pavements. The boxes (dotted lines) indicate the region of interface where visually it could be observed that materials from the two layers have varying properties.

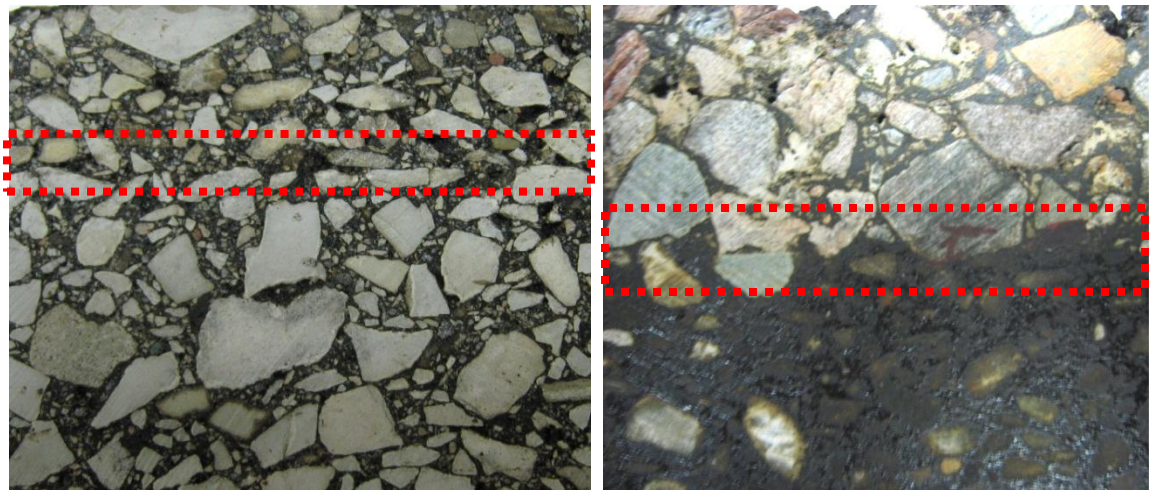

Figure 6-15: Cross Section of Asphalt Pavements showing Interfaces between Different Construction Courses

The current state of practice in modeling of asphalt concrete pavements is to assign infinitesimally small thickness to the interface between different asphalt courses or lifts. In the current example, this type of approach is labeled as “Stepped Interface” due to jump in material properties at the boundary. The viscoelastic FGM FE analysis procedure developed in this dissertation may be a useful tool for the simulation of viscoelastic interfaces. This example compares the responses obtained for graded versus stepped interfaces for asphalt pavements. Furthermore it demonstrates the capability of formulations presented herein to simulate the graded interfaces.

6.5.2 Pavement Section

The pavement section from Louisiana State Highway, LA34 located near town of Monroe in northern Louisiana is selected as the basis for constructing the simulation model. The pavement section is constructed in form of overlay-interlayer system. This pavement is part of the NSF sponsored reflective cracking study by Paulino et al. [12]. Figure 6-16 shows the picture of pavement section, which undergoes heavy truck traffic due to its close proximity to paper mill.

6.5.3 FE Model and Boundary Conditions

The finite element model for the pavement analysis is developed on basis of the pavement information obtained from site visits as well as the cross section details obtained from construction plans and cored samples. Figure 6-17 shows the cross section of the pavement as utilized for FE model construction. The FE simulations are performed using an assumption of 2D axisymmetric conditions.

As described previously, the focus of this example is to compare two simulation approaches for interfaces between asphalt concrete construction lifts, Figure 6-17 illustrates the two simulation approaches regarding the representation material gradation.

Figure 6-16: Pavement Section (LA34 near Monroe, LA)

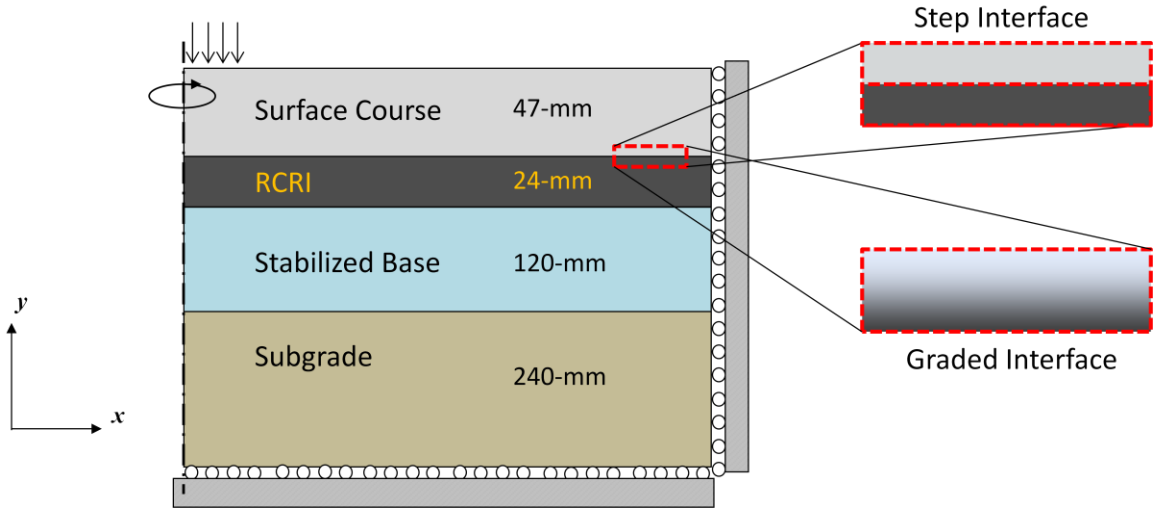

Figure 6-17: Pavement Cross Section and FE Model Schematics

Two key properties are needed for accurate simulation of graded interfaces, (1) height or width of interface, and (2) distribution of material properties within the interface. In this example, the following assumptions are made:

- The width of the interface is 9.5 mm; this assumption is made on the basis of the nominal maximum aggregate sizes (NMAS) of the asphalt mixtures. The surface course is a 19 mm NMAS mixture and the RCRI mixture is 4.75 mm NMAS.

- The material properties are assumed to be transitioning in linear fashion from one mixture to another over the thickness of interface. A better approach for obtaining viscoelastic property gradation at the interfaces would be to incorporate micromechanical approaches such as those proposed by Yin et al. [144], which, preferably, would be validated through experiments. This has been identified as one of the future extensions of this dissertation.

6.5.4 AC Material Properties

Wagoner et al. [16] have tested and analyzed the field core samples from LA34 highway. The relaxation moduli for overlay and interlayer mixtures are shown in Figure 6-18. The variation of material properties at the interface for "step interface" and "graded interface" are shown in Figure 6-19 and Figure 6-20 respectively. Notice the mismatch of properties at midpoint of interface for the stepped approach.

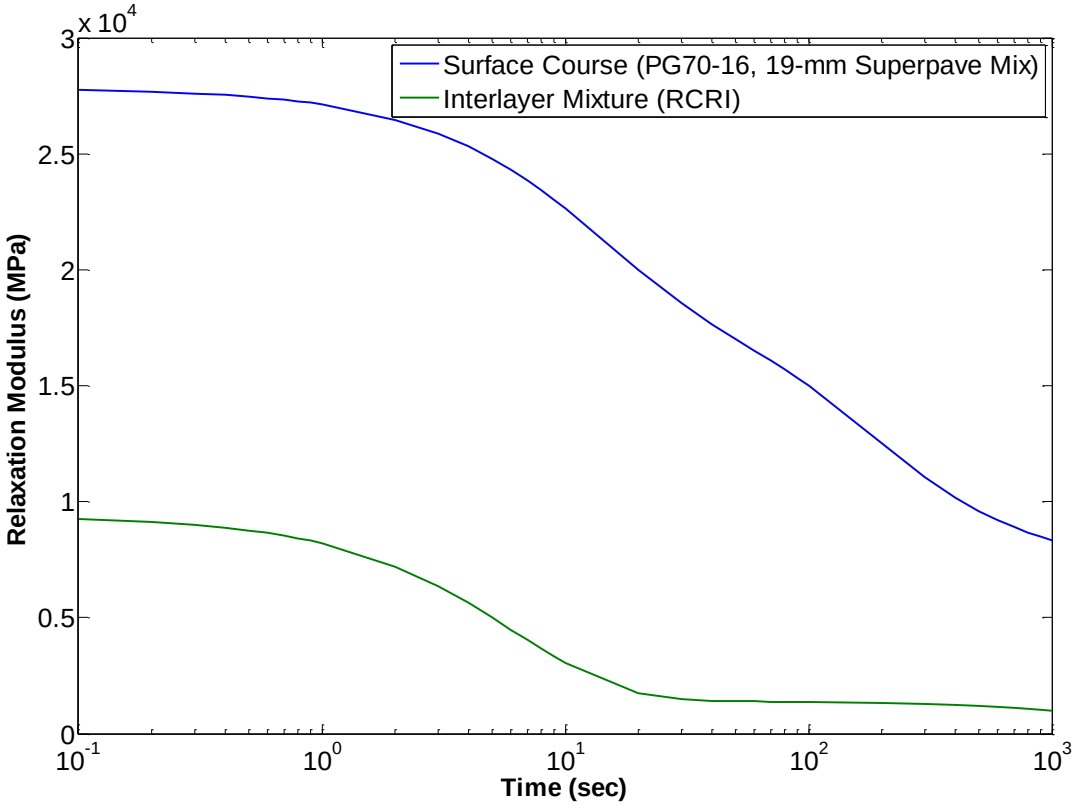

Figure 6-18: Relaxation Modulus for Surface and Interlayer Mixtures

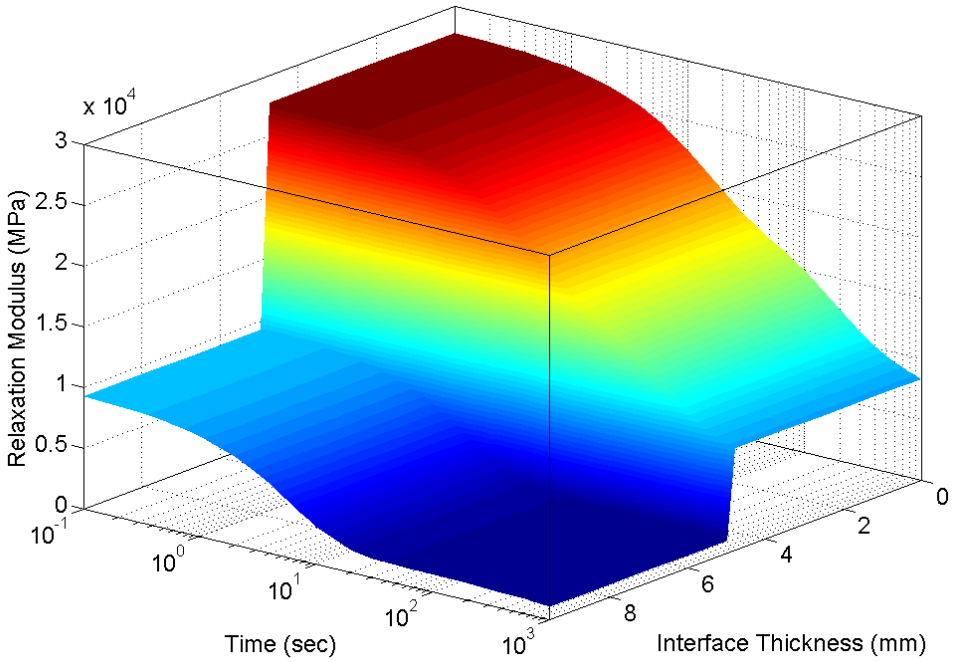

Figure 6-19: Relaxation Modulus Variation for Step Interface

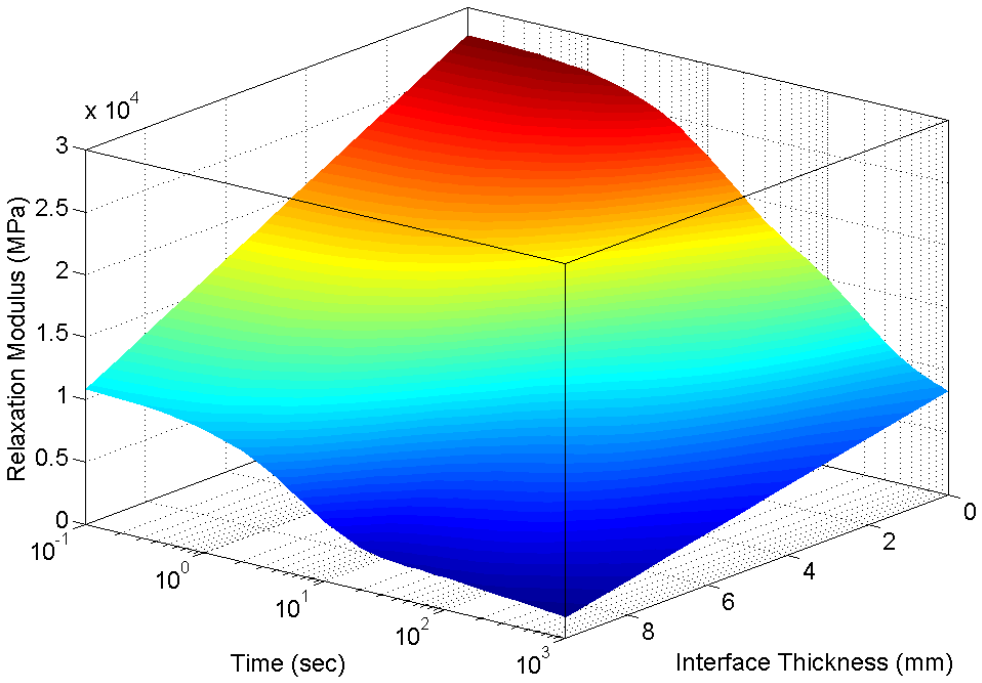

Figure 6-20: Relaxation Modulus Variation for Graded Interface

6.5.5 Results

The response parameter that is utilized for comparing the two simulation approaches is the stresses in horizontal direction directly under the tire load. Figure 6-21 shows the variation of stresses as function of height of asphalt layers. The results are presented for 10, 100, and 100 second loading times. Notice that the stresses exhibit non-physical "jump" at the step interface. This jump in stresses is illustrated in Figure 6-22; the plot shows variation of as much as 49% between the predicted tensile stresses at the bottom of overlay. The tensile stresses at bottom of overlay are important for reflective cracking simulations. In particular, the tensile stresses are compared with tensile strength of material and that serves as the threshold parameter for onset of damage.

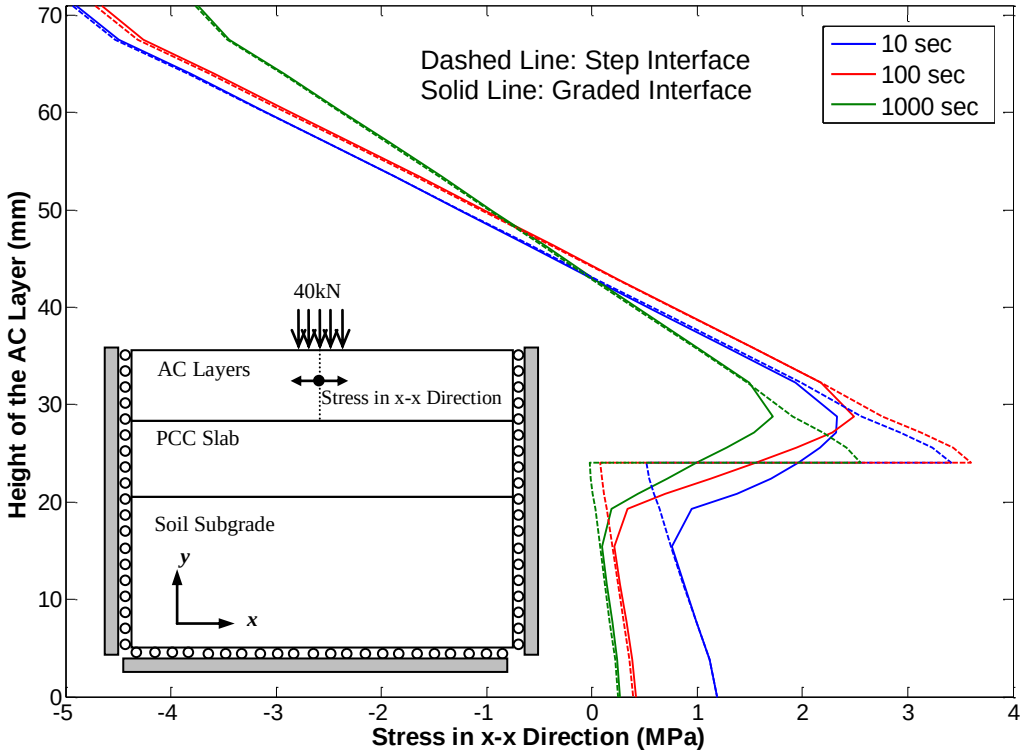

Figure 6-21: Stress in Horizontal Direction (x-direction) directly under the Tire Load (different loading times are shown)

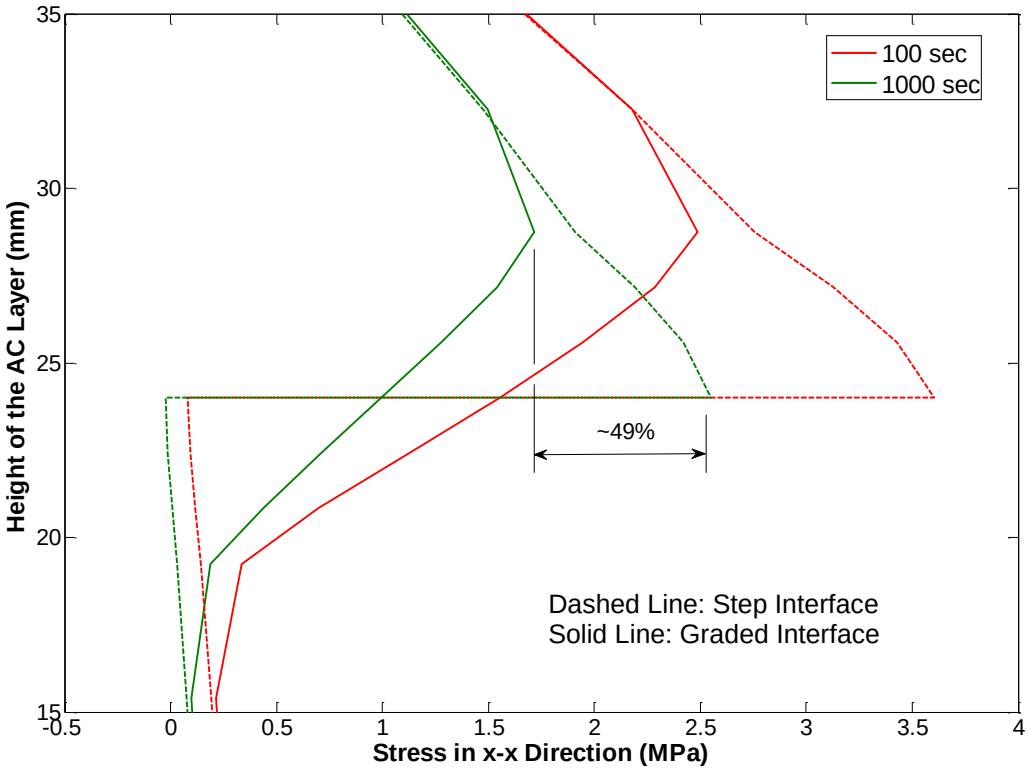

Figure 6-22: Stress in Horizontal Direction (x-direction) at Interface

The variations of peak tensile stresses within the interface with loading times are shown in Figure 6-23. The plot shows peak stresses for graded interface and three set of plots for step interface: (1) peak stress for surface course, (2) peak stress for RCRI, and (3) Average of surface course and RCRI stresses. The motivation for plotting average stresses for step interface is to demonstrate that simple averaging of responses (stresses or strains) at the interface significantly over predicts the response compared to graded interface. For the current example the averaging yields as much as 30% higher values when compared to graded interface.

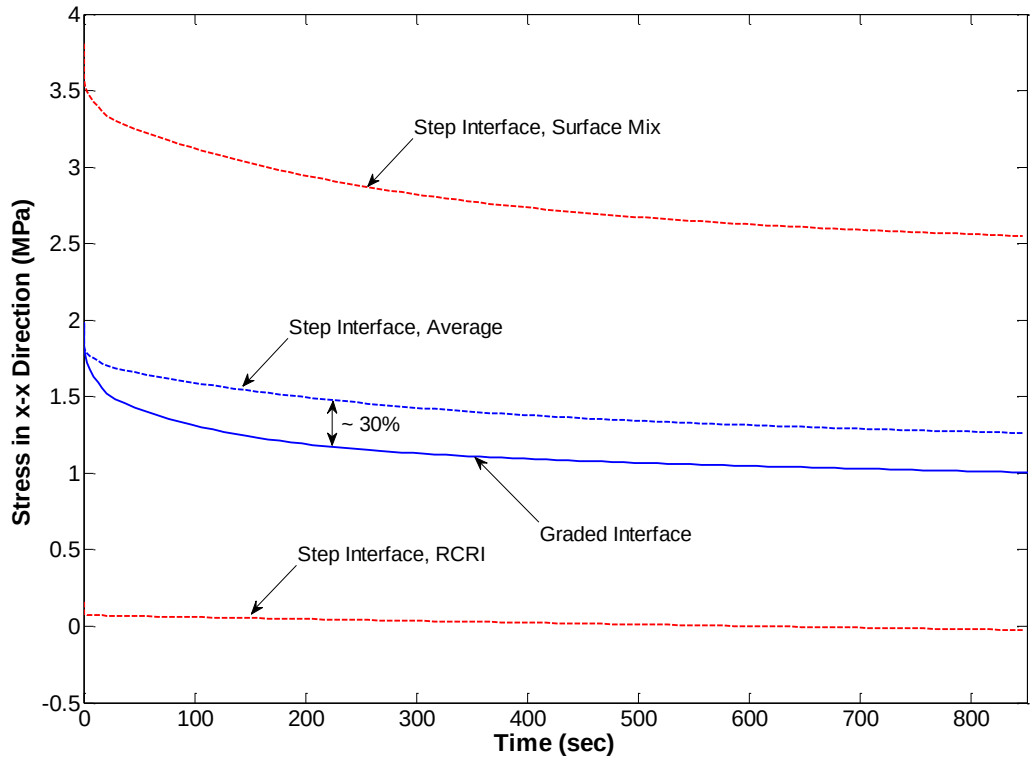

Figure 6-23: Peak Tensile Stresses in the Overlay

6.5.6 Summary and Findings

An example is presented for an overlay-interlayer pavement system based on an actual pavement section on Louisiana state highway 34. The interface between overlay and interlayer is modeled using two approaches, a more conventional step interface and a more physical graded interface. The graded interface is assumed to have thickness of 9.5mm and the viscoelastic properties are assumed to be varying linearly within the interface. Based on this limited study on asphalt concrete layer interface, the following key points are observed:

- The physical interfaces between different asphalt lifts require special modeling considerations.
- Assumption of interface with infinitesimal thickness (step interface) yields unrealistic stress responses.
- The limited study shown here demonstrated a significant variation between peak tensile stresses obtained from step and graded interfaces.

- The average stresses from step interfaces were also found to be significantly greater than those obtained from graded interface.
- More work is needed to identify:
    - Thickness/Length scale of asphalt concrete interfaces; and
    - Property variations within the interface. A micromechanical approach might be a useful tool for generating the required inputs for the graded interface model.

6.6 SUMMARY

Three case studies for conventional, full-depth and overlay-interlayer asphalt pavement systems are simulated and the key results are discussed. For each of the cases the viscoelastic FGM FE methods developed in Chapters 4 and 5 are utilized. The results from viscoelastic FGM analysis approach are contrasted with conventional asphalt pavement simulation approaches. Results reveal the strength of viscoelastic FGM procedure over conventional approaches, such as, layered gradation or stepped interfaces. The predictions from layered approaches are found to be significantly deviant from FGM predictions for same computational costs. By increasing the mesh refinements and in-turn the computational costs, the responses from layered gradations starts to approach the FGM representations. The key finding from the case studies is that for accurate and efficient simulation of asphalt pavements the viscoelastic FGM analysis is necessary.

CHAPTER 7 – CONCLUSIONS AND EXTENSIONS

7.1 SUMMARY AND FINDINGS

This dissertation describes the development, implementation, verification and application of viscoelastic FGM finite-element analysis procedures. Two formulations have been presented, (1) correspondence principle based, and (2) recursive time integration procedure, respectively.

A viscoelastic characterization procedure using the indirect tensile test is presented and comparisons are made between regular and flattened test geometries. In depth verification is performed for the formulations developed and implemented in this thesis. The verification examples demonstrate the accuracy and efficiency of the proposed procedures, when compared to conventional approaches. Three types of asphalt pavement systems have been simulated using the procedure developed herein. The results are compared against the conventional simulation approaches. The application examples further demonstrate the superiority of the proposed approaches over the conventional methods.

The key findings identified on the basis of research conducted in this study are summarized as follows:

- The indirect tensile creep test (IDT) can be utilized for determination of viscoelastic properties of asphalt concrete at low and intermediate test temperatures.
- The flattened IDT geometry is a viable alternative to regular IDT for viscoelastic characterization of asphalt concrete at low and intermediate temperatures.
- Non-homogeneous form of generalized Maxwell model is selected as the constitutive model of choice for the formulations developed herein.

- The correspondence principle (CP) based finite element procedure for viscoelastic FGM problems presented in Chapter 4 is capable of accurate and efficient simulation of non-homogeneous viscoelastic boundary value problems.
- In this study, the collocation method is found as the method of choice for numerical Laplace inversion.
- The recursive time-integration finite-element procedure for viscoelastic FGM problems presented in Chapter 5 is capable of accurate and efficient simulation of non-homogeneous viscoelastic boundary value problems.
- The generalized isoparametric formulation (GIF) extended to non-homogeneous viscoelastic finite elements makes for an attractive simulation method for asphalt pavements when compared to conventional approaches such as use of layered gradations.
- Verification examples for CP-based and time-integration finite element implementations ensure the veracity of the formulations and the implementations discussed in this dissertation.
- Comparisons with commercial software ABAQUS® for both CP-based and time-integration formulations further verifies and demonstrates the importance of the procedures developed in this study.
- Stationary crack tip fields have been determined for a radially graded viscoelastic FGM under Mode-I loading conditions. The results demonstrate the significant variation in the stresses with both space and time. This demonstrates the importance of considering of both spatial and temporal variations when simulating viscoelastic FGMs.
- Ignoring aging and temperature induced property gradients in asphalt concrete yield significant errors in the predicted responses.
- Significant deviations were found between graded and stepped interface modeling approaches for asphalt pavements. The deviation is anticipated to be

greatest for pavement systems with greater mismatch between layer properties, for example, that which is present in some overlay-interlayer systems.

7.2 CONCLUSIONS

Based on the findings from this study following conclusions can be drawn:

- The non-homogeneous viscoelastic analyses procedures presented in this dissertation are suitable and preferred for simulation of asphalt pavement systems.
- The proposed procedures yield greater accuracy and efficiency over conventional approaches for simulation of non-homogeneous viscoelastic problems.
- The layered approach for simulation of aging and temperature induced property gradients in asphalt concrete can yield significant errors; the most pronounced errors are at layer interfaces in the stress and strain quantities.
- The interface between asphalt concrete layers can be realistically simulated using the procedures developed in this thesis.
- In a limited study of aged full-depth asphalt pavements, the shear strains at the tire edge were found to be the most critical response.
- In case of layered approaches, at the layer interfaces the average of results from each material can be significantly different when compared to continuous FGM results at the same location. This difference is usually exaggerated with time when the time dependent (viscous) portion of material has spatial gradation.

7.3 FUTURE EXTENSIONS

Based on the finding and conclusions from this study following extensions are recommended:

- Further verification and validations are required for the flattened indirect tensile test for viscoelastic characterization and strength determination of asphalt

concrete. Verifications should include numerical simulation of the creep tests for different test geometries. Comparisons should be made between numerically determined viscoelastic properties with inputted properties to the analysis model. Analysis procedure similar to that utilized by Buttlar and Roque [43] could be used for development of correction factors if necessary.

- In the current study generalized Maxwell model was used for constitutive representation of non-homogeneous viscoeasltic material, the formulations should be extended to other commonly used models for asphalt concrete such as 2P2S1D model proposed by Olard et al. [49, 50].
- Limited data is available on variation of viscoelastic properties of asphalt concrete with age, the procedures developed in this thesis depend significantly on availability of this information. More testing and analysis should be performed to further verify and validate aging prediction models. The widely utilized global aging model by Mirza and Witczek [33] has been validated only for binder viscosity tests and amplitude of complex moduli.
- One of the key application areas of this dissertation research is thermal and reflective cracking predictions in asphalt pavement systems. The development from this research enables realistic simulation of age and temperature induced property gradients in bulk material, which significantly increases accuracy over the current state of practice. Future extension to graded viscoelastic cohesive fracture model is necessary to further enhance the accuracy of pavement crack modeling. Song [87] has worked on preliminary development of rate and temperature dependent cohesive fracture model and Braham et al. [145] have performed fracture characterization of asphalt concrete with varying degree of aging, these could be used as the basis for further development.
- The numerical inversion schemes studied in this thesis such as collocation method or Laguerre's functions are computationally inefficient. Approximate inversion formulae have been proposed by Schapery and Park [114] and Park and Kim [146], amongst others. These should be explored to increase efficiency

of CP-based implementations due to their significantly lower computational costs.

- Micromechanics considerations for prediction of graded viscoelastic properties should be studied. This is of particular interest for fracture simulation of significantly heterogeneous material such as asphalt concrete. Figure 7-1 demonstrates the effect of material heterogeneity during the fracture through asphalt concrete. Different failure modes are evident in the pictures, including cohesive failure of asphalt mastic, cracking of aggregates, and adhesive failure of interface between aggregate and mastic. Previously Kim and Paulino [147] have utilized micromechanical models for elastic simulation of fracture in FGMs and Yin et al. [148] described micromechanical models for prediction of viscoelastic properties of asphalt mastics.

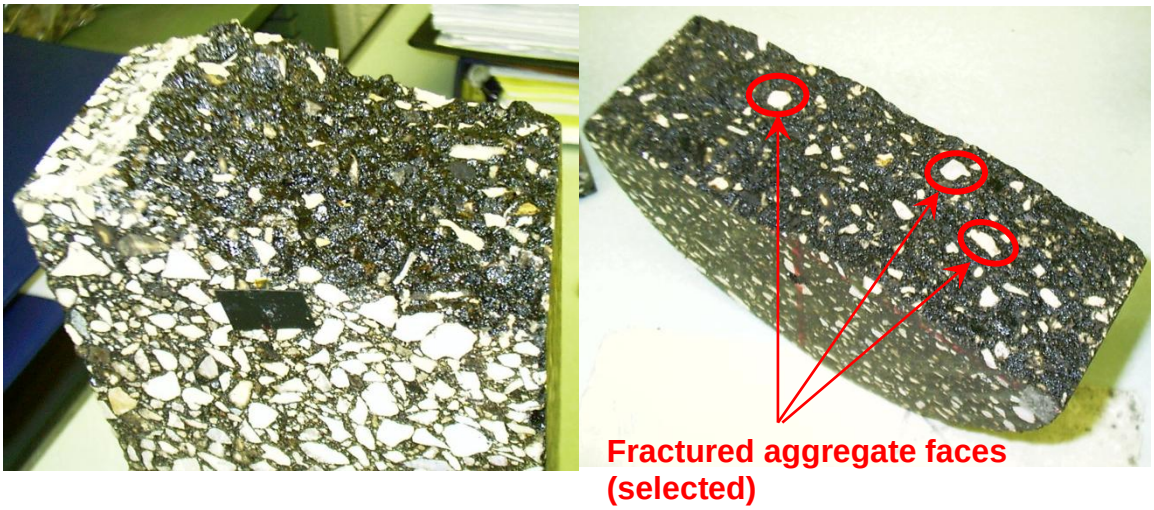

Figure 7-1: Fractured Faces of Asphalt Concrete Specimens

- This thesis explored incremental and recursive formulations for performing time-integration. Further evaluations of these methods are needed to study the theoretical basis of these numerical schemes. Krenk [149] has recently studied the energy conservation in Newmark time integration algorithms, similar analyses should be carried out for the time integration schemes studied in this dissertation.
- Finally, it is recommended that the current formulations be implemented in form of user defined elements (UEL) in commercial software ABAQUS®. The key motivation is to take benefit of efficient pre-processing, analysis and post-processing interfaces as well as for utilization of ABAQUS® finite-element mesh library of asphalt pavements developed previously [12].

7.4 SOME APPLICATIONS OF THE PRESENT RESEARCH

Few examples of have been presented in Chapters 4, 5, and 6 demonstrating the application of this research. There are broad areas of application for the present research within the field of asphalt pavements as well as outside. Some of the immediate applications for the current work are identified here:

- The viscoelastic FGM analysis described in this dissertation can be used for analysis and design of asphalt pavements. Based on the distress mechanism of interest the aging and temperature conditions can be chosen as the sources of non-homogeneities.
- The present analysis codes can be utilized as material selection tools for asphalt pavement and overlay systems. Using the aged and unaged viscoelastic properties the simulation code allows practicing engineers to make comparisons between different combinations of asphalt materials at different aging levels. Similar comparisons and selections are possible for selection of appropriate materials based on the anticipated climatic conditions.
- Bonded overlay systems are becoming popular structural and functional improvement strategies for deteriorated pavements. These type of systems

consists of emulsified asphalt tack coats with high application rates. During the process of lay-down and construction the tack coat wicks upwards into the asphalt concrete layer, as illustrated in Figure 7-2. This type of bonded overlay system exhibits significant viscoelastic property gradients through the thickness due to the spatially graded of tack-coat distribution. The present research provides a useful tool for the study of bonded overlay systems.

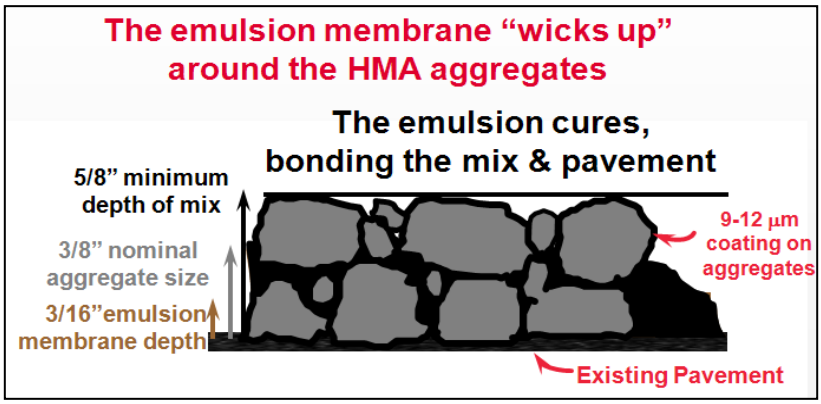

Figure 7-2: Tack Coat Emulsion Wicking up (reproduced from [150])

- Hilton [28, 29] has proposed designer viscoelastic FGMs that are tailored for a various applications using analytical formulations. The analyses procedures developed in this dissertation can be applied in similar fashion for design of viscoelastic FGMs for complicated boundary value problems for which, analytical solutions are not available.
- Many geotechnical materials exhibit viscoelastic behavior, for example behavior of sands as recently demonstrated by Bang et al. [151]. Factors such as moisture distribution [152, 153], temperature non-homogeneity [154], pore distribution [155] etc. commonly yield naturally existing and man-made geotechnical FGMs. The analyses procedures described in this dissertation can be applied for simulation of naturally exiting and man-made geotechnical deposits and their interactions with civil engineering structures.
- Portland cement concrete (PCC) and paste exhibits creep behavior necessitating viscoelastic analysis [156, 157], the properties depend on temperature [158] and

extent of cement hydration [156]. The viscoelastic FGM analysis is appropriate for simulation of PCC during the course of curing (short term) as well as long term creep.

- Significant amount of plant and animal tissues exhibit graded viscoelastic properties, one such example is human bones where porosity distribution makes it a viscoelastic FGM [159-161]. Analysis of biomaterials is another application of the present research.
- Other application areas of the present research include engineering materials that exhibit non-homogeneous viscoelasticity as a result of varied sources such as, temperature distribution, aging, moisture distribution, radiation, and curing. The applications vary across broad realm ranging from food industry [162] to metallurgy [3, 163] to polymer science [164].

CHAPTER 8 – NOMENCLATURE

The symbols and notations used throughout this dissertation are described herein. Unless otherwise indicated the symbols used in the text, equations, figures and tables refer to the list provided below.

8.1 CONSTITUTIVE RELATIONSHIP

x : Location

t : Time

T : Temperature

i, j, k, l : Subscripts with values of 1, 2, and 3 used in conjunction with summation convention

α : Coefficient of thermal expansion and contraction

$C_{ijkl}(x)$: Stiffess tensor

$C_{ijkl}(x,t)$: Relaxation modulus tensor

$D_{ijkl}(x,t)$: Creep compliance tensor

$G(x,t)$: Shear or Deviatoric relaxation modulus

$J(x,t)$: Shear or Deviatoric creep compliance

$K(x,t)$: Bulk or Volumetric relaxation modulus

$M(x,t)$: Bulk or Volumetric creep compliance

$\eta_{ijkl}(x)$: Viscosity

$(\bullet_{ijkl})_h$: Elastic or viscous contribution from h unit of generalized model

τ_{ijkl} : Relaxation time

λ_{ijkl} : Retaradation time

$\sigma_{ij}(t)$: Stress tensor

$\varepsilon_{ij}(t)$: Strain tensor

$\xi_{ijkl}(t,T)$:Reduced time

$a_{ijkl}(T)$: Time-temperature superposition shift factors

δ_{ij} : Kronecker's delta

Superscript d indicate deviatoric (shear) component

8.2 FINITE-ELEMENT FORMULATION

π :Potential

u_i : Displacements

P_i: Prescribed tractions

q_i : Nodal displacement vector

N_i : Isoprarametric shape functions

B_i : Derivative of shape functions

f_i : Element mechanical force vector

f_i^{th} : Element thermal force vector

k_{ij} : Element stiffness matrix

F_i : Global mechanical force vector

F_i^{th} : Global thermal force vector

K_{ij} : Global stiffness matrix

K_{ij}^e : Elastic component of stiffness matrix

K_{ij}^t : Viscous component of stiffness matrix

8.3 TIME INTEGRATION SCHEMES

t_n : Time at increment n

Δt : Time step size

$\Delta\xi(T,t_n)$: Reduced time increment corresponding to real time increment, Δt

$v_{ij}^1(x,t_n)$ & $v_{ij}^2(x,t_n)$: Viscous contributions in the element kernel for recursive method

$R_i(t_n)$: Solutions from previous time steps contributing to current time step

REFERENCES

[1] "Guide for Mechanistic-Empirical Design of New and Rehabilitated Pavement Structures," ARA Inc., ERES Consultants, NCHRP Project 1-37A Final Report, 2002.

[2] C. Billotte, P.J. Carreau, and M.C. Heuzey, (2006) "Rheological characterization of a solder paste for surface mount applications," *Rheologica Acta,* **45:**374.

[3] S. Koric, and B.G. Thomas, (2008) "Thermo-mechanical models of steel solidification based on two elastic visco-plastic constitutive laws," *Journal of Materials Processing Technology,* **197:**408.

[4] J. Sladek, V. Sladek, and C. Zhang, (2005) "Stress analysis in anisotropic functionally graded materials by the MLPG method," *Engineering Analysis with Boundary Elements,* **29:**597-609.

[5] J.N. Reddy, and R.A. Arciniega, (2007) "Large deformation analysis of functionally graded shells," *International Journal of Solids and Structures,* **44:**2036-52.

[6] A. Hollaender, J.E. Klemberg-Sapieha, and M.R. Wertheimer, (1995) "Polymer oxidation induced by vacuum-ultraviolet emission," *Surface and Coatings Technology,* Vol. 74-75 55.

[7] J.R. Roesler, G.H. Paulino, C. Gaedicke, A. Bordelon, and K. Park, (2007) "Fracture behavior of functionally graded concrete materials for rigid pavements," *Transportation Research Record,* **2037:**40-49.

[8] H. Diab, and Z. Wu, (2007) "Nonlinear constitutive model for time-dependent behavior of FRP-concrete interface," *Composites Science and Technology,* **67:**2323.

[9] Y.H. Huang, "Pavement Analysis and Design," Prentice-Hall, Inc., Englewood Cliffs, New Jersey, 1993.

[10] P. Blankenship, N. Iker, and J. Drbohlav, (2004) "Interlayer and design considerations to retard reflective cracking," *Transportation Research Record,* **1896:**177-186.

[11] M. Marasteanu, A. Zofka, M. Turos, X. Li, R. Velasquez, X. Li, C. Williams, J. Bausano, W. Buttlar, G. Paulino, A. Braham, E. Dave, J. Ojo, H. Bahia, A. Gallistel, and

J. McGraw, "Investigation of Low Temperature Cracking in Asphalt Pavements," Minnesota Department of Transportation, Research Services MS 330, St. Paul, MN 55155, Report: 776, 2007.

[12] G.H. Paulino, W.G. Buttlar, P.B. Blankenship, E.V. Dave, M.P. Wagoner, and S.H. Song, "Reflective crack control treatment and design procedures: a new integrated approach," National Science Foundation, CMS 0219566, Washington, DC, 2007.

[13] M.P. Wagoner, W.G. Buttlar, G.H. Paulino, and P.B. Blankenship, (2005) "Investigation of the fracture resistance of hot-mix asphalt concrete using a disk-shaped compact tension test," *Transportation Research Record,* **1929:**183-192.

[14] M.P. Wagoner, W.G. Buttlar, and G.H. Paulino, (2005) "Disk-shaped compact tension test for asphalt concrete fracture," *Proceedings of the Society for Experimental Mechanics, Inc,* **52:**270-7.

[15] M.P. Wagoner, W.G. Buttlar, and G.H. Paulino, (2005) "Development of a single-edge notched beam test for the study of asphalt concrete fracture," Geo-Frontiers 2005, 137-149.

[16] M.P. Wagoner, W.G. Buttlar, G.H. Paulino, and P.B. Blankenship, (2006) "Laboratory testing suite for characterization of asphalt concrete mixtures obtained from field cores," *Journal of Asphalt Paving Technologists,* Proceedings of the Annual Meeting, Association of Asphalt Paving Technologists, Vol. 75 815-852.

[17] M.P. Wagoner,"Fracture Tests for Bituminous Aggregate Mixtures: Laboratory and Field Investigations," Doctorate Thesis, University of Illinois at Urbana-Champaign, Urbana, IL, 2006.

[18] S.H. Song, G.H. Paulino, and W.G. Buttlar, (2006) "Simulation of crack propagation in asphalt concrete using an intrinsic cohesive zone model," *Journal of Engineering Mechanics,* **132:**1215.

[19] S.H. Song, G.H. Paulino, and W.G. Buttlar, (2006) "A bilinear cohesive zone model tailored for fracture of asphalt concrete considering viscoelastic bulk material," *Engineering Fracture Mechanics,* **73:**2829-2848.

[20] S.H. Song, G.H. Paulino, and W.G. Buttlar, (2006) "Simulation of crack propagation in asphalt concrete using an intrinsic cohesive zone model," *Journal of Engineering Mechanics,* **132:**1215-1223.

[21] S.H. Song,"Fracture of Asphalt Concrete: A Cohesive Zone Modeling Approach Considering Viscoelastic Effects," Doctorate Thesis, University of Illinois at Urbana-Champaign, Urbana, IL, 2006.

[22] E.V. Dave, S.H. Song, W.G. Buttlar, and G.H. Paulino, (2007) "Reflective and Thermal Cracking Modeling of Asphalt Concrete Overlays," Proceedings of the Advance Characterization of Pavement and Soil Engineering Materials – 2007, Vol. 2 1241-1252.

[23] E.V. Dave, A.F. Braham, W.G. Buttlar, G.H. Paulino, and A. Zofka, (2008) "Integration of Laboratory Testing, Field Performance Data, and Numerical Simulations for the Study of Low-Temperature Cracking," Proceedings of the 6th RILEM International Conference on Cracking in Pavements, Vol. 1 369-378.

[24] W.G. Buttlar, G.H. Paulino, and S.H. Song, (2006) "Application of graded finite elements for asphalt pavements," *Journal of Engineering Mechanics,* **132:**240-249.

[25] S. Suresh, and A. Mortensen, "Functionally Graded Materials," The Institute of Materials, IOM Communications Ltd., London, 1998.

[26] M.A.A. Cavalcante, S.P.C. Marques, and M. Pindera, (2007) "Parametric formulation of the finite-volume theory for functionally graded Materials-part I: analysis," *Journal of Applied Mechanics,* **74:**935-45.

[27] Y. Miyamoto, W.A. Kaysser, B.H. Rabin eds., "Functionally Graded Materials: Design, Processing and Applications," Kluwer Acedemic, Dordrecht, The Netherlands, 1999,

[28] H.H. Hilton, (2005) "Optimum linear and nonlinear viscoelastic designer functionally graded materials - Characterizations and analysis," *Composites Part A: Applied Science and Manufacturing,* **36:**1329-1334.

[29] H.H. Hilton, (2006) "Tailored designer functionally graded materials for minimizing probabilistic creep buckling failures in linear viscoelastic columns with large deformations and follower loads," 47th AIAA/ASME/ASCE/AHS/ASC Structures, Structural Dynamics and Materials Conference, Vol. 1 328-344.

[30] N.W. Garrick, (1995) "Nonlinear differential equation for modeling asphalt aging," *Journal of Materials in Civil Engineering,* **7:**265.

[31] E.C.N. Silva, M.C. Walters, and G.H. Paulino, (2006) "Modeling bamboo as a functionally graded material: lessons for the analysis of affordable materials," *Journal of Materials Science,* **41:**6991-7004.

[32] J.F. Branthaver, J.C. Petersen, R.E. Robertson, J.J. Duvall, S.S. Kim, P.M. Harnsberger, T. Mill, E.K. Ensley, F.A. Barbour, and J.F. Schabron, "Binder Characterization and Evaluation, Volume 2: Chemistry," Strategic Highway Research Program, National Research Council, Final Report, SHRP A-368, Washington, DC, 1993.

[33] M.W. Mirza, and M.W. Witczak, (1996) "Development of a global aging system for short and long term aging of asphalt cements," *Journal of Asphalt Paving Technologists,* Proceedings of the Annual Meeting, Association of Asphalt Paving Technologists, Vol. 64 393-430.

[34] A.K. Apeagyei,"Antioxidant Treatment for Asphalt Binders and Mixtures," Doctorate Thesis, University of Illinois at Urbana-Champaign, Urbana, IL, 2006.

[35] A.D. Chiasson, C. Yavuzturk, and K. Ksaibati, (2008) "Linearized approach for predicting thermal stresses in asphalt pavements due to environmental conditions," *Journal of Materials in Civil Engineering,* **20:**118.

[36] J. Kim, and W.G. Buttlar, (2002) "Analysis of reflective crack control system involving reinforcing grid over based-isolating interlayer mixture," *Journal of Transportation Engineering,* **128:**375-384.

[37] B. Saad, H. Mitri, and H. Poorooshasb, (2006) "3D FE analysis of flexible pavement with geosynthetic reinforcement," *Journal of Transportation Engineering,* **132:**402.

[38] J. Baek, and I.L. Al-Qadi, (2006) "Finite element method modeling of reflective cracking initiation and propagation: Investigation of the effect of steel reinforcement interlayer on retarding reflective cracking in hot-mix asphalt overlay," *Transportation Research Record,* **1949:**32-42.

[39] W.G. Buttlar, G.H. Paulino, and S.H. Song, (2006) "Application of graded finite elements for asphalt pavements," *Journal of Engineering Mechanics,* **132:**240-249.

[40] K. Nam, and H.U. Bahia, (2004) "Effect of binder and mixture variables on glass transition behavior of asphalt mixtures," *Journal of Asphalt Paving Technologists,* Proceedings of the Annual Meeting, Association of Asphalt Paving Technologists, Vol. 73 89-119.

[41] J.M. Krishnan, and K.R. Rajagopal, (2003) "Review of the uses and modeling of bitumen from ancient to modern times," *Applied Mechanics Reviews,* **56:**149-214.

[42] F.L. Roberts, P.S. Kandhal, E.R. Brown, "Hot Mix Asphalt Materials, Mixture Design, and Construction," NAPA Research and Education Foundation, Lanham, Maryland, 1996.

[43] W.G. Buttlar, and R. Roque, (1994) "Development and evaluation of the strategic highway research program measurement and analysis system for indirect tensile testing at low temperatures," *Transportation Research Record,* **1454:**163-171.

[44] AASHTO, "Standard Test Method for Determining the Creep Compliance and Strength of Hot Mix Asphalt (HMA) Using the Indirect Tensile Test Device (T-322),"

American Association of State Highway and Transportation Officials, Washington, DC, 2004.

[45] ASTM, "Standard Specification for Performance Graded Asphalt Binder," Vol. D6373-99, 1999.

[46] D.W. Christensen, and R.F. Bonaquist, "Evaluation of Indirect Tensile Test (IDT) Procedures for Low-Temperature Performance of Hot Mix Asphalt," Federal Highway Administration, NCHRP-530, United States, 2004.

[47] C. Huet,"Etude par une méthode d'impédance du comportement viscoélastique des matériaux hydrocarbonés," Doctorate Thesis, Faculté des Sciences de l'université de Paris, Paris, 1963.

[48] G. Sayegh,"Variation des modules de quelques bitumes purs et bétons bitumineux," Doctorate Thesis, Faculté des Sciences de l'université de Paris, Paris, 1965.

[49] H. Di Benedetto, B. Delaporte, and C. Sauzéat, (2007) "Three-dimensional linear behavior of bituminous materials: Experiments and modeling," *International Journal of Geomechanics,* **7:**149-157.

[50] F. Olard, H. Di Benedetto, A. Dony, and J.C. Vaniscote, (2005) "Properties of bituminous mixtures at low temperatures and relations with binder characteristics," *Materials and Structures,* **38:**121-126.

[51] H. Di Benedetto, F. Olard, C. Sauzéat, and B. Delaporte, (2004) "Linear viscoelastic behaviour of bituminous materials: from binders to mixes," *Road Materials and Pavement Design,* **5:**163-202.

[52] B. Delaporte, H. Di Benedetto, P. Chaverot, and G. Gauthier, (2007) "Linear viscoelastic properties of bituminous materials: from binders to mastics," *Journal of Asphalt Paving Technologists*, Proceedings of the Annual Meeting, Association of Asphalt Paving Technologists, Vol. 76 393-430.

[53] H.U. Bahia, and D.A. Anderson, (1995) "Development of the bending beam rheometer; Basics and critical evaluation of the rheometer," ASTM, Proceedings of the Conference on Physical Properties of Asphalt Cement Binders, Vol. 1241 28-50.

[54] M.W. Witczak, and O.A. Fonseca, (1996) "Revised predictive model for dynamic (complex) modulus of asphalt mixtures," *Transportation Research Record,* **1540:**15-23.

[55] T.K. Pellinen, and M.W. Witczak, (2002) "Use of stiffness of hot-mix asphalt as a simple performance test," *Transportation Research Record,* **1789:**80-90.

[56] T.K. Pellinen, M.W. Witczak, and R.F. Bonaquist, (2004) "Asphalt mix master curve construction using sigmoidal fitting function with non-linear least squares

optimization," Recent Advances in Materials Characterization and Modeling of Pavement Systems, 83-101.

[57] J. Bari, and M.W. Witczak, (2006) "Development of a new revised version of the Witczak E* Predictive Model for hot mix asphalt mixtures," *Journal of Asphalt Paving Technologists,* Proceedings of the Annual Meeting, Association of Asphalt Paving Technologists, Vol. 75 381-424.

[58] D.W. Christensen Jr., T. Pellinen, and R.F. Bonaquist, (2003) "Hirsch model for estimating the modulus of asphalt concrete," *Journal of Asphalt Paving Technologists,* Proceedings of the Annual Meeting, Association of Asphalt Paving Technologists, Vol. 72 97-121.

[59] Z. Zhang, and G.H. Paulino, (2007) "Wave propagation and dynamic analysis of smoothly graded heterogeneous continua using graded finite elements," *International Journal of Solids and Structures,* **44:**3601-3626.

[60] J.H. Kim, and G.H. Paulino, (2005) "Consistent formulations of the interaction Integral method for fracture of functionally graded materials," *Journal of Applied Mechanics,* **72:**351-64.

[61] G.H. Paulino, and J.H. Kim, (2007) "The weak patch test for nonhomogeneous materials modeled with graded finite elements," *Journal of the Brazilian Society of Mechanical Sciences and Engineering,* **29:**63-81.

[62] S.H. Song, and G.H. Paulino, (2006) "Dynamic stress intensity factors for homogeneous and smoothly heterogeneous materials using the interaction integral method," *International Journal of Solids and Structures,* **43:**4830-4866.

[63] Y.D. Lee, and F. Erdogan, (1995) "Residual/thermal stresses in FGM and laminated thermal barrier coatings," *International Journal of Fracture,* **69:**145-65.

[64] M.H. Santare, and J. Lambros, (2000) "Use of graded finite elements to model the behavior of nonhomogeneous materials," *Journal of Applied Mechanics,* **67:**819-22.

[65] J.H. Kim, and G.H. Paulino, (2002) "Isoparametric graded finite elements for nonhomogeneous isotropic and orthotropic materials," *Journal of Applied Mechanics,* **69:**502-14.

[66] M.C. Walters, G.H. Paulino, and R.H. Dodds Jr., (2004) "Stress-intensity factors for surface cracks in functionally graded materials under mode-1 thermomechanical loading," *International Journal of Solids and Structures,* **41:**1081-118.

[67] E.C.N. Silva, R.C. Carbonari, and G.H. Paulino, (2007) "On graded elements for multiphysics applications," *Smart Materials and Structures,* **16:**2408-2428.

[68] H.H. Hilton, and J.J. Piechocki, (1962) "Shear Center Motion in Beams with Temperature Dependent Linear Elastic or Viscoelastic Properties," Proceedings of the Forth U.S. National Congress of Applied Mechanics, 1279-1289.

[69] R.A. Schapery, "A Method for Predicting Crack Growth in Nonhomogeneous Viscoelastic Media," Texas A and M Univ College Station Mechanics and Materials Research Center, United States, 1977.

[70] J. Sladek, V. Sladek, C. Zhang, and M. Schanz, (2006) "Meshless local Petrov-Galerkin method for continuously nonhomogeneous linear viscoelastic solids," *Computational Mechanics,* **37:**279-289.

[71] W.J. Chang, T.H. Fang, and Y.C. Yang, (2007) "Thermoviscoelastic analysis of polymeric film on an elastic substrate with graded interlayer," *Japanese Journal of Applied Physics, Part 1: Regular Papers and Short Notes and Review Papers,* **46:**1604-1607.

[72] G.H. Paulino, and Z.H. Jin, (2001) "Correspondence principle in viscoelastic functionally graded materials," *Journal of Applied Mechanics,* **68:**129-32.

[73] S. Mukherjee, and G.H. Paulino, (2003) "The elastic-viscoelastic correspondence principle for functionally graded materials, revisited," *Journal of Applied Mechanics,* **70:**359-63.

[74] Z.H. Jin, (2006) "Some notes on the linear viscoelasticity of functionally graded materials," *Mathematics and Mechanics of Solids,* **11:**216-24.

[75] Y.H. Huang, (1973) "Stresses and Strains in Viscoelastic Multilayer Systems Subjected To Moving Loads," *Highway Research Record,* **457:**60-71.

[76] J. Uzan, M. Livneh, and I. Ishai, (1980) "Thickness Design of Flexible Pavements with Different Layer Structures," *Australian Road Research,* **10:**8-20.

[77] J. Uzan, (2004) "Permanent deformation in flexible pavements," *Journal of Transportation Engineering,* **130:**6-13.

[78] C.D. Whiteoak, (1990) "Analytical pavement design using programs for personal computers," *Highways and Transportation,* **37:**31-35.

[79] L. Khazanovich, and Q. Wang, (2007) "MnLayer: High-performance layered elastic analysis program," *Transportation Research Record,* **2037:**63-75.

[80] W. Alkasawneh, E. Pan, F. Han, R. Zhu, and R. Green, (2007) "Effect of temperature variation on pavement responses using 3D multilayered elastic analysis," *International Journal of Pavement Engineering,* **8:**203-212.

[81] R.P. Elliott, and M.R. Thompson, "Mechanistic Design Concepts for Conventional Flexible Pavements," Illinois State Dept. of Transportation, Springfield, IL, UILU-ENG-85-2001, United States, 1985.

[82] H.I. Ling, and H. Liu, (2003) "Finite element studies of asphalt concrete pavement reinforced with geogrid," *Journal of Engineering Mechanics,* **129:**801-811.

[83] S. Mun, M.N. Guddati, and Y. Kim, (2004) "Fatigue cracking mechanisms in asphalt pavements with viscoelastic continuum damage finite-element program," *Transportation Research Record,* **1896:**96-106.

[84] M. Novak, B. Birgisson, and R. Roque, (2003) "Tire Contact Stresses and Their Effects on Instability Rutting of Asphalt Mixture Pavements: Three-Dimensional Finite Element Analysis," *Transportation Research Record,* **1853:**150-156.

[85] W.G. Buttlar, B.J. Dempsey, and D. Bozkurt, "Evaluation of Reflective Crack Control Policy," Illinois Transportation Research Center, ITRC-IA-H1, United States, 1999.

[86] L.A. Myers, R. Roque, and B. Birgisson, (2001) "Propagation mechanisms for surface-initiated longitudinal wheelpath cracks," *Transportation Research Record,* **1778:**113-121.

[87] S.H. Song,"Fracture of Asphalt Concrete: A Cohesive Zone Modeling Approach Considering Viscoelastic Effects," Doctorate Thesis, University of Illinois at Urbana-Champaign, Urbana, IL, 2006.

[88] Q.Z. Wang, X.M. Jia, S.Q. Kou, Z.X. Zhang, and P.A. Lindqvist, (2004) "The flattened Brazilian disc specimen used for testing elastic modulus, tensile strength and fracture toughness of brittle rocks: Analytical and numerical results," *International Journal of Rock Mechanics and Mining Sciences,* **41:**245-253.

[89] Q.Z. Wang, and L.Z. Wu, (2004) "The flattened Brazilian disc specimen used for determining elastic modulus, tensile strength and fracture toughness of brittle rocks: Experimental results," *International Journal of Rock Mechanics and Mining Sciences,* **41:**1A 05 1-5.

[90] E.V. Dave, A.F. Braham, W.G. Buttlar, and G.H. Paulino, (2007) "Development of a flattened indirect tension test for asphalt concrete," SEM Annual Conference and Exposition on Experimental and Applied Mechanics 2007, Vol. 2 1088-1097.

[91] H.H. Hilton, (2001) "Implications and constraints of time-independent Poisson ratios in linear isotropic and anisotropic viscoelasticity," *Journal of Elasticity,* **63:**221-251.

[92] H.R. Hertz, (1881) "Ueber die Berührung fester elastischer Körper," *Journal Für Die Reine Und Angewandte Mathematik (Crelle's Journal),* **92:**1.

[93] G. Hondros, (1959) "The evaluation of poisson's ratio and the modulus of materials of a low tensile resistance by the brazilian (indirect tensile) test with particular reference to concrete," *Australian Journal of Applied Science,* **10:**243-268.

[94] G.D. Airey, and B. Rahimzadeh, (2004) "Combined bituminous binder and mixture linear rheological properties," *Construction and Building Materials,* **18:**535-548.

[95] E. Masad, and A. Papagiannakis, "Pavement Design and Materials," John Wiley and Sons, Inc., Hoboken, NJ, 2008.

[96] E.V. Dave, A.F. Braham, W.G. Buttlar, and G.H. Paulino, (2009) "Development of a Flattened Indirect Tension Test for Asphalt Concrete," *To be Submitted for Journal Publication.*

[97] H.H. Hilton, "Viscoelastic Analysis," *Engineering Design for Plastics,* Reinhold, New York, 1964, pp. 199.

[98] R.M. Christensen, "Theory of Viscoelasticity," Dover Publications, Inc., Mineola, New York, 1982.

[99] W.T. Read Jr., (1950) "Stress analysis for compressible viscoelastic materials," *Journal of Applied Physics,* **21:**671-674.

[100] H.H. Hilton, and S. Yi, (1993) "Anisotropic viscoelastic finite element analysis of mechanically and hygrothermally loaded composites," *Composites Engineering,* **3:**123-35.

[101] H.H. Hilton, Personal Communication, "Limitations on use of correspondence principle".

[102] R.D. Cook, D.S. Malkus, M.E. Plesha, "Concepts and applications of finite element analysis," *Fourth Edition,* John Wiley & Sons, Inc., New York, 2001.

[103] J.N. Reddy, "An introduction to finite element method," *Third Edition,* McGraw Hill, New York, 2005.

[104] M.E. Gurtin, (1963) "Variational Principles in the Linear Theory of Viscoelasticity," *Archives of Rational Mechanics and Analysis,* **36:**179-185.

[105] R.L. Taylor, K.S. Pister, and G.L. Goudreau, (1970) "Thermomechanical Analysis of Viscoelastic Solids," *International Journal of Numerical Methods in Engineering,* **2:**45-59.

[106] G.V. Narayanan, and D.E. Beskos, (1982) "Numerical operational methods for time-dependent linear problems," *International Journal for Numerical Methods in Engineering,* **18:**1829-1854.

[107] D.E. Beskos, and G.V. Narayanan, (1983) "Dynamic response of frameworks by numerical Laplace transform," *Computer Methods in Applied Mechanics and Engineering,* **37:**289-307.

[108] H. Stehfest, (1970) "Numerical inversion of Laplace transforms," *Communications of the ACM,* **13:**47-9.

[109] A. Sutradhar, G.H. Paulino, and L.J. Gray, (2002) "Transient heat conduction in homogeneous and non-homogeneous materials by the Laplace transform Galerkin boundary element method," *Engineering Analysis with Boundary Elements,* **26:**119-132.

[110] F. Durbin, (1974) "Numerical inversion of Laplace transforms: an efficient improvement to Dubner and Abate's method," *Computer Journal,* **17:**371-6.

[111] W.T. Weeks, (1966) "Numerical inversion of Laplace transforms using Laguerre functions," *Journal of the ACM,* **33:**419-429.

[112] B.S. Garbow, G. Giunta, J.N. Lyness, and A. Murli, (1988) "Software for an implementation of Weeks' method for the inverse Laplace transform problem," *ACM Transactions on Mathematical Software,* **14:**163-70.

[113] R.A. Schapery, (1965) "Method of viscoelastic stress analysis using elastic solutions," *Franklin Institute Journal,* **279:**268-289.

[114] R.A. Schapery, and S.W. Park, (1999) "Methods of interconversion between linear viscoelastic material functions. Part II - an approximate analytical method," *International Journal of Solids and Structures,* **36:**1677-1699.

[115] S. Yi,"Finite Element Analysis of Anisotropic Viscoelastic Composite Structures and Analytical Determination of Optimum Viscoelastic Material Properties," Doctorate Thesis, University of Illinois, Urbana, IL, 1992.

[116] T.L. Cost, and E.B. Becker, (1970) "A multidata method of approximate Laplace transform inversion," *International Journal for Numerical Methods in Engineering,* **2:**207-19.

[117] R.A. Schapery, "A Note on Approximate Methods Pertinent to Thermo-Viscoelastic Stress Analysis," U.S. Department of Commerce, Report: GALCIT-SM-62-40, United States, 1962.

[118] I.L. Hopkins, and R.W. Hamming, (1957) "On creep and relaxation," *Journal of Applied Physics,* **28:**906-909.

[119] E.H. Lee, and T.G. Rogers, (1962) "Solution of viscoelastic stress analysis problems using measured creep or relaxation functions," Proceedings of the ASME Annual Meeting.

[120] N.M. Newmark, (1959) "Method of computation for structural dynamics," *Journal of the Engineering Mechanics (ASCE),* **85:**67-94.

[121] F. Dubois, C. Chazal, and C. Petit, (2002) "Viscoelastic crack growth process in wood timbers: an approach by the finite element method for mode I fracture," *International Journal of Fracture,* **113:**367.

[122] P. Ellsiepen, and S. Hartmann, (2001) "Remarks on the interpretation of current non-linear finite element analyses as differential-algebraic equations," *International Journal for Numerical Methods in Engineering,* **51:**679.

[123] S. Hartmann, (2002) "Computation in finite-strain viscoelasticity: finite elements based on the interpretation as differential-algebraic equations," *Computer Methods in Applied Mechanics and Engineering,* **191:**1439.

[124] S. Hartmann, and J. Wensch, (2007) "Finite element analysis of viscoelastic structures using Rosenbrock-type methods," *Computational Mechanics,* **40:**383.

[125] A.D. Mesquita, and H.B. Coda, (2002) "Alternative Kelvin viscoelastic procedure for finite elements," *Applied Mathematical Modelling,* **26:**501.

[126] A.R. Zak, (1968) "Structural analysis of realistic solid-propellant materials," *Journal of Spacecraft and Rockets,* **5:**270-275.

[127] O.C. Zienkiewicz, M. Watson, and I.P. King, (1968) "A numerical method of visco-elastic stress analysis," *International Journal of Mechanical Sciences,* **10:**807-27.

[128] S. Yi, and H.H. Hilton, (1994) "Dynamic finite element analysis of viscoelastic composite plates in the time domain," *International Journal for Numerical Methods in Engineering,* **37:**4081-96.

[129] S. Yi, H.H. Hilton, and M.F. Ahmad, (1997) "A finite element approach for cure simulation of thermosetting matrix composites," *Computers and Structures,* **64:**383-8.

[130] M.A. Zocher, S.E. Groves, and D.H. Allen, (1997) "A three-dimensional finite element formulation for thermoviscoelastic orthotropic media," *International Journal for Numerical Methods in Engineering,* **40:**2267-88.

[131] H. Poon, and M.F. Ahmad, (1998) "Material point time integration procedure for anisotropic, thermo rheologically simple, viscoelastic solids," *Computational Mechanics,* **21:**236-242.

[132] H. Yang, and Z. Han, (2004) "Solving non-linear viscoelastic problems via a self-adaptive precise algorithm in time domain," *International Journal of Solids and Structures,* **41:**5483.

[133] R.M. Haj-Ali, and A.H. Muliana, (2004) "Numerical finite element formulation of the Schapery non-linear viscoelastic material model," *International Journal for Numerical Methods in Engineering*, **59:**25.

[134] A. Muliana, and K.A. Khan, (2008) "A time-integration algorithm for thermo-rheologically complex polymers," *Computational Materials Science,* **41:**576.

[135] S. Sawant, and A. Muliana, (2008) "A thermo-mechanical viscoelastic analysis of orthotropic materials," *Composite Structures,* **83:**61.

[136] A.M. Freudenthal, and M. Shinozuka, "Shrinkage Stresses in Case-Bonded Viscoelastic Hollow Cylinder of Infinite Length," TR-1 CU-1-61-ONR 266(78), United States, 1961.

[137] A.M. Freudenthal, and M. Shinozuka, (1963) "Shrinkage stresses in a thick-walled viscoelastic cylinder bonded to a rigid case," *AIAA Journal,* **1:**107-115.

[138] M.L. Williams, (1957) "On stress distribution at base of stationary crack," *Journal of Applied Mechanics,* **24:**109-114.

[139] J.W. Eischen, (1987) "Fracture of nonhomogeneous materials," *International Journal of Fracture,* **34:**3-22.

[140] P.R. Marur, and H.V. Tippur, (2000) "Numerical analysis of crack-tip fields in functionally graded materials with a crack normal to the elastic gradient," *International Journal of Solids and Structures,* **37:**5353-5370.

[141] J.H. Kim,"Mixed-Mode Crack Propagation in Functionally Graded Materials," Doctorate Thesis, University of Illinois at Urbana-Champaign, Urbana, IL, 2003.

[142] J. Eftis, N. Subramonian, and H. Liebowitz, (1977) "Biaxial load effects on the crack border elastic strain energy and strain energy rate," *Engineering Fracture Mechanics,* **9:**753-764.

[143] A.K. Apeagyei, W.G. Buttlar, and B.J. Dempsey, (2008) "Investigation of Cracking Behavior of Antioxidant-Modified Asphalt Mixtures," *Journal of Asphalt Paving Technologists,* Proceedings of the Annual Meeting, Association of Asphalt Paving Technologists, Vol. 77.

[144] H.M. Yin, G.H. Paulino, W.G. Buttlar, and L.Z. Sun, (2007) "Micromechanics-based thermoelastic model for functionally graded particulate materials with particle interactions," *Journal of the Mechanics and Physics of Solids,* **55:**132-160.

[145] A.F. Braham, W.G. Buttlar, T. Clyne, M.O. Marasteanu, and M. Turos, (2009) "The Effect of Long Term Laboratory Aging on Asphalt Concrete Fracture Energy,"

Journal of Asphalt Paving Technologists, Proceedings of the Annual Meeting, Association of Asphalt Paving Technologists, Vol. 78.

[146] S.W. Park, and Y.R. Kim, (2001) "Fitting prony-series viscoelastic models with power-law pre-smoothing," *Journal of Materials in Civil Engineering,* **13:**26-32.

[147] J.H. Kim, and G.H. Paulino, (2003) "An accurate scheme for mixed-mode fracture analysis of functionally graded materials using the interaction integral and micromechanics models," *International Journal for Numerical Methods in Engineering,* **58:**1457-1497.

[148] H.M. Yin, W.G. Buttlar, G.H. Paulino, and H. Di Benedetto, (2008) "Assessment of existing micro-mechanical models for asphalt mastics considering viscoelastic effects," *Road Materials and Pavement Design,* **9:**31-57.

[149] S. Krenk, (2006) "Energy conservation in Newmark based time integration algorithms," *Computer Methods in Applied Mechanics and Engineering,* **195:**6110-6124.

[150] M. Exline, (2009) "Thin Bonded Overlay Systems for Flexible and Rigid Pavement Rehabilitation," *Transportation and Highway Engineering Conference,* Technical Presentation, Session: Local Roads and Streets.

[151] D.P.V. Bang, H. Di Benedetto, A. Duttine, and A. Ezaoui, (2007) "Viscous behaviour of dry sand," *International Journal for Numerical and Analytical Methods in Geomechanics,* **31:**1631-58.

[152] V. Sanchez-Giron, E. Andreu, and J.L. Hernanz, (2001) "Stress relaxation of five different soil samples when uniaxially compacted at different water contents," *Soil and Tillage Research,* **62:**85-99.

[153] C. Wei, and K.K. Muraleetharan, (2007) "Linear viscoelastic behavior of porous media with non-uniform saturation," *International Journal of Engineering Science,* **45:**698-715.

[154] A.M. Vinogradov, (1985) "Generalized approach to the structure-soil interaction analysis with time and temperature effects," POAC 85: The 8th International Conference on Port and Ocean Engineering under Actic Conditions. Vol. 1 468-477.

[155] W. Dong Guo, (2000) "Visco-elastic consolidation subsequent to pile installation," *Computers and Geotechnics,* **26:**113-144.

[156] Z.C. Grasley, and D.A. Lange, (2007) "Constitutive modeling of the aging viscoelastic properties of Portland cement paste," *Mechanics of Time-Dependent Materials,* **11:**175-98.

[157] Z.P. Bazant, and G. Li, (2008) "Comprehensive database on concrete creep and shrinkage," *ACI Materials Journal,* **105:**635-637.

[158] Z.P. Bazant, G. Cusatis, and L. Cedolin, (2004) "Temperature effect on concrete creep modeled by microprestress- solidification theory," *Journal of Engineering Mechanics,* **130:**691-699.

[159] E. Garner, R. Lakes, T. Lee, C. Swan, and R. Brand, (2000) "Viscoelastic dissipation in compact bone: implications for stress-induced fluid flow in bone," *Journal of Biomechanical Engineering,* **122:**166-72.

[160] R. Schaller, S. Barrault, and P. Zysset, (2004) "Mechanical spectroscopy of bovine compact bone," *Materials Science and Engineering: A,* 13th International Conference on Internal Friction and Ultrasonic Attenuation in Solids, Vol. A370 569-74.

[161] P.L. Chandran, and V.H. Barocas, (2004) "Microstructural mechanics of collagen gels in confined compression: poroelasticity, viscoelasticity, and collapse," *Journal of Biomechanical Engineering,* **126:**152-66.

[162] R. Subramanian, K. Muthukumarappan, and S. Gunasekaran, (2006) "Linear viscoelastic properties of regular- and reduced-fat pasteurized process cheese during heating and cooling," *International Journal of Food Properties,* **9:**377-393.

[163] I. Jackson, J.D. Fitz Gerald, and H. Kokkonen, (2000) "High-temperature viscoelastic relaxation in iron and its implications for the shear modulus and attenuation of the Earth's inner core," *Journal of Geophysical Research,* **105:**23605.

[164] S.A.R. Hashmi, and U.K. Dwivedi, (2009) "SiC dispersed polysulphide epoxy resin based functionally graded material," *Polymer Composites,* **30:**162-168.